REGULATION OF METABOLISM BY THE ONCOPROTEIN C-MYC

by

Lia Rae Edmunds

Biochemistry, Washington and Jefferson College, 2008

Submitted to the Graduate Faculty of

Molecular Genetics and Developmental Biology in partial fulfillment

of the requirements for the degree of

Doctor of Philosophy

University of Pittsburgh

2015

UNIVERSITY OF PITTSBURGH

MOLECULAR GENETICS AND DEVELOPMENTAL BIOLOGY

This dissertation was presented

by

Lia Rae Edmunds

It was defended on

November, 2015

and approved by

Eric S. Goetzman, Ph.D., Medical Genetics

Robert M. O'Doherty, Ph.D., Endocrinology

Bennet Van Houten, Ph.D., Molecular Genetics and Developmental Biology

Dissertation Advisor: Edward V. Prochownik, M.D., Ph.D., Pediatric Hematology/Oncology

REGULATION OF METABOLISM BY THE ONCOPROTEIN C-MYC

Lia Rae Edmunds, Ph.D.

University of Pittsburgh, 2015

c-Myc (hereafter Myc), a transcription factor that regulates a variety of cellular functions including growth and differentiation, is deregulated in many different types of cancers. Myc regulates the Warburg effect and oncogenic biosynthesis, but also many aspects of metabolism, believed to be a pivotal point of transformation. Myc is known to control glycolysis and glutaminolysis but little is known about the interplay between glucose, amino acid, and fatty acid oxidation. We hypothesize Myc integrates glucose, amino acid, and fatty acid utilization for energy, and either loss- or gain-of-function will disrupt metabolic homeostasis.

Loss of Myc in rat fibroblasts elicits a severe energy deficit, including diminished acetyl-coA levels, to which they respond by enhancing FAO and lipid uptake and storage. Using an in vivo model, we found murine hepatocytes respond to Myc ablation with a milder phenotype. They display metabolic defects, including reduced respiratory chain capacity and an increased metabolic rate when fed a high-fat diet. Additionally, hepatocytes had major lipid defects including transcriptional deregulation, lipid accumulation and increased FAO.

Reduced ATP in Myc KO fibroblasts constitutively activates AMPK, a protein which limits anabolism for catabolism, leading us to hypothesize AMPK may play a role in Myc deregulated phenotypes. We found AMPK controls mitochondrial structure and function in conjunction with Myc over-expression, via redox state, electron transport chain (ETC) capacity, and TCA cycle dehydrogenases. Additionally, AMPK KO cells demonstrate transcriptional and translational differences and differential responses in regulating glycolysis, which results in

metabolite dysfunction, when exposed to Myc over-expression. Thus, AMPK is critical to supporting metabolic pathways in response to Myc deregulation.

To ascertain if Myc plays a role in hepatic proliferative capacity, we turned to a mouse model of hereditary tyrosinemia. We definitively proved that Myc is not required for prolonged hepatocyte proliferation, even in direct competition with Myc-replete hepatocytes. Proliferating KO hepatocytes were associated with a pro-inflammatory environment that correlated with worsening lipid accumulation and lipid oxidation-mediated liver damage, a phenotype reminiscent of non-alcoholic fatty liver-like disease. Throughout this work, we reveal Myc-regulated metabolism is vital for maintaining lipid homeostasis and energy production, but dispensable for sustained hepatic proliferation.

TABLE OF CONTENTS

LIST OF TABLES

LIST OF FIGURES

PREFACE

CHAPTER 2 ACKNOWLEDGEMENTS

This research was originally published in the Journal of Biological Chemistry.

Edmunds LR, Sharma L, Kang A, Lu J, Vockley J, Basu S, Uppala R, Goetzman ES, Beck ME, Scott D, Prochownik EV.

c-Myc programs fatty acid metabolism and dictates acetyl-CoA abundance and fate.

J Biol Chem. 2015 Aug 14;290(33):20100

CHAPTER 3 ACKNOWLEDGEMENTS

This research was originally published in PLoS One.

Edmunds LR, Sharma L, Wang H, Kang A, d'Souza S, Lu J, McLaughlin M, Dolezal JM, Gao X, Weintraub ST, Ding Y, Zeng X, Yates N, Prochownik EV.

c-Myc and AMPK Control Cellular Energy Levels by Cooperatively Regulating Mitochondrial Structure and Function.

PLoS One. 2015 Jul 31;10(7):e0134049.

CHAPTER 4 ACKNOWLEDGEMENTS

This chapter corresponds to research which will be published concurrently entitled “Abnormal Lipid Processing but Normal Long-Term Repopulation Potential of *myc-/-* Hepatocytes”.

Edmunds LR, Otero PA, Sharma L, D’Souza S, Dolezal JM, David S, Lu J, Lamm L, Basantani M, Zhang P, Sipula IJ, Li L, Zeng X, Ding Y, Ding F, Beck ME, Vockley J, Monga SPS, Kershaw EE, O’Doherty RM, Kratz LE,Yate NA, Goetzman EP, Scott D, Duncan AW, and Prochownik EV.

These works were supported by a pre-doctoral fellowship award from the Children’s Hospital of Pittsburgh of UPMC Health Systems Research Advisory Committee.

ABBREVIATIONS

Oxidative Phosphorylation (OXPHOS); Electron transport chain (ETC); Fatty acid β-oxidation (FAO); Reactive oxygen species (ROS); Very-long/Long/Medium/Short chain fatty acids (VL/L/M/SCFAs); Pyruvate Dehydrogenase (PDH); Pyruvate Dehydrogenase Kinase (PDK); Pyruvate dehydrogenase phosphatase (PDP); Pyruvate carboxylase (PC); Pyruvate kinase (PK); Phospho(enol)pyruvate (PEP); Glutathione (GSH [reduced] and GSSG [oxidized]); Acetyl coenzyme A (AcCoA); Murine embryonic fibroblasts (MEFs); Fumarylacetoacetate Hydrolase

(FAH); 2-(2-Nitro-4-Trifluoro-Methyl-Benzoyl)-1,3-Cyclo-Hexanedione (NTBC); Blue Native Gel Electrophoresis (BNGE); Super complexes (SCs); ATP synthase (Complex V, also V_m [monomer] and V_d [dimer]); Isocitrate Dehydrogenase (IDH); Malic Dehydrogenase (MDH); Glycerol 3-Phosphate Dehydrogenase (G3PDH) ; Succinate Dehydrogenase (SDH, also Complex II); AMP-Activated Protein Kinase (AMPK); Oil Red O (ORO); False Discovery Rate (FDR, q-value); Cytochrome P450 (Cyp450); Farnesoid X Receptor (FXR); Liver X Receptor (LXR); Respiratory Exchange Ratio (RER); Oxygen Consumption Rate (VO_2); Carbon Dioxide Production Rate (VCO_2); Oxygen consumption rate (OCR); Extracellular acidification rate (ECAR) Non-alcoholic fatty liver disease (NAFLD); Non-alcoholic steatohepatitis (NASH)

1.0 INTRODUCTION

The *MYCC* gene is among the most frequently deregulated oncogenes in human tumors. At basal expression levels, c-Myc (hereafter Myc) functions as a transcription factor to inhibit differentiation and promote proliferation [13]. However, when the protein is amplified or over-expressed, the resulting deregulated expression can result in cellular transformation [14]. In normal cells, Myc has been proposed to control cell cycle progression, differentiation, apoptosis, and mitochondrial biogenesis and function [4, 15-17]. It has been suggested that deregulated Myc merely amplifies global expression of already-transcribed genes, contingent on estimates that Myc can regulate 10-15% of the genome [14]. However, this appears to be an oversimplification, based on the abundance of specific genes involved in cell cycle, growth, metabolism, protein and ribosomal biogenesis, and mitochondrial function [18]. Myc deregulation in tumorigenesis affects many metabolic pathways, but its direct role in tumor cell metabolism is poorly understood. A fuller understanding of Myc's regulation of metabolism may provide key weaknesses, which can be exploited by novel therapies.

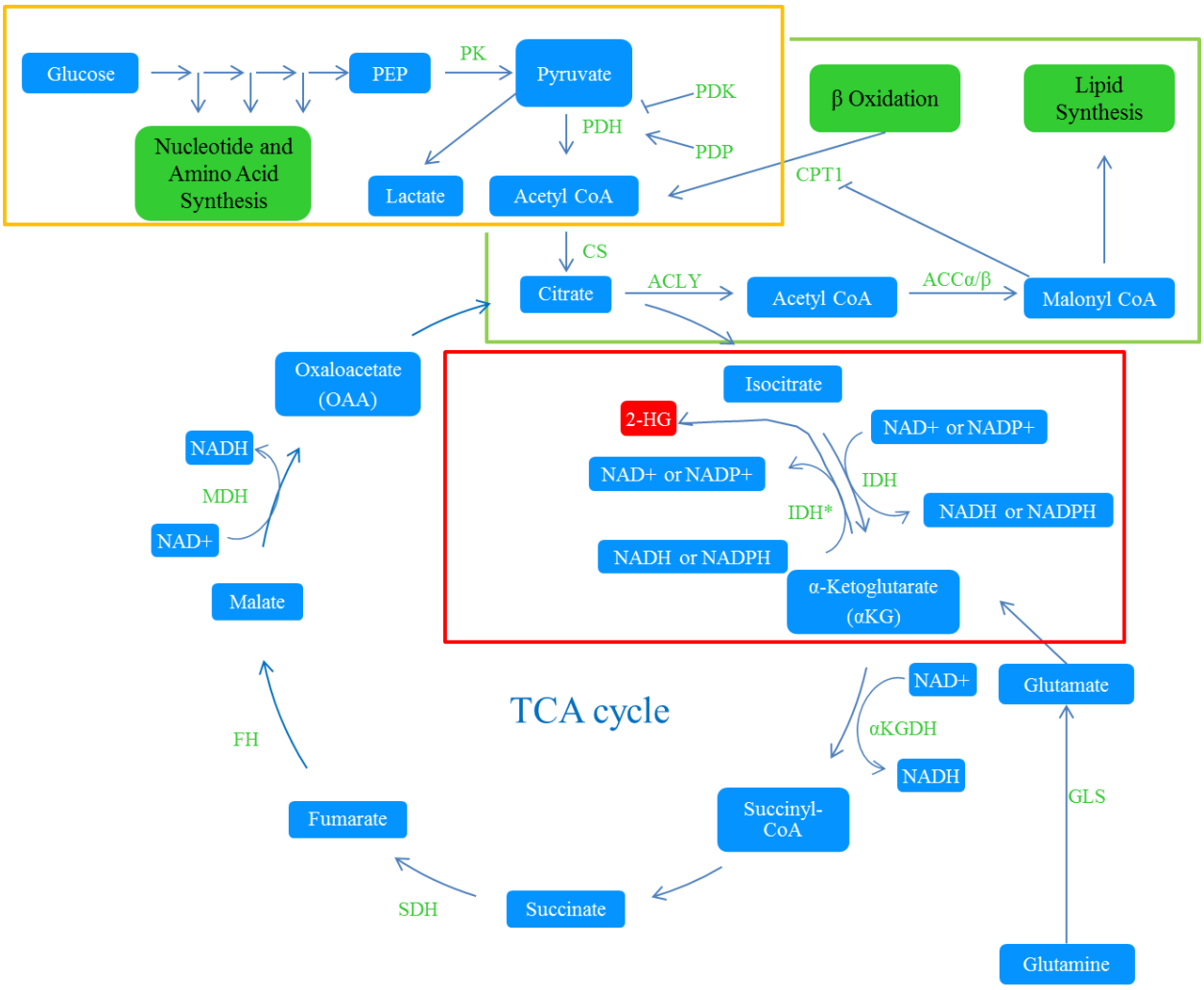

Figure 1: Schematic of Metabolic Pathways. Yellow box indicates glycolysis and potential biosynthetic offshoots. Green box illustrates FAO and de novo fatty acid synthesis pathway. Red box is an example of oncogenic manipulation of the TCA cycle and production of the oncometabolite 2HG. IDH3 is the isoform responsible for TCA cycle reduction of NAD+ to NADH, while IDH1 (cytoplasmic) and IDH2 (mitochondrial) reduce NADP+ to NADPH. Abbreviations: Phosphoenol Pyruvate (PEP), Pyruvate Kinase (PK), Pyruvate Dehydrogenase (PDH), ATP Citrate Lyase (ACLY), Citrate Synthase (CS), Malate Dehydrogenase (MDH), Fumarate Hydrolase (FH), Succinate Dehydrogenase (SDH), α-Ketogluterate Dehydrogenase (α-KGDH), Isocitrate Dehydrogenase (IDH), 2-Hydroxyglutarate (2HG).

1.1 TUMOR METABOLISM

It was once believed the deregulated metabolism of tumors was merely a byproduct of their rapid proliferation, but it is now considered to be one of the hallmarks of cancer [19]. Otto Warburg introduced the idea of altered cancer metabolism when he discovered that tumor cells accumulate lactate in the process of breaking down glucose (glycolysis), despite an ample supply of oxygen to reduce glucose down to TCA cycle substrates (Figure 1, yellow box) [20]. Many tumors preferentially use aerobic glycolysis at the cost of reduced ATP production because it confers the proliferative advantage of providing the necessary anabolic precursors needed to proliferate [21]. Canonical biochemical pathways used to generate energy in normal tissues are re-routed to synthetic intermediates for nucleic acids, amino acids, and lipids production [21, 22]. The described glutamine addiction of Myc-expressing tumors results because Warburg respiration depletes the TCA cycle of intermediates, which can be restored by glutamine conversion to α-ketoglutarate [23-25]. The oncogenic environment is rich in substrates to be broken down for oxidative phosphorylation, but cannot provide the anabolic intermediates or reducing equivalents for biosynthetic reactions [26]. This is strong motivation for proliferative pathways to regulate cellular metabolism, and also why many cancer-driving mutations usurp this control.

If neoplastic transformation depends in part on altering the metabolic microenvironment, it is increasingly understood that many oncogenes and tumor suppressors must play a vital role in regulating metabolism. For example, p53, a well-known tumor suppressor, activates metabolic arrest in the setting of glucose depletion; however, when p53 is lost or mutated, proliferation can proceed unchecked despite lack of available nutrients [27]. p53 mutations also increase the expression of genes involved in cholesterol biosynthesis (mevalonate) pathways [28], suggesting

that successful oncogenic transformation alters cellular metabolism on many fronts. Many other cancer-associated mutations can reprogram metabolism, such as loss-of-function mutations in fumarate dehydrogenase (FH) and succinate dehydrogenase (SDH) or gain-of-function mutations in isocitrate dehydrogenase (IDH), that produce aberrant metabolites ("oncometabolites") [21, 29-31]. Mutations in FH and SDH cause abnormal accumulation of fumarate and succinate, while mutations in IDH reverse the normal flow of the TCA cycle and switch production of NADH to consumption of NADPH, with the consequences being a high level of 2-hydroxyglutarate [32, 33]. These metabolites can cause transformation by obstructing normal regulation of α-ketoglutarate dioxygenases, causing deregulation in fatty acid metabolism, oxygen sensing, and epigenetic modifications (as reviewed in [34]). Another example is the canonical breakdown of acetyl CoA through the TCA cycle, which is not normally re-synthesized into lipids in a starved state. Acetyl CoA is converted to citrate and then α-ketoglutarate (Figure 1, red box) to generate ATP producing intermediates. Tumor metabolism can reverse the TCA cycle to convert glutamine to citrate, and then increase activity of ATP Citrate Lyase (ACLY) to utilize acetyl CoA for lipid synthesis [19, 35]. Far from being a mere coincidence, the deregulation of metabolism is a necessary and directed step for oncogenic transformation and proliferation.

1.2 MYC AND METABOLIC REPROGRAMMING

Myc is directly responsible for a variety of changes in transformed and non-transformed cells, though the response is tissue- and context-specific [25, 36]. Myc is a major regulator of the

Warburg effect and will increase glucose uptake and lactate production [21, 22]. Myc drives a rapid switch from fatty acid oxidation (FAO) and pyruvate oxidation via the TCA cycle to aerobic glycolysis, the pentose phosphate shunt, and glutamine oxidation [1, 37, 38]. Myc overexpression also modulates the alternative splicing from pyruvate kinase isoform 1 to 2 (PKM1/2), which results in less carbon flow from glucose to acetyl CoA [38, 39]. PKM2 has a higher activation energy (k_m) and lower activity level (k_{cat}), allowing upstream intermediates to build up and be re-directed into the above-mentioned anabolic pathways. The Warburg effect can further negatively regulate PKM through tyrosine phosphorylation and reactive oxygen species (ROS) which destabilize it from the tetrameric (active) to dimeric (inactive) form [21]. Myc tumorigenesis requires MondoA, a transcription factor that works by sensing nutrients, specifically glycolytic intermediates that accumulate due to reduced PKM activity [40, 41]. As Myc stimulates Warburg metabolism, the anabolic products feed back on and reinforce Myc-driven tumorigenesis in a targeted and essential part of transformation.

1.3 MYC AND FATTY ACID METABOLISM

Lipid metabolism can also be disrupted by cancer metabolism, potentially through Myc (Figure 1, green box). Each cell type, transformed or un-transformed, has a unique metabolic profile based on its individual needs. Fatty acid oxidation can be preferred over glucose breakdown because one molecule of palmitate, a long-chain fatty acid, yields 129 molecules of ATP while glucose yields only 38. While fatty acids are a rich energy source, they tend to induce lipid peroxidation and result in cellular damage, and are used by tissues which can respond by

repairing damage or replacing the cell [42]. On the other hand, tissues which require a constant, reliable source of energy tend to use glucose, which can be supplied throughout the body by the liver [42]. To further complicate the matter, bioavailability plays a major role in how a tissue fulfils its unique energy needs.

Mitochondrial fatty acid β-oxidation (FAO) is the main pathway for breakdown of most fatty acids, though some oxidation can occur in peroxisomes [43]. Peroxisomal β-oxidation of fatty acids is uncoupled to any respiratory chain and results in H_2O_2 production and heat [44]. Because loss of Myc results in lipid accumulation, peroxisome oxidation of this lipid may result in increased ROS in Myc knockout models and in human diseases like non-alcoholic fatty liver disease (NAFLD) and non-alcoholic steatohepatitis (NASH) [45, 46]. While shorter chain fatty acids can diffuse through the mitochondrial membrane to be used for fatty acid oxidation [47], longer chain fatty acids require more active processing and facilitated transport into the mitochondria, specifically by the rate-limiting enzyme carnitine palmitoyltransferase 1 (CPT1) [48, 49]. Fatty acyl chains are joined to CoA in the mitochondrial matrix and are broken down to yield NADH, $FADH_2$, and acetyl CoA by iterative cycles of oxidation/hydration [50]. Both prostate [51] and pancreatic [52] cancers rely on FAO as the major energy producing pathway and inhibition of FAO in leukemia [53] and glioblastomas [54] will induce apoptosis. Prostate tumors are particularly dependent on FAO because of a decreased ability to utilize glucose [55, 56], which results in an increased uptake of fatty acids [57] and an over-expression of β-oxidation enzymes [58].

Rather than oxidized for ATP, fatty acids can be directly incorporated into new lipids to provide membranes for rapidly growing normal or cancer cells [59]. Typically, there exists an equilibrium between β−oxidation and *de novo* fatty acid synthesis, but safeguards are in place to

keep both from occurring simultaneously. Mechanistically, CPT1 is inhibited by malonyl CoA, a product of synthesizing acetyl CoA into long chain fatty acids by Acetyl CoA Carboxylase (ACCα/β) (Figure 1, green box) [50]. The energy state of the cell dictates whether CPT1 or ACCα/β is active and AMPK controls this through phosphorylation of ACCα/β. Phosphorylation inhibits ACCα/β, resulting in FAO up-regulation and inhibition of fatty acid synthesis [60]. Though FAO is stimulated in some types of cancer, CPT1 is more often down-regulated in cancers, tipping the balance in favor of increased fatty acid synthesis [61, 62]. Enhanced lipid synthesis is more often associated with different types of cancers, such as breast and ovarian tumors, and is driven by the expression of ACLY and fatty acid synthase (FASN) [63-68]. In instances of cancers where fatty acid β–oxidation (FAO) is favored over fatty acid synthesis, the Warburg effect might dictate the fate of all other available substrates, leaving the transformed cells reliant on fatty acids as a source of ATP.

While much is known regarding Myc regulation of glucose and glutamine metabolism, Myc control over lipid metabolism is still an emerging field. In chapters 2 and 4, we attempt to distinguish lipid profiles of cells driven by oncogenic Myc signaling, compared to normal cells, and cells removed from Myc signaling. The removal of Myc may initiate a switch from glycolysis to FAO, so we studied each of these situations to determine how the cell transports, directs, and breaks down fatty acids. On one hand, Myc signaling necessitates de novo synthesis for a large supply of macromolecular precursors. Previous studies have shown pharmacologic inhibition of Myc by the drug 10058-F4 results in diminished fatty acid synthesis [69] and Myc directly contributes glucose-derived acetyl coA to lipid biosynthesis [70]. On the other hand, the proliferating cell also requires ATP and other studies show that induction of Myc increases fatty acid oxidation [71]. Since oxidation and *de novo* synthesis do not occur simultaneously under

normal circumstances, this could be an issue of cell type or bioavailability, or this could be a Myc-specific phenomenon. Another novel, Myc-specific occurrence is the lipid accumulation that occurs with genetic or pharmacological inhibition of Myc [69, 72]. In this work, we begin to determine the cause and effect of Myc-deplete induced lipid accumulation.

1.4 AMPK AND MYC

A primary regulator of cellular metabolism in most eukaryotic cells is AMP-activated protein kinase, or AMPK, which is activated in response to energetic stress (i.e. high AMP:ATP ratios) to promote survival [73]. This involves the stimulation pathways to increase ATP production, such as glucose and fatty acid uptake and oxidation and mitochondrial biogenesis (Figure 2 and [74, 75]). Along with that comes concurrent inhibition of anabolic processes such as protein and glycogen synthesis [74]. As an important regulator of metabolism, it seems an obvious target for controlling the tumor microenvironment and AMPK acts as an energy sensor at the intersection of several tumor suppressor pathways. However, mutations in AMPK are relatively rare events in cancer, suggesting that metabolic elasticity is important for tumor survival. Upstream or downstream regulators can be modified so proliferation continues in spite of AMPK activation. For example, the tumor suppressor LKB1 directly regulates AMPK activity upstream [76], while TSC2 [77] and p53 [27] are downstream. Mutations in these proteins are more common and control certain aspects of AMPK function to promote proliferation, while allowing AMPK otherwise autonomic function.

AMPK can be activated, and thereby controlled, in a variety of ways (Figure 2). The classical pathway is in response to the ratio of AMP and ADP:ATP, but it can also be activated by less well-characterized modes such as calcium or magnesium, by the drugs resveratrol and metformin, and by oxidative (H_2O_2) and genotoxic stress [74]. Non-canonical activation of AMPK may be another way to promote survival while oncogenic drivers are subverting metabolism but maintaining a normal AMP:ATP ratio.

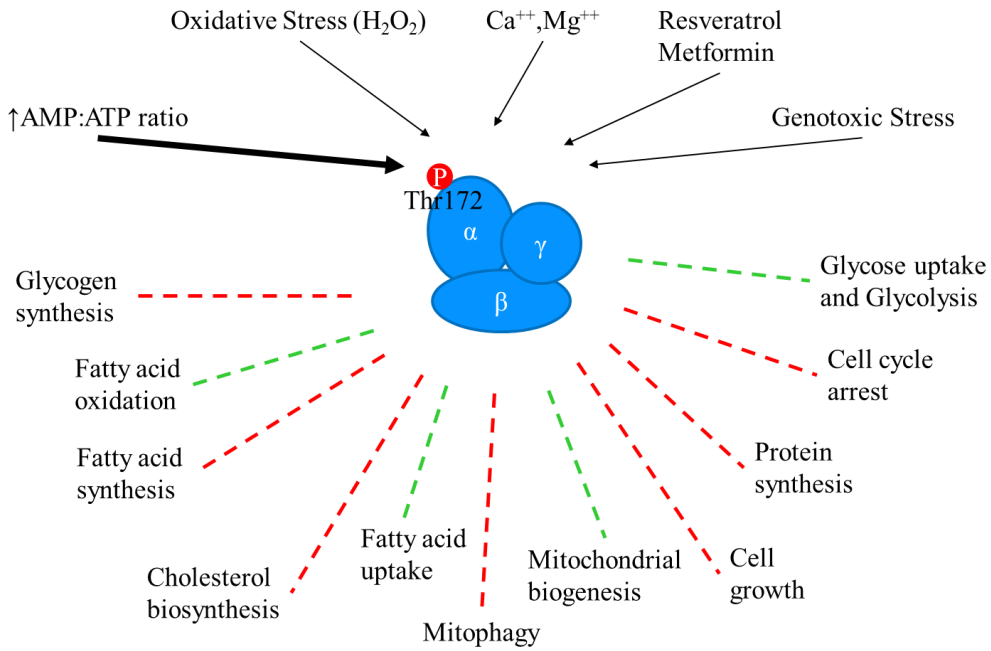

Figure 2: Regulation of AMPK. Activation of AMPK via phosphorylation of Thr172 can occur through canonical (thick arrow) or non-canonical (thin arrows) means. AMPK activation then stimulates catabolic pathways (green dashed lines) and inhibits anabolic pathways (red dashed lines).

Myc positively regulates cell growth and a number of synthetic pathways, in direct opposition of AMPK action in an energy crisis. But both Myc and AMPK enhance glucose and fatty acid oxidation. So though the two proteins control metabolism differently, AMPK may interact with Myc-driven metabolism to maintain metabolic homeostasis. For instance, the loss

of Myc results in activation of AMPK [78]. This may be purely circumstantial as loss of Myc reduces ATP and AMPK is conceivably activated to restore depleted ATP. In other circumstances, AMPK can inhibit Myc biosynthetic pathways and suppress tumor growth, in effect counteracting Myc activation [79]. Faubert *et al.* used a Myc-driven model of B-cell lymphoma to show deletion of AMPK cooperated with Myc to enhance lymphogenesis [79]. Yet there must also be some yet-undiscovered adaptability to the response between AMPK and Myc, because in of Myc-driven osteosarcoma, loss of AMPK resulted in increased cell death [80]. Given the conflicting roles for these two proteins controlling metabolism, it seems clear the end result is tissue- and context-dependent. The flexibility conferred by AMPK may be necessary for later stage tumors, but loss of AMPK may be beneficial in the early stages of tumorigenesis.

By promoting survival, AMPK could cooperate with oncogenic drivers and is thus advantageous for cellular survival. What coordination exists and how it is regulated remains largely unknown. In chapter 3, we study the interaction between AMPK and Myc. To determine if AMPK is necessary for Myc-driven proliferation, murine embryonic fibroblast line with ablated AMPK activity was used to study the initiation of Myc deregulation. Because Myc stimulates both energy production and energy utilization at a high cost to the cell, AMPK may dampen the true Myc response. When AMPK is absent, we can evaluate how this crosstalk affects Myc-directed metabolism.

1.5 MYC AND PROLIFERATION

While Myc has long been implicated in the regulation of cellular proliferation, apoptosis, and cell growth [81, 82], the actual role in normal tissue physiology remains elusive and at times contradictory. The simple explanation that regulation by Myc seems to be tissue- and situation-specific includes exceptions based on age and experimental model. The loss of Myc in bone marrow severely disrupts normal hematopoietic proliferation and homeostasis [83]. Trumpp *et al*. determined that when mice were lacking a single Myc allele (heterozygous null), they had overall reduced organ size [84]. They found cell number was reduced in spleen, lymph nodes, and bone marrow, but no differences in cell size, indicating that loss of even a single copy of Myc causes some reduction in proliferation and a smaller total number of cells in these organs [84]. On the other hand, genetic ablation of Myc in villi and intestinal crypts by Bettess *et al*. showed no difference in small intestine development of adults [85]. Soucek *et al*. used a dominant negative Myc mutant to cause global inhibition of Myc transcription, which caused only minor proliferative damage in high-turnover tissues like skin, testes, and gut epithelia, which resolved when Myc was restored [86]. The remaining tissues, including moderately proliferating tissue like lung, pancreas, liver and kidney, all exhibited no structural or proliferative changes [86].

Several groups have studied liver or hepatocyte specific proliferation when Myc is reduced or completely ablated. Even these studies on single organs produce considerably dissimilar results (Table 1). Sanders *et al*. used a model similar to that employed in chapter 4, namely an albumin-driven Cre recombinase which excised the endogenous *myc* gene, flanked by LoxP sites (“floxed”), in a hepatocyte-specific manner. They found there to be no difference in

liver size, weight, architecture or hepatocyte proliferation [87]. Li *et al*. deleted floxed *myc* alleles from the liver in 6 week old mice with adenovirus-driven Cre introduced through tail vein injection, and found deceased proliferation after a partial hepatectomy, but otherwise complete regeneration 7 days [88]. Baena *et al.* used an Mx-Cre deletion induced though pI:pC injections in newborns and in 6 week old mice, resulting in $myc^{FLOX/FLOX}$ excision throughout the liver [89]. They found increased liver:body weight and apoptosis, decreased liver function, and pyknotic nuclei [89]. While Baena *et al*. observed a decrease in hepatocyte size, Li *et al*. reported an increase and Sanders *et al*. found no change. All of these models do have some things in common: 1) none found any compensation by Myc family members N-Myc or L-Myc; and 2) they all made use of 2/3rd partial hepatectomy, to drive proliferation and increase stress in the liver. However, in order to replace the lost tissue (typically ~70% of the entire hepatic mass), the remaining hepatocytes need undergo only ~1.5 cell divisions, which is not very stringent proliferative stress.

Table 1: Summary of papers published on Myc's role in liver regeneration

	Baena (2005) - c-Myc regulates cell size and ploidy but is not essential for postnatal proliferation in liver	**Li (2006) - Conditional Deletion of c-myc Does Not Impair Liver Regeneration**	**Sanders (2012) - Postnatal liver growth and regeneration are independent of c-myc in a mouse model of conditional hepatic c-myc deletion.**
Method of Myc deletion	endogenous myc gene with loxP sites crossed with mx-cre mice Four polyinosinic: polycytidylic acid i.p. injections deletion induced 2 days after birth or at 6 weeks for PH	endogenous myc gene with loxP sites adenovirus-driven Cre recombinase tail vein injections All experiments were performed on mice ~6 weeks	endogenous myc gene with loxP sites albumin-driven Cre recombinase hepatocyte specific 8-10 week old mice were used for regeneration experiments
Liver weight			No difference

Body weight	decreased (10wk)		
Liver/body weight	Increased	no difference	No difference
PH- liver/carcass weight ratio		no difference (2 and 7 days), difference at 5 days post	No difference
Liver architecture	disorganized parenchyma	disorganized	No difference
Cell size - Hepatocyte	decreased - 10day and 10wk	enlarged, also enlarged post HP	
Hepatocytes/field	Increased	decreased (7days post HP), no difference (2days post HP)	
Proliferation of hepatocytes	BrdU increased-6wk, however no major difference	no difference	
PH - hepatocyte proliferation	decreased (PCNA - 48h)	decreased - day 7	slight decrease (48h post; Ki-67 +ve), not significant
Nuclei	Pyknotic	enlarged	
Polyploidy	decreased - 10 wk	increase - 4N hepatocytes, decrease - 2N, no change in 8N	
Binucleated cells	Decreased		
Apoptosis	increased- 10day and 10wk (TUNEL)		
Levels of Myc/ Myc-related proteins	No difference (n-myc, l-myc, b-myc, max, mad, mxi, mad3, mad4, mnt)	no change (l-myc, n-myc)	no change (L-myc, b-Myc, Max; n-myc below detection level)
Oxidaive Status of hepatocytes	increased 10day and 10wk (DCFH-DA)		
Conclusions	Liver regeneration is compromised 2 days post PH c-Myc required for polyploidy in hepatocytes C-myc regulates cell size and number in liver	Liver regeneration after PH within 7 days	c-Myc not required for hepatocyte proliferation and protein synthesis in liver

Our goal in chapter 4 is to clarify Myc's necessity in adult hepatocyte proliferation using a much more demanding model of repopulation – a mouse model of hereditary tyrosinemia where the recipient *fah*-deficient cells slowly die while Myc WT or KO donor hepatocytes repopulate the existing liver architecture. To further characterize the proliferating hepatocyte, we

examine Oxphos and biosynthetic capacity, which may be reduced in the absence of Myc signaling. Additionally, the consequences of proliferative stress are evaluated in terms of lipid accumulation and oxidative or inflammatory stress, which was briefly characterized in chapter 2. In vivo, the large accumulation of lipids in the liver may result in a disease similar to non-alcoholic fatty liver disease, which is characterized by steatosis, increased inflammation and fibrosis[90].

2.0 C-MYC PROGRAMS FATTY ACID METABOLISM AND DICTATES ACETYL COA ABUNDANCE AND FATE

2.1 INTRODUCTION

Cells dividing rapidly in response to normal or oncogenic signals have metabolic profiles distinct from those of their quiescent counterparts. Because they must coordinate mass accretion and division, they devote considerable resources to generating macromolecular precursors [19, 26]. To support these processes, they must also be equipped to generate large amounts of ATP, usually by increasing glucose and glutamine utilization by the TCA cycle [91]. Given this increased demand for energy and the fact that many of the macromolecular precursors originate from glycolytic and TCA cycle intermediates [19, 26], dividing cells undergo a process of metabolic re-programming whereby the shunting of these intermediates into anabolic pathways assumes a more prominent role than during quiescence. An example of this occurs with the Warburg effect whereby glycolysis, normally utilized by resting cells to generate ATP anaerobically, continues to function aerobically to supply certain essential amino acids, nucleotides and pentose sugars for macromolecular bio-synthesis [19, 91, 92].

The dependence of dividing cells on the Warburg effect has occasionally been misconstrued as indicating that they minimize energy production via oxidative phosphorylation (Oxphos). In fact, provided sufficient oxygen, both glycolysis and Oxphos are often concurrently

increased in tumor cells [93, 94]. A particularly instructive example of this occurs with Myc oncoprotein de-regulation which, in addition to stimulating glycolysis, also increases mitochondrial mass, Oxphos and electron transport chain (ETC) function [4, 95]. Although basal ATP levels do not change, its half-life is shortened [4] and likely reflects its increased utilization for anabolic processes. In contrast, Myc-deficient cells, such as *myc*-/- rat fibroblasts (KO cells) [95], have dramatically lower ATP levels and turnover that correlate with reduced glycolysis, Oxphos, replication and cell mass relative to their *myc*+/+ wild-type (WT) counterparts or to KO cells whose Myc expression is restored (KO-Myc cells) [4]. The mitochondrial changes documented in KO cells include an overall paucity of these organelles, atrophy of those which remain and structural and functional ETC defects [4, 95].

The enhanced utilization of glucose and glutamine that accompanies Myc over-expression correlates with increased uptake of these substrates and their consumption in the glycolytic pathway and TCA cycle, respectively. Myc positively regulates a majority of glycolytic enzymes and increases glutamine's conversion to glutamate and α-ketoglutarate by both transcriptional and post-transcriptional mechanisms [37, 91, 92].

Another highly efficient energy source derives from mitochondrial fatty acid β-oxidation (FAO), which, like glycolysis, yields acetyl CoA, the entry-level TCA cycle substrate. During proliferation, acetyl CoA's immediate downstream product, citrate, can also be converted back to acetyl CoA in the cytoplasm where, in ATP-consuming processes, it can be used for *de novo* lipid or steroid bio-synthesis [68, 96]. While considerable effort has been devoted to delineating the means by which glucose and glutamine metabolism are regulated by Myc [37, 91, 92], our understanding of how Myc supervises the transport, directionality and metabolism of fatty acids and their catabolites remains incomplete. In the current work, we have studied how WT, KO and

KO-Myc rat fibroblasts differ in this regard. Our studies indicate that, in an apparent effort to compensate for their ATP deficit and poor utilization of glucose and glutamine as energy-generating substrates, KO cells preferentially transport and oxidize long chain fatty acids (LCFAs) such as palmitate. The channeling of LCFAs into the TCA cycle is facilitated not only by the up-regulation of enzymes involved in their transport and β-oxidation but also by a concurrent down-regulation of acetyl CoA consumption for anabolic purposes. Because KO cells oxidize LCFAs more rapidly, their rate of incorporation into neutral lipids is lower than that of WT or KO-Myc cells. These latter cells utilize their neutral lipid stores for anabolic purposes to a greater extent, while KO cells eventually accumulate a higher stored neutral lipid content. Similar studies, which traced the fate of the freely diffusible medium chain fatty acid (MCFA) octanoate and the two carbon molecule acetate indicated that their metabolism was also altered to maximize their conversion to acetyl CoA. The importance of acetyl CoA as a critical metabolic intermediate that links these opposing functions was further underscored by demonstrating that its supply is also regulated by additional Myc-dependent enzymes including pyruvate dehydrogenase (PDH), which converts pyruvate to acetyl CoA; acetyl CoA acetyltransferase (Acat1/2), which participates in FAO and directs the catabolism of certain amino acids into acetyl CoA, and acetyl CoA synthase 2 (AceCS2) and cytoplasmic acetyl CoA hydrolase (cACH), which regulate the balance between acetate and acetyl CoA. Despite these compensatory changes, KO cells remained profoundly depleted of acetyl CoA. Collectively, these studies identify adaptive pathways through which exogenous fatty acid substrates, ranging from LCFAs to simple two carbon units, can be converted to acetyl CoA, which in KO cells is then preferentially directed toward replenishing ATP. KO cells resort to multiple strategies to correct their acetyl CoA and ATP deficits. These include generating acetyl CoA from multiple

sources, redirecting it into an otherwise compromised TCA cycle, and minimizing its use for purposes other than ATP generation.

2.2 RESULTS

2.2.1 Uptake and oxidation of fatty acids by KO cells

To quantify fatty acid utilization among WT, KO and KO-Myc cells, we exposed them to ^{14}C-radio-labeled palmitate or ^{14}C-octanoate as representative long- and short-medium chain fatty acids, respectively [97, 98]. In each case, the ^{14}C tag resided on the carboxylic acid moiety, which allowed us to test the integrity and interdependence of at least seven distinct enzymatic steps in the β-oxidation pathway. These include the placement of the trans-double bond between C2 and C3 by very long- or medium-chain acyl CoA dehydrogenase , the production of L-B-hydroxyacyl CoA by enoyl CoA hydratase, the conversion of L-B-hydroxyacyl CoA to B-ketoacyl CoA by B-hydroxyacyl CoA dehydrogenase and thiolysis between C2 and C3 of B-ketoacyl CoA to produce acetyl CoA. Upon entry into the TCA cycle, ^{14}C-tagged acetyl CoA would need to be conjugated with oxaloacetate before eventually surrendering its tag as CO_2 during the conversion of isocitrate to α-ketoglutarate. Importantly, LCFA oxidation is also dependent on the rate at which the substrate is actively transported across the plasma and mitochondrial membranes and into the mitochondrial matrix [99]. These steps may not necessarily parallel CO_2 production given that LCFAs can also be stored cytoplasmically as neutral lipids or utilized for anabolic rather than catabolic purposes. MCFAs can be utilized

similarly although they enter mitochondria passively without contributing to neutral lipid pools [47, 99]. Thus, differences in MCFA uptake should better reflect the rate of β-oxidation. As seen in Fig. 3*A*, the rate of ^{14}C-palmitate oxidation was similar in WT and KO-Myc cells after adjusting for differences in mitochondrial mass ($p=0.58$), but was nearly 25-fold higher in KO cells ($p<0.0001$). Similar studies performed with ^{14}C-octanoate (Fig. 3*B*) also showed a >5-fold higher rate of β-oxidation in KO cells. Thus, despite their markedly slower proliferation and their reduced mitochondrial function, KO cells actually utilize a larger amount of LCFAs and MCFAs for energy generation than do their Myc-replete counterparts.

We next asked whether the observed differences in FAO among the above three cell lines were associated with differences in their fatty acid uptake rates. As seen in Fig. 3*C*, ^{14}C-palmitate uptake was highest in KO cells, in keeping with their overall greater utilization of this substrate for FAO. A higher rate of ^{14}C-octanoate uptake by KO-Myc cells was also consistent with their preferential utilization of this substrate for processes other than FAO (Fig. 3*C*). Interestingly, WT and KO-Myc cells showed distinct preferences for LCFAs and MCFAs, with the former cells demonstrating a greater uptake of palmitate than octanoate whereas the reverse was true for KO-Myc cells. Thus, KO cells have a selective uptake for both LCFAs and MCFAs and utilize them more efficiently as FAO substrates. However, each cell line possesses a distinct pattern of LCFA and MCFA uptake that presumably reflects differential usage for processes other than FAO.

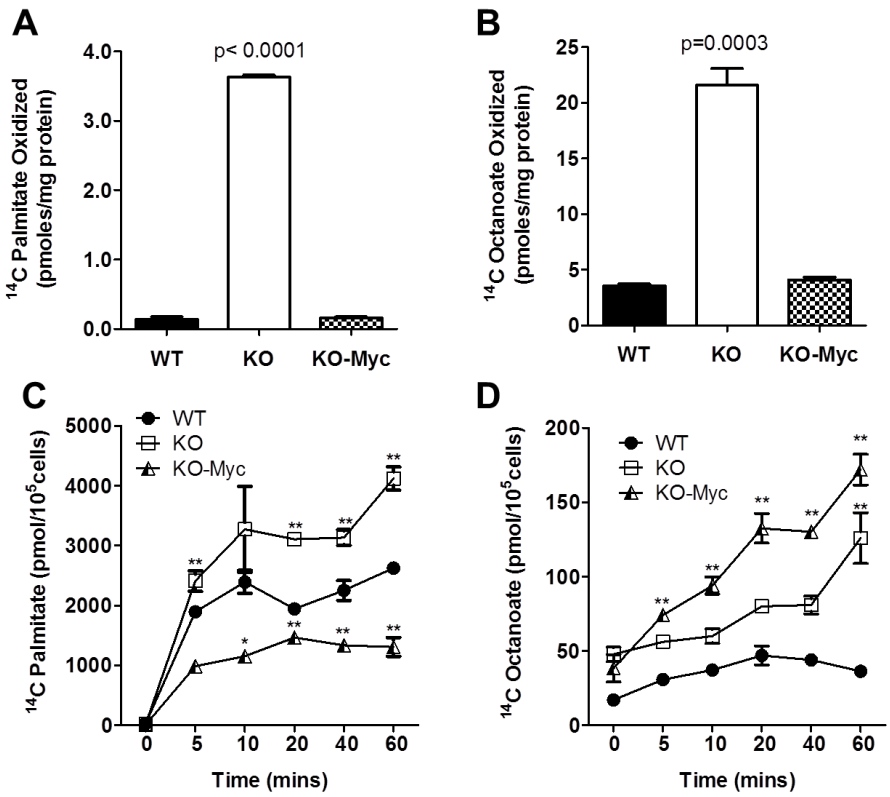

Figure 3: Differential utilization and uptake of LCFAs and MCFAs by WT, KO and KO-Myc cells. (A) β-oxidation of 14C-palmitate. (B) β-oxidation of 14C-octanoate. (C) Uptake of 14C-palmitate. (D) Uptake of 14C-octanoate. Each point represents the mean of triplicate determinations +/- 1 S.E.M. p values are expressed relative to WT cells (*=p<0.05, **=p<0.001)

2.2.2 Differential utilization of fatty acids

The initial stage of FAO involves the iterative insertion of a trans double bond between the C2 and C3 carbon atoms of the acyl CoA thioester substrate in a reaction that, for palmitate, is catalyzed by very long-chain acyl CoA dehydrogenase (ACADVL) and, for octanoate, by medium-chain acyl CoA dehydrogenases (ACADM) [100]. To determine whether the preferential utilization of palmitate and octanoate for FAO by KO cells could be explained by

differences in these enzymes, we measured their activities [101]. As seen in Fig. 4*A* and *B*, both ACADVL and ACADM activities were increased significantly in KO cells after adjusting to mitochondrial mass, thus providing an explanation for their more efficient utilization of these substrates.

The foregoing studies were designed to evaluate the fate of fatty acids as energy-generating catabolic substrates but did not explain how the acetyl CoA generated from their catabolism was utilized for anabolic purposes. To address this, we labeled the cell lines with ^{3}H-palmitate and followed the incorporation of its tag into both phospho- and neutral lipid pools [98]. Because octanoate is not incorporated into neutral lipids, we measured the transfer of its ^{14}C-tag into phospholipids only. The rate of incorporation of the ^{3}H tag of palmitate into both neutral lipids (Fig. 4*C*) and phospholipids (Fig. 4*D*) and the ^{14}C-octanoate tag into phospholipids (Fig. 4*E*) was significantly lower in KO cells.

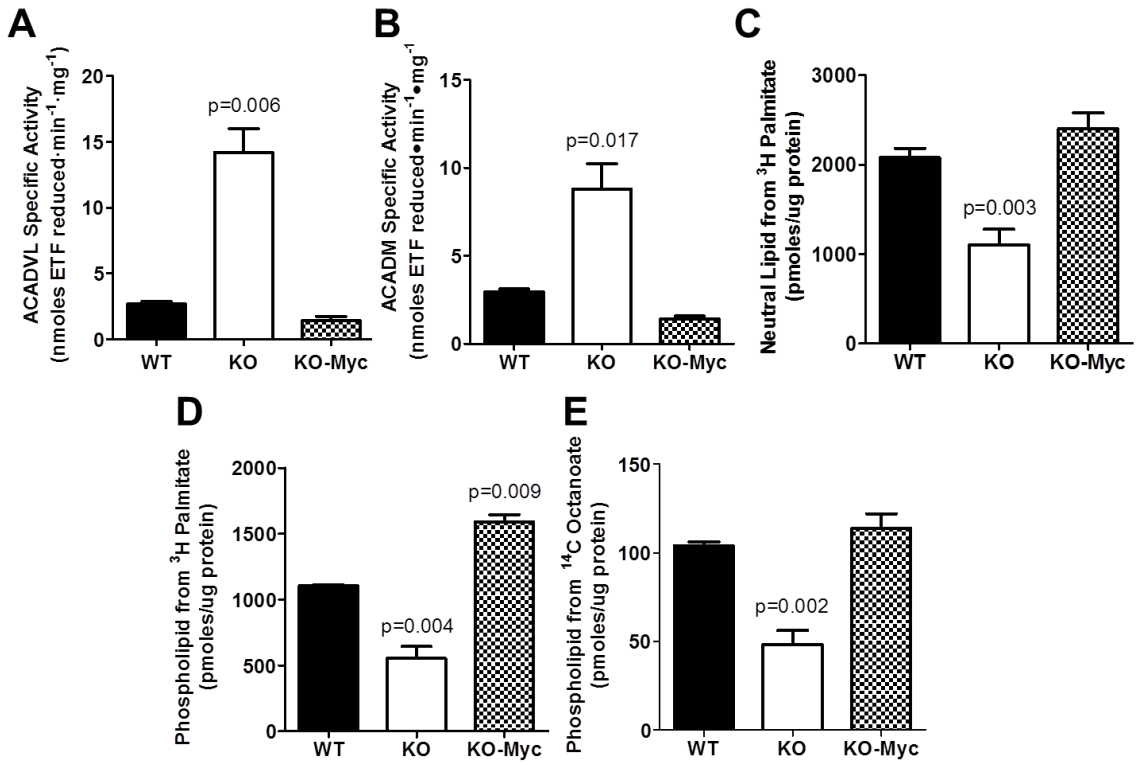

Figure 4: ETF assays for ACADVL and ACADM activities and incorporation of LCFAs and MCFAs into neutral and phospholipids in WT, KO and KO-Myc cells. (*A*) ACADVL enzymatic activity. Mean values are depicted +/- 1 S.E.M. Results were normalized to account for differences in mitochondrial mass among the three cell types[4]. (*B*) ACADM activity. Results are presented as described for *A*. (*C*) Incorporation of 3H-palmitate into neutral lipids. (*D*) Incorporation 3H-palmitate of into phospholipids. (*E*) Incorporation of 14C-octanoate into phospholipids.

2.2.3 Neutral Lipid Accumulation in KO cells

Previous studies have shown that N-Myc inhibition in neuroblastoma cells increases their neutral lipid content [69]. We therefore next asked whether fatty acid uptake and utilization were balanced by assessing differences in basal neutral lipid content. Each cell line was stained with the neutral lipid-specific probe BODIPY-493/503 and visualized by fluorescence microscopy to

assess its neutral lipid content. WT and KO-Myc cells demonstrated low-level accumulation of BODIPY-493/503 in contrast to KO cells in which considerable amounts of the dye could be detected (Fig. 5*A* and *B*). In other experiments, we confirmed the presence of excess neutral lipid staining in KO cells by Oil Red O staining (Fig. 5*C*). Using two different approaches, we confirmed that the accumulation of neutral lipids was a direct and rapid consequence of Myc inactivation. First, treatment of WT cells with the Myc inhibitor 10058-F4 [102] significantly increased BODIPY-493/503 uptake (Fig. 5*D*). Additionally, reduction of Myc protein levels in A549 human lung cancer cells using tetracycline-dependent conditional expression of a Myc shRNA produced a similar result (Fig. 5*E* and *F*). Collectively, these findings support the idea that neutral lipid accumulation in KO cells is a direct consequence of Myc depletion and mitochondrial dysfunction.

To better define the relationship between fatty acid transport and metabolism and the generation and utilization of acetyl CoA, we utilized real-time qRT-PCR to quantify transcripts encoding the enzymes described above plus select others to allow an overview of the activity of relevant pathways (Fig. 6*A*). Transcripts were grouped into six functional categories representing fatty acid transport and FAO, *de novo* lipid and steroid biosynthesis, neutral lipid storage and the generation of acetyl CoA from acetate and pyruvate. This last category included transcripts for the pyruvate dehydrogenase (PDH) E1 subunit and its regulators, pyruvate dehydrogenase kinase 1 (PDK1) and pyruvate dehydrogenase phosphatase 2 (PDP2), which are responsible for the phosphorylation-dependent inactivation and activation, respectively, of E1 [103]. Also included were transcripts for pyruvate carboxylase (PC) which catalyzes an anaplerotic reaction important for gluconeogenesis and lipid biosynthesis and irreversibly re-directs pyruvate to oxaloacetate to

limit the former's conversion to acetyl CoA [104]. We also examined transcripts for the pyruvate kinase isoforms PKM1 and PKM2, which catalyze the irreversible conversion of phosphoenolpyruvate (PEP) to pyruvate during glycolysis. PKM2 is typically more abundant in rapidly proliferating cells and has a significantly higher Km for PEP [105, 106]. This may better allow for the accumulation of upstream glycolytic intermediates, thus facilitating their channeling into collateral, anabolic pathways in support of proliferation-associated mass accretion [106, 107]. Consistent with this idea, the activity of PKM2 is subject to negative regulatory control by ATP and possibly by acetyl CoA as well [21, 26, 105].

The results of transcriptional profiling (Fig. 6*B*) were largely consistent with our foregoing studies. First, they indicated that KO cells up-regulate transcripts encoding enzymes involved in the production of acetyl CoA for energy generation while down-regulating those involved in anabolism such as *de novo* lipid and steroid biosynthesis (Fig. 6*A*). One example of the potential precision of this re-programming in KO cells was seen in the case of the 5-fold change in the relative ratio of acetyl CoA carboxylase 1 and 2 isoforms (ACC1 and ACC2), which function in fatty acid synthesis and β-oxidation, respectively [108]. Also notably up-regulated in KO cells were several transcripts such as phosphatidic acid phosphatase types 2b and c (Ppap2b and Ppap2c) and diacylglycerol acyltransferase 1 (Dgat1), which encode key enzymes involved in the shunting of fatty acids into neutral lipid storage pools [109, 110].

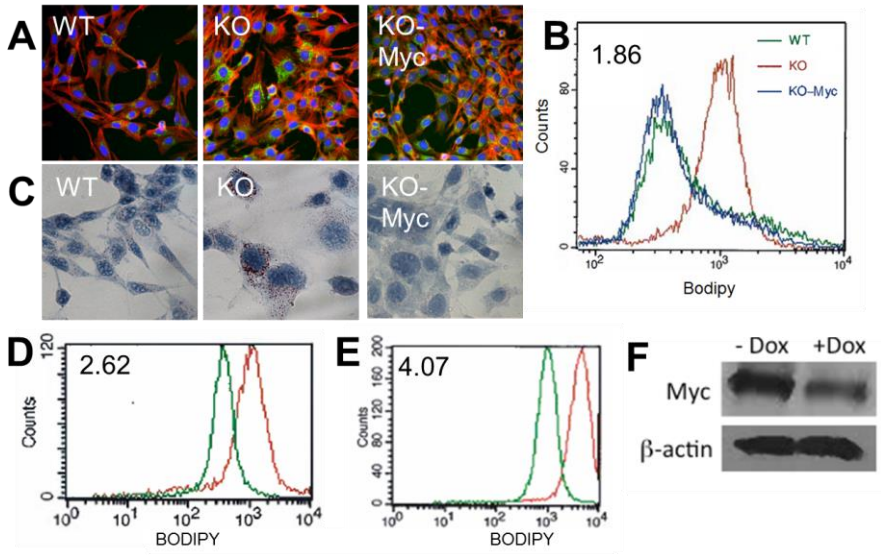

Figure 5: Neutral Lipid Accumulation in KO cells. (*A*) Staining of cells for neutral lipids. WT, KO and KO-Myc cells were plated onto glass microscope slides and allowed to grow to sub-confluency before being fixed and stained with BODIPY-493/503 and counter-stained with Texas red-labeled phalloidin and DAPI. Representative fields are shown. (*B*) Quantification of neutral lipid staining. Each of the indicated cell types was stained with BODIPY-493/503 and assessed by flow cytometry. (*C*) Oil Red O staining. Each of the indicated cell types were plated as in (*A*), and stained with Oil Red O. (*D*) 10058-F4-mediated inhibition of endogenous Myc leads to the accumulation of neutral lipids. WT cells in log-phase growth were exposed to 50 µM 10058-F4 (22) for 48 hr before being stained with BIODIPY-493/503 and assessed by flow cytometry. The number in the upper left corner is the ratio of the mean intensity of staining of cells with (red) and without (green) 10058-F4 exposure. (*E*) Induction of shMyc in A549 cells leads to neutral lipid accumulation. A549 cells (ca. 10% confluency) were allowed to grow for an additional 3 days in the absence (green) or presence (red) of 2.5 µg/ml Doxycline (Dox) before being stained with BODIPY-493/503 as described for (*B*). (*F*) Immunoblots demonstrating a reduction in endogenous Myc protein levels following a 3 day exposure to

2.2.4 AMPK is Myc-responsive

Some of the above-discussed enzymes are regulated post-translationally by AMP-dependent protein kinase (AMPK), a serine/threonine kinase that is itself activated by phosphorylation in response to low ATP/(AMP+ADP) ratios [74]. A role for AMPK in maintaining adenosine nucleotide homeostasis stems from its inhibition of ATP-consuming processes such as macromolecular synthesis and cell proliferation along with its stimulation of ATP-generating reactions such as glycolysis and Oxphos [111]. Among the enzymes depicted in Fig. 6 whose activities are down-regulated by AMPK-mediated phosphorylation are ACC1, which catalyzes the conversion of acetyl CoA to malonyl CoA in the initial step of fatty acid synthesis; fatty acid synthase (FASN), which converts malonyl CoA into palmitate; and HMG-CoA reductase (HMGCR), the rate-limiting step in the biosynthesis of cholesterol and other steroids [111]. AMPK-mediated phosphoryl-ation of the palmitate cell surface receptor CD36 has also been reported to increase its rate of cycling between the cell membrane and intracellular compartments thereby affecting the normal balance between FAO and lipid accumulation in favor of the latter [112, 113]. Finally, although not known to be a direct AMPK target, carnitine palmitoyltransferase I (CPT1) is suppressed by malonyl CoA, such that ACC1 inhibition by AMPK would likely increase FAO [114].

To determine whether the altered metabolic pathways of KO cells might be susceptible to post-translational modulation by AMPK, we compared the levels of total and active (Thr_{172}-phosphorylated) forms of AMPK in WT, KO and KO-Myc cells. KO cells showed marked constitutive Thr_{172} phosphorylation as well as increased total AMPK levels (Fig. 6*C*). These

findings are in keeping with the profound ATP deficit of KO cells [4] and suggest that, despite AMPK's constitutive activation, it is unable to correct the energy deficit.

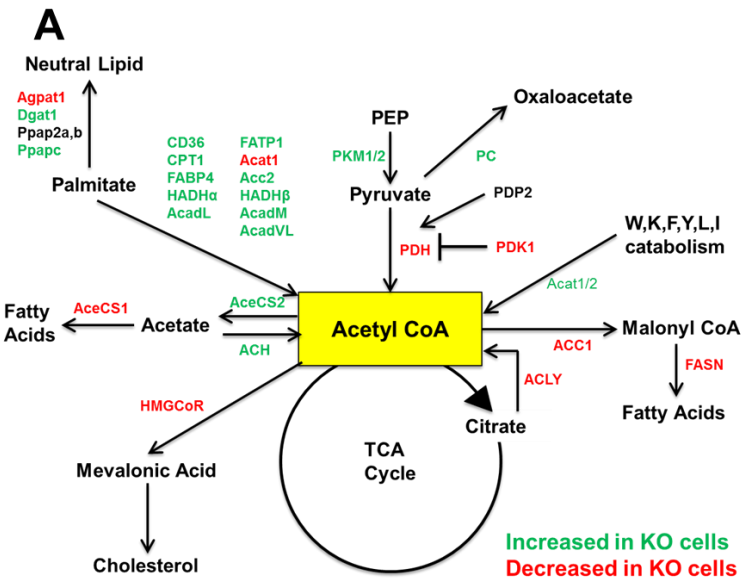

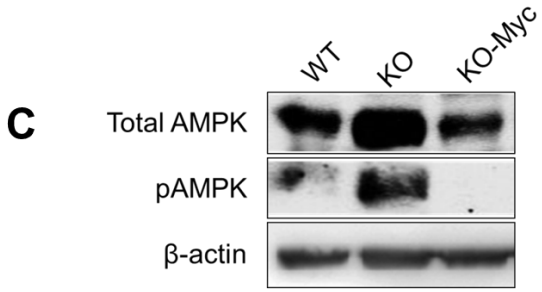

		WT	KO	KO-MYC
FA Transport	CD36	1.0	11.1	43.3
	CPT1	1.0	3.8	0.5
	FABP4	1.0	2.7	0.0
	FATP1 (Scl271a	1.0	1.9	0.7
FA Oxidation	Acat1	1.0	0.7	2.0
	HADHa	1.0	1.8	0.5
	HADHb	1.0	1.7	0.6
	ACADL	1.0	1.8	1.5
	ACADM	1.0	1.4	0.5
	ACADVL	1.0	1.9	0.9
Lipid/ cholesterol Synthesis	ACC1	1.0	0.3	0.7
	ACC2	1.0	1.5	1.7
	ACLY	1.0	0.6	2.3
	FASN	1.0	0.3	2.0
	Agpat1	1.0	0.1	1.1
NL storage	Dgat1	1.0	2.4	0.8
	Gpat1 (Gpam)	1.0	5.5	1.8
	Ppap2a	1.0	1.0	2.5
	Ppap2b	1.0	1.0	1.2
	Ppap2c	1.0	5.8	24.7
	HMGCR	1.0	0.6	2.3
Pyruvate → Acetyl CoA Conversion	PC	1.0	1.8	1.7
	PDH (Pdha1)	1.0	0.7	1.2
	PDK1	1.0	0.5	60.3
	PDP2	1.0	0.9	0.2
	PKM1	1.0	1.6	0.8
	PKM2	1.0	1.5	0.7
Acetate → AcCoA Conversion	AceCS1	1.0	0.6	1.4
	AceCS2	1.0	36.6	0.3
	cACH (Acot12)	1.0	4.5	0.5

Figure 6: Alteration of metabolic pathways in KO cells. (*A*) Pathways depicting the generation and utilization of acetyl CoA in KO cells. The major sources of mitochondrial acetyl CoA include the glycolytic intermediate pyruvate; long and medium chain fatty acids such as palmitate and octanoate; acetate and a subset of amino acids that includes tryptophan, lysine, phenylalanine, tyrosine, leucine and isoleucine. Cytoplasmic acetyl CoA can also be generated from the mitochondrial TCA substrate citrate in a reaction involving ACLY and from acetate by AceCS2. Acetyl CoA's fate in pathways other than the TCA cycle primarily include its conversion to malonyl CoA during fatty acid synthesis. In addition, pyruvate, the direct glycolytic precursor of acetyl CoA, can be diverted from this pathway by an anaplerotic reaction involving its conversion to oxaloacetate that is catalyzed by pyruvate carboxylase (PC) and palmitate can be diverted into neutral lipids. The activity of pyruvate dehydrogenase (PDH), which catalyzes the conversion of pyruvate to acetyl CoA is also negatively regulated by pyruvate dehydrogenase kinase1 (PDK1) and positively regulated by pyruvate dehydrogenase phosphatase 2 (PDP2). Based on transcriptional profiling shown in (*B*), enzymes whose transcripts are up-regulated in KO cells are depicted in green and those which are down-regulated are depicted in red. (*B*) Transcript expression. For simplicity, transcripts and proteins are designated by common acronyms. Transcripts that were significantly up-regulated in KO cells are indicated in green and those that are down-regulated are depicted in red. The values of transcripts in WT cells were arbitrarily set at 1 (black). Transcripts are arranged according to the functional categories of their representative enzymes. Each value represents the mean of triplicate determinations for each transcript. (*C*) AMPK is up-regulated in KO cells. Immunoblots of total cell lysates from WT, KO and KO-Myc cells were probed with antibodies for total AMPK or phospho-AMPK (pThr172).

2.2.5 KO cells maximize their accumulation of acetyl CoA by increasing its production and decreasing its utilization for purposes other than TCA cycle utilization

The E1 subunit of the mitochondrial PDH complex catalyzes pyruvate decarboxylation, which is the first and rate-limiting step in its irreversible conversion to acetyl CoA (Fig. 7*A*) [115]. In addition to its regulation by PDK1 and PDP2 [103, 116, 117], PDHE1 is under additional negative feedback control by acetyl CoA and positive control by ATP by virtue of the latter's inhibitory effect on PDP2 [118]. Furthermore, ATP and ADP exert positive and negative control, respectively, over PDK1 (Fig. 7*A*). Although the transcripts encoding these proteins were modestly down-regulated in KO cells (Fig. 7*B*), the complexity of PDHE1 post-translational regulation demanded that we actually measure its activity and thereby gauge the overall extent to which it was subject to control by these various and often opposing regulatory factors. As shown in Fig. 7*B*, KO cells contained ca. 8 times as much PDH activity as WT and KO-Myc cells. Although immunoblotting showed modest differences in PDHE1 protein levels among the three cell lines (Fig. 7*C*), it demonstrated more dramatically, in both KO and KO-Myc cells, the relative under-phosphorylation of PDHE1 on Ser_{293}, the site whose modification by PDK1 and PDP2 most affects its activity [74]. Further consistent with the increased PDH activity in KO cells was their higher levels of PDP2 relative to WT cells. In contrast, no differences in the levels of PDK1 were observed between WT and KO cells. Although KO-Myc cells contained nearly 5-fold lower levels of PDP2 transcripts than WT cells and 60-fold higher levels of PDK1 transcripts (Fig. 6*B*), this was not reflected in PDH activity (Fig. 7*B*).

Another source of acetyl CoA is acetate, which, in the whole animal, is typically supplied by bacterial fermentation in the colon, by the metabolic breakdown of acetaldehyde and by the action of enzymes such as sirtuins and histone deacetylases [119]. Like octanoate, acetate is both freely diffusible and readily available for metabolism in both the cytosol and mitochondria. Consistent with the notion that KO cells attempt unsuccessfully to normalize acetyl CoA levels, we note that AceCS2 transcript levels were elevated by nearly 40-fold in KO cells whereas those for AceCS1 were modestly decreased (Fig. 6*B*). AceCS2, a mitochondrial enzyme, converts acetate to acetyl CoA for utilization by the TCA cycle whereas AceCS1, which is cytoplasmic, is more important for fatty acid synthesis [120]. Thus, the >60-fold changes in the AceCS1:AceCS2 ratio described above would be expected to greatly favor acetate conversion into acetyl CoA in the mitochondria. Further consistent with, and perhaps contributing to, the reduced utilization of acetate for fatty acid synthetic pathways was the finding that transcripts for cACH, which converts acetyl CoA back to acetate in the cytoplasm [121], were increased 4.5-fold in KO cells. Indeed, when cells were incubated with ^{14}C-acetate, KO cells incorporated the least amount of ^{14}C-tag, particularly into phospholipids (Fig. 7*D* and *E*).

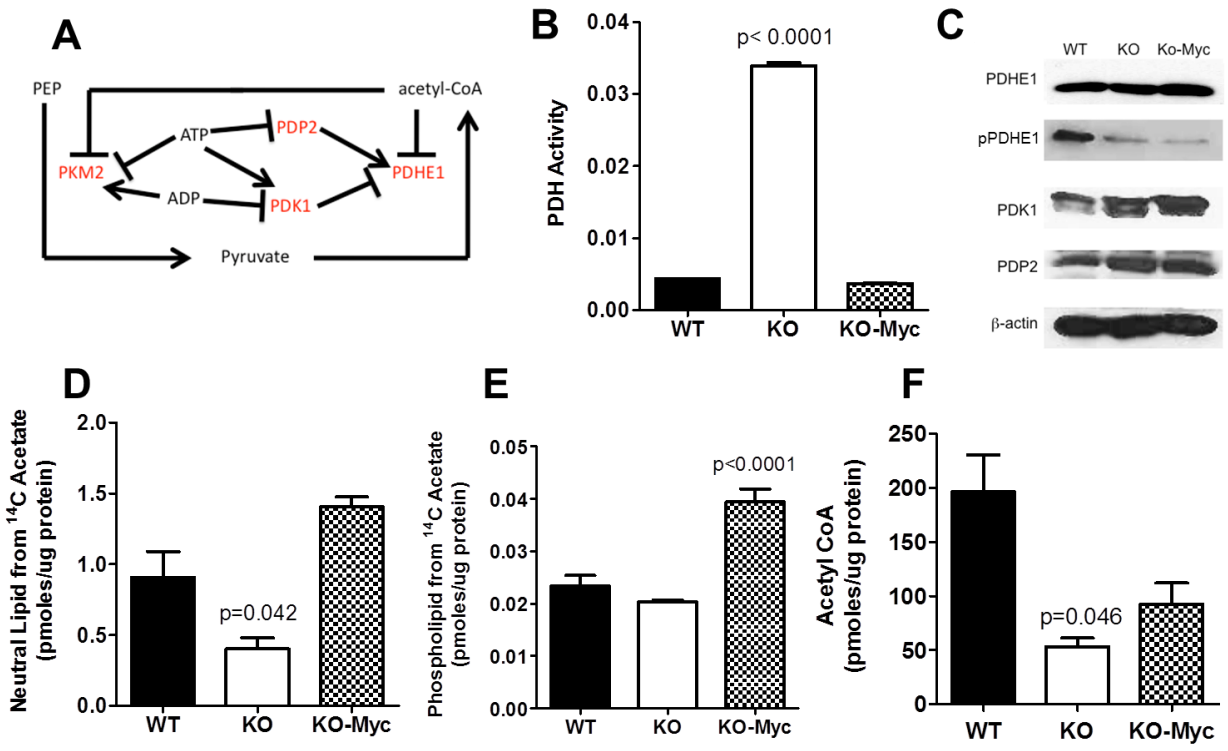

Figure 7: Myc-regulated control of acetyl CoA generation from pyruvate. (*A*) Outline of the reaction and its regulatory network. The E1 subunit of the mitochondrial PDH complex is subject to negative feedback inhibition by acetyl CoA and to enzymatic regulation by the inhibitory kinase PDK1 and the stimulatory phosphatase PDP2 via Ser293 phosphorylation on the E1 subunit of PDH. PDK1 is subject to additional positive control by ATP and to negative control by ADP, whereas PDP2 is subject to negative control by ATP. In addition, the PKM2 isoform, which is less efficient at converting PEP to pyruvate, is under positive regulatory control by ADP and negative regulatory control by ATP and acetyl CoA. (*B*) PDH activity in WT, KO and KO-Myc cells after adjusting for differences in mitochondrial mass. (*C*) Immunoblots for PDHE1, phospho(Ser293)-PDHE1 (pPDHE1), PDK1 and PDP2. A β-actin blot was included as a protein loading control. (*D*) and (*E*), Acetate incorporation in neutral lipids and phospholipids, respectively. (*F*) Total acetyl CoA levels in WT, KO and KO-Myc cells. Each point represents the mean of quadruplicate determinations +/- 1 S.E.M.

Finally, we measured steady-state levels of acetyl CoA. As seen in Fig. 7*F*, both KO and KO-Myc cells contained reduced levels of acetyl CoA relative to WT cells, although the latter did not reach statistical significance. Together with the previous results (Fig. 6*B*), these findings are most compatible with the idea that KO cell metabolism is directed primarily at maximizing the generation of acetyl CoA for use by the TCA cycle and minimizing its utilization for anabolic reactions. Despite maximal efforts to produce more acetyl CoA, KO cells remain unable to maintain normal levels of this substrate.

2.3 DISCUSSION

Numerous studies support the idea that Myc's importance in promoting cell proliferation derives in part from its ability to ensure the provision of adequate supplies of anabolic substrates and ATP to support macromolecular syntheses [19, 24, 37, 91, 92]. Myc's silencing is associated with numerous metabolic and proliferative consequences that ultimately can be traced to defects in glycolysis and mitochondrial structure and function [4, 17, 122]. That these factors are rate-limiting for proliferation is supported by findings shown here and elsewhere that, even when provided with adequate energy-generating substrates such as glucose, glutamine and fatty acids, KO cells remain chronically ATP-depleted and respond by activating AMPK in a futile attempt to remedy this energy deficit (Fig. 6*C*). However, because two of the major responses to AMPK activation include the up-regulation of glycolysis and Oxphos, both of which are Myc-dependent [4, 74, 91, 92], the AMPK response is ultimately abortive despite its chronicity.

KO cells respond to their ATP deficit by up-regulating FAO and many of the transcripts associated with LCFA uptake, transport and metabolism (Fig. 6*A* and *B*). Palmitate oxidation, which begins with ACADVL, is further enabled by the high activity of this enzyme in KO cell mitochondria. Thus, despite their reduced overall mass, atrophic structure and relatively poor utilization of substrates such as glucose and glutamine [4, 17], KO cell mitochondria disproportionately oxidize LCFAs. They also contain higher ACADM activity and preferentially oxidize octanoate whose transport into cells and mitochondria, unlike that of palmitate, is passive.

Importantly, the transcriptional profiles depicted in Fig. 6*B* represent steady state levels in otherwise isogenic cells that have adapted to long-term differences in Myc expression and have distinct metabolic behaviors [95]. While these differences may not necessarily reflect "direct" Myc targets [123, 124], they are nonetheless useful in that they reveal long-term strategies employed by Myc-compromised cells to compensate for their inherent metabolic disadvantages. In this regard AMPK, whose level of activation is clearly inversely related to Myc levels (Fig. 7*C*), is a well-known regulator of many of the same process controlled by Myc such as FAO, fatty acid synthesis, glycolysis and Oxphos [74]. However, since the ultimate metabolic function of Myc is to increase ATP synthesis in support of anabolism and proliferation [4] whereas AMPK's function is to conserve energy until the ATP:ADP/AMP balance is restored, the integrated effects we observe based on steady state transcripts may reflect a metabolic compromise between these opposing actions [79].

In a seemingly paradoxical finding, KO cells were found to possess the highest stores of neutral lipids (Fig. 5*A*-*C*) despite incorporating the least amount of ^{3}H-palmitate into this

compartment (Fig. 4*C*). This latter finding is likely attributable to the fact that a large proportion of palmitate entering KO cells is immediately utilized for FAO (Fig. 3*A*) whereas in Myc-replete cells, larger amounts of the fatty acid are directed into neutral lipid pools (Fig. 4*C*). The extremely slow rate of KO cell proliferation [95] minimizes the need for these neutral lipid pools to serve as sources for phospholipid synthesis. Reduced demand for neutral lipid mobilization thus permits KO cells to accumulate higher neutral lipid stores despite their lower rates of accumulation. In contrast, WT and KO-Myc cells synthesize phospholipids at higher rates (Fig. 4*C*) and thus mobilize neutral lipids much more rapidly for this purpose (Fig. 4*D*) thus preventing their accumulation. The highly dynamic nature of neutral lipid stores is further evidenced by the rapidity with which they accumulate following Myc inhibition (Fig. 5*D* and *E* and [69]).

A major finding of the current study is that KO cells, in addition to deriving a considerable fraction of their acetyl CoA from FAO, also maximize its production from other sources and minimize its utilization for purposes other than energy production. For example, reduced levels of transcripts involved in fatty acid synthesis such as those for ATP citrate lyase (ACLY), ACC1 and FASN support the notion that KO cells minimize their incorporation of acetyl CoA into lipids. That this down-regulation occurs throughout the pathway and involves its most proximal enzyme (ACLY) would seem to favor the retention of citrate within the TCA cycle to ensure its utilization for Oxphos. Further consistent with this was the finding that ACC2, proposed to be more important than ACC1 for FAO [108], was up-regulated in KO cells, whereas ACC1 was down-regulated. High levels of palmitate within KO cells might further inhibit fatty acid synthesis by virtue of the well-known tendency of the substrate to suppress

ACC1 [125]. A similar attempt to direct acetyl CoA away from synthetic pathways was observed with the down-regulation in KO cells of transcripts for HMGCR, the rate-limiting enzyme of the mevalonate pathway [126]. Both ACC1 and HMGCR are also further suppressed by AMPK [74]. The down-regulation of PC also serves indirectly to maximize the availability of pyruvate for conversion into acetyl CoA by diverting it away from the anaplerotic pathway that furnishes oxaloacetate. Other pathways through which acetyl CoA production is maximized are up-regulated in KO cells and include those involving its AceCS2-mediated synthesis directly from acetate and the catabolism of selected amino acids by Acat 1 and 2.

The PDH-mediated conversion of pyruvate to acetyl CoA provides yet another example of how KO cells attempt to selectively utilize acetyl CoA for ATP generation (Fig. 7*A*). This reaction is particularly noteworthy as it illustrates the complex and interdependent regulation that Myc and adenine nucleotides may exert over acetyl CoA levels as well as the negative feedback control that acetyl CoA itself provides. PDH activity, which is increased in KO cells (Fig. 7*B*) is positively controlled by the PDP2 phosphatase and negatively controlled by the PDK1 kinase [103, 115-117]. The net result is PDHE1 de-phosphorylation and activation (Fig. 7*C*). Non-enzymatic control is exerted by the repressive action of acetyl CoA; by ATP, which inhibits PDP2 and stimulates PDK1; and by ADP, which represses PDK1 (Fig.7*A*) [103, 115-117]. Given that the intracellular milieu of KO cells is one in which both acetyl CoA and ATP levels are low, these small molecules likely exert significant additional influence on PDH activity. The relatively normal PDH activity in KO-Myc cells, despite its hypo-phosphorylation, suggests that factors other than those examined here may play additional roles in its regulation [103].

Another factor that might also influence acetyl CoA levels in KO cells is PKM2, whose ability to catalyze the conversion of phosphoenolpyruvate (PEP) to pyruvate is accelerated by ADP and inhibited by ATP and acetyl CoA (Fig. 7*A*) [105, 106, 127]. Because this reaction is one of only three in the entire glycolytic pathway that is irreversible, it provides a relatively stable source of the substrate. It is noteworthy that both PKM2 and PKM1 are equally up-regulated in KO cells in contrast to KO-Myc cells where they are coordinately down-regulated. In the latter case, where ATP generated by Oxphos is already abundant, this may permit PEP and its upstream precursors to accumulate and be diverted into anabolic pathways.

Although both KO and KO-Myc cells have lower levels of acetyl CoA (Fig. 7*F*), the origins and consequences of these deficits are likely quite different. In KO cells, we believe this arises primarily from reduced ability to produce acetyl CoA within atrophic and dysfunctional mitochondrial that reduces the overall acetyl CoA supply, despite an increased in PDH activity as discussed above. In contrast, the acetyl CoA deficiency of KO-Myc cells likely reflects the proliferative strain imposed upon them as they attempt to keep pace with high levels of fatty acid synthesis and high rates of ATP turnover [4]. Thus, the reduced level of acetyl CoA in KO-Myc cells more likely represents the accelerated rate at which this substrate is utilized in contrast to KO cells in which acetyl CoA production is compromised. This suggests that the supply of acetyl CoA may represent a potential proliferative and metabolic bottleneck that might be exploited in a therapeutic setting, particularly in cancers that are Oxphos-dependent.

2.4 EXPERIMENTAL PROCEDURES

2.4.1 Cell culture

All cell lines were routinely maintained as previously described [4]. KO-Myc cells were generated through the use of stable transduction with a lentiviral vector encoding a full-length human Myc cDNA [4]. A549-shMyc cells were generated by infecting A549 human alveolar lung cancer cells with a pTRIPZ lentiviral vector encoding red fluorescent protein and a shRNA directed against human Myc, both of which were tetracycline-inducible (Thermo Fisher, Waltham, MA). All lentiviral packaging and infections were performed as previously described [122] under BSL2+ conditions and were approved by the University of Pittsburgh Biosafety Committee. Stable transfectants were selected and maintained in puromcycin-containing medium (1 µg/ml) as described above.

2.4.2 ^{14}C-palmitate and ^{14}C-octanoate uptake and β-oxidation studies

FAO was quantified as previously described [98]. Briefly, $2x10^4$ WT and KO-Myc cells and $4x10^4$ KO cells (all >90% viable) were seeded into 24-well tissue culture plates and allowed to attach overnight. The following day, medium was removed and the cells were incubated at 37C for 30 min. in PBS. 200 µL of fresh PBS containing 1 mM carnitine (Santa Cruz Biotechnology, Santa Cruz, CA) and 0.2 µCi BSA-bound [1-^{14}C]-palmitate (sp. act. = 32 mCi/mmol), (Perkin-Elmer, Waltham, MA) or 0.1 µCi ^{14}C-octanoate (sp. act. = 55 mCi/mmol), (American Radiolabelled Chemicals, St. Louis, MO) was then added. $^{14}CO_2$ was collected onto filters

soaked in 0.6N KOH which were placed in a collection apparatus made from a 0.4 ml Eppendorf tube and maintained under air-tight seal at 37C for 2 hr [97]. The medium was then acidified by adding 20 µL 6M perchloric acid to release additional dissolved CO_2. Filters were removed after 60 min and released $^{14}CO_2$ was quantified from quadruplicate samples on a Beckman LS6500 scintillation counter. Counts were adjusted so as to normalize for any differences in total protein content among the three groups of cells (generally <10%). p values were calculated using 1-way ANOVA followed by Bonferroni's post-hoc comparisons test. To measure ^{14}C-palmitate and ^{14}C-octanoate uptake, cells were plated as described above the day prior to labeling. Monolayers were washed twice with PBS and then incubated in fresh PBS (200 µL) for 30 min. Fatty acid-free BSA-bound ^{14}C palmitate (0.2 µCi/well) with 1 mM carnitine was incubated for the appropriate time periods. After thorough washing, the cells were lysed in 160 µL 5% SDS and subjected to scintillation counting as described above. Results from triplicate samples were normalized to protein content. All experiments were repeated two additional times with comparable results.

2.4.3 Incorporation of ^{3}H-palmitate, ^{14}C-octanoate and ^{14}C-acetate into lipids

Cells were plated as described for oxidation studies except that tritiated palmitate was utilized [98]. The next day, they were starved for 1 hr in PBS and then labeled for 1 hr in 200 µL of fresh PBS containing 0.5 µCi BSA-bound [9,10-^{3}H(N)]palmitate (sp. act. = 32 mCi/mmol) (Perkin-Elmer, Waltham, MA), ^{14}C-octanoate (0.1 µCi) containing 1 mM carnitine or 0.2 µCi ^{14}C-Na acetate (Perkin-Elmer, sp. act. = 54.3 mCi/mmol). The cells were then washed twice in warm PBS, and fresh PBS with 1 mM carnitine was added for 2 hr. Cells were then lysed with 25 µl

6N KOH and an organic extraction was performed in 1 ml of methanol: chloroform (1:1), which was then removed and dried under nitrogen. After adding ice-cold acetone to the dried lipid film and incubating at -20 C overnight, the phospholipid pellet was separated by centrifugation (14,000 x g, 30 mins at 4C). Both neutral and phospholipids were re-dissolved in 50 µL of chloroform for quantification. The labeled fractions were quantified by scintillation counting as described above. Each assay was performed in triplicate and p values were calculated using 2 way ANOVA followed by Bonferroni's post-hoc comparison.

2.4.4 Enzyme assays

Measurements of very-long and medium chain acyl CoA dehydrogenase activities (ACADVL and ACADM, respectively) in cell-free extracts were performed using the anaerobic electron transfer flavoprotein (ETF) fluorescence reduction assay as previously described [101]. Measurements were performed with a LS50B fluorescence spectrophotometer (Perkin-Elmer, Waltham, MA) with a heated cuvette block set to 32C. One unit of activity was defined as the amount of enzyme necessary to completely reduce 1 µmol of ETF in 1 min. Each assay was performed in duplicate and one-way ANOVA followed by Bonferroni's post-hoc comparisons tests were performed in all statistical analyses. Assay results were adjusted to account for previously determined differences in mitochondrial mass based on staining with 10-n-nonyl-acridine orange (NAO) [4].

PDH activity was quantified using an enzyme activity microplate assay kit (MitoSciences, Eugene, OR). 5 nearly confluent 100 mm plates of cells were harvested by trypsinization, washed twice in PBS, flash frozen in liquid nitrogen and stored at -80 C until

ready to assay. Each assay utilized 1 mg of total cellular protein in 200 µl of the buffer provided by the supplier. The remainder of the assay was completed according to the supplier's protocol.

2.4.5 Visualization and quantification of neutral lipids

Cells were plated in 12 well dishes containing sterile glass coverslips and cultured overnight. They were then washed once in PBS and stained with Bodipy-493/503 Neutral Lipid stain (Molecular Probes/Thermo-Fisher: final concentration = 10 µg/ml) in complete D-MEM for 30 minutes at 37 C. After washing in PBS the cells were fixed for 30 minutes at room temperature in PBS-2% paraformaldehyde, and permeabilized in PBS-0.1% Triton-X 100 for 5 min. After 3 additional washes in PBS, the coverslips were blocked in 1% BSA for 30 min and co-stained with 0.165 mg/ml Texas Red Phallodin (Life Technologies, Grand island, NY) and 0.1 mg/ml 4′,6-diamidino-2-phenylindole (DAPI) Nuclear Stain (Sigma-Aldrich, St. Louis, MO) final and mounted. Representative fields were imaged on an Olympus IX81 Motorized Inverted Confocal Microscope using Olympus Fluoview software (Ver.2.1c).

Neutral lipid content was quantified using a modification of a previously described protocol [128]. Briefly, 10^6 cells were trypsinized, collected in PBS and stained at 25C for 30 min in the dark using Bodipy-493/503 (final concentration = 10 µg/ml in complete D-MEM). Flow cytometry was performed using a FACStar flow cytometer (Becton-Dickinson Biosciences, San Jose, CA). Each experiment was performed in triplicate with similar outcomes.

Oil Red O staining was performed using standard histologic techniques following growth of cells on coverslips, which were air-dried and stained with both Oil Red O and H&E.

2.4.6 Immunoblotting

Western blots were performed as previously described [4]. Antibodies used included those for total AMPK (Rabbit polyclonal IgG, 1:1,000, Cell Signaling Technology, Beverly, MA, cat. no. 2532) or phospho-AMPK ($pThr_{172}$) (Rabbit monoclonal IgG, 1:2,000 Cell Signaling, cat. no. 4188), PDHE1 (Mouse monoclonal IgG, 1:1,000, Santa Cruz Biotechnology, Santa Cruz, CA. cat. no. SC-377092) or phospho-PDH ($pSer_{293}$) (Rabbit monoclonal IgG, 1:10,000, EMD Millipore, Billerica, MA, cat. no. ap1062) PDK1 (Rabbit monoclonal IgG, 1:1,000, Cell Signaling, cat. no. 3820) and PDP2 (Rabbit polyclonal IgG, 1:500, Biovision, Inc., Milpitas, CA cat. no. 3944). Endogenous Myc protein was assessed with the mouse monoclonal antibody 9E10 (Santa Cruz) as previous described [4]. Protein loading was confirmed using a β-actin mAb (1:2,000, Santa Cruz cat. no. 3700). Blots were developed using a SuperSignal™ West Pico Chemiluminescent Substrate kit (Thermo Fisher).

2.4.7 RNA isolation and real time qRT-PCR

RNA was isolated from 80-90% confluent cell culture wells using a Qiagen RNAeasy Mini Kit, according to manufacturer's instruction (Qiagen, Inc. Chatsworth, CA). Residual DNA was removed using a TURBO DNA-free™ DNase Treatment and Removal Kit (Life Technologies). PCR reactions were conducted with Power SYBR® Green RNA-to-CT™ 1-Step Kit (Life Technologies), using a StepOnePlus™ Real-Time PCR System (Applied Biosystems, Inc. Carlsbad, CA). qRT-PCR primers were designed using Primer3web software (http://bioinfo.ut.ee/primer3/) and were synthesized by International DNA Technologies, Inc.

(Coralville, IA). Reactions were optimized such that only single bands of the predicted size were visualized upon gel electrophoresis (primer sequences and conditions are found in Table 2 and 3). Each qRT-PCR reaction was performed in triplicate with variations among samples seldom exceeding 5%. Statistical analysis was performed using Student's t-test.

Table 2: Transcripts evaluated by qRT-PCR and the functions of their encoded proteins

Symbol:	Description (mRNA):	Accession ID:	Pathway
CD36	CD36 molecule (thrombospondin receptor)	NM_031561	FA Transport
CPT1	carnitine palmitoyltransferase 1a, liver	NM_031559	FA Transport
FABP4	fatty acid binding protein 4, adipocyte	NM_053580	FA Transport
FATP1 (Scl271a)	solute carrier family 27 (fatty acid transporter) 1	NM_053580	FA Transport
Acat1	acetyl-CoA acetyltransferase 1	NM_017075.2	FA Oxidation
HADHa	hydroxyacyl-CoA dehydrogenase (trifunctional protein), alpha subunit	NM_130826.2	FA Oxidation
HADHb	hydroxyacyl-CoA dehydrogenase (trifunctional protein), beta subunit	NM_133618.2	FA Oxidation
ACADL	acyl-CoA dehydrogenase, long chain	NM_012819	FA Oxidation
ACADM	acyl-CoA dehydrogenase, C-4 to C-12 straight chain	NM_016986.2	FA Oxidation
ACADVL	acyl-CoA dehydrogenase, very long chain	NM_012891	FA Oxidation
ACC1	acetyl-CoA carboxylase alpha	NM_022193	FA Synthesis
ACC2	acetyl-CoA carboxylase beta	NM_053922	FA Synthesis
ACLY	ATP citrate lyase	NM_016987	FA Synthesis
FASN	fatty acid synthase	NM_017332	FA Synthesis
Agpat1	1-acylglycerol-3-phosphate O-acyltransferase 1	NM_212458	Lipid/ cholesterol Synthesis
Dgat1	diacylglycerol O-acyltransferase 1	NM_053437	Lipid/ cholesterol Synthesis
Gpat1 (Gpam)	glycerol-3-phosphate acyltransferase, mitochondrial	NM_017274	Lipid/ cholesterol Synthesis
Ppap2a	phosphatidic acid phosphatase type 2A	Nm_022538	Lipid/ cholesterol Synthesis
Ppap2b	phosphatidic acid phosphatase type 2b	Nm_138905	Lipid/ cholesterol Synthesis
Ppap2c	phosphatidic acid phosphatase type 2c	Nm_139252	Lipid/ cholesterol Synthesis
HMGCR	3-hydroxy-3-methylglutaryl-CoA reductase	NM_013134.2	Lipid/ cholesterol Synthesis
PC	pyruvate carboxylase	NM_012744.2	Pyruvate → Acetyl CoA Conv.
PDH (Pdha1)	pyruvate dehydrogenase (lipoamide) alpha 1	NM_001004072	Pyruvate → Acetyl CoA Conv.
PDK1	pyruvate dehydrogenase kinase, isozyme 1	BC089783	Pyruvate → Acetyl CoA Conv.
PDP2	pyruvate dehydrogenase phosphatase isoenzyme 2	AF062741.1	Pyruvate → Acetyl CoA Conv.
PKM1	pyruvate kinase, muscle, isoform 1	NM_053297	Pyruvate → Acetyl CoA Conv.
PKM2	pyruvate kinase, muscle, isoform 2	NM_053297	Pyruvate → Acetyl CoA Conv.
AceCS1	acyl-CoA synthetase short-chain family member 2 (cytoplasmic)	NM_001107793	Acetate → AcCoA Conv.
AceCS2	acyl-CoA synthetase short-chain family member 1 (mitochondrial)	NM_001106524	Acetate → AcCoA Conv.
cACH (Acot12)	acyl-CoA thioesterase 12	NM_130747	Acetate → AcCoA Conv.

Table 3: Sequences and annealing temperatures for all PCR primers used for Fig. 4*B*.

Symbol:	Forward Primer Sequence (5' → 3')	Reverse Primer Sequence (5' → 3')	Product Length (bps)	Annealing Temp.
CD36	ATTGGGAAAGTTATTGCGACATG	AACC1GCATAGATGGACCTG	124	62
CPT1	AACACCATCCACGCCATAC	GAAGTATTGAAGAGTCGCTCCC	125	62
FABP4	GATTTCCTTCAAACTGGGCG	ACTTTCCATCCCACTTCTGC	119	62
FATP1 (Scl271a)	GGACCCTAACTCAATGTACCAG	TCAAAGCCTTCACGCTGTAG	141	62
Acat1	TGCTACACGAACTCCCATTG	ATGACGTTGCCCATGTAGAC	147	62
HADHa	AGGCACTCACATCCTTCGAA	GAGAGCAGATGTGTTGCTGG	194	58
HADHb	GCCTTTGCTGTTTCTCGAATG	TGCTAACTGTGTCTTTTCCTGG	133	62
ACADL	CCTGCTTGGCATCAACATTG	TCTGAATGGAGGCTGAAACC	126	62
ACADM	CAAGAGAGCCTGGGAACTTG	CCCCAAAGAATTTGCTTCAA	154	60
ACADVL	GGCTCGGATGGCTATTCTG	CACTCATCTGTCACTTTCCAGG	150	58
ACC1	AAGGCTATGTGAAGGATGTGG	GAGGTTAGGGAAGTCATCTGC	137	62
ACC2	TTTGAGACCCCTTTGAGCC	AGTAACCCCACACGTTCTTG	148	62
ACLY	TTACGAGTGATGGGAGAAGTTG	AGGAAGTTGGCAGTGTGAG	149	62
FASN	GGCGTACACCCAGAGCTACC	GATGAGGTCCACAGCAGCAG	178	62
Agpat1	GTTCCCTCGACCTGCTTG	AATGAAGATGACTCCTGCCAG	125	62
Dgat1	GACAGCGGTTTCAGCAATTAC	GGGTCCTTCAGAAACAGAGAC	149	62
Gpat1 (Gpam)	CTGCTCACCTTCATCCTCTTC	CGTCAAGCCTCCGTCTTATG	133	62
Ppap2a	GAACAGAAGGTCAGGGAAGG	AACTGTAGCATGGGTCGTAAG	143	62
Ppap2b	ACTACAAACACCATCCTAGCG	CTTGAAGAGGTCAGACACGAAG	95	62
Ppap2c	CCCTGCTAATGTCACCGAG	AAGAACTGAACGGTGGGC	147	62
HMGCR	GCCTCGACCTAATGAAGAGTG	AGTTTGTAGGCTGGGATGTG	120	62
PC	TCATCCCCAACATCCCATTC	GTTAAGGGAGTCAAAGATCCGG	146	62
PDH (Pdha1)	TCTGGCCTGCAAGTATAATGG	CCATAGCGGTTATTCTCACAGATG	150	62
PDK1	TCGAAAACC1TTGGAAGCA	ATGGGACGGAACATAAACCA	181	60
PDP2	GTTCTCCACATGGTGGCTTT	ACACCTTGTCGGTCTTCCAC	226	60
PKM1	AGCATGATCAAGAAGCCACG	TCTCGAGCTATCAGGTGCTG	155	58
PKM2	CTCCTTCAAGTGCTGCAGTG	CATGGCCAAGTTCACACGAA	502	58
AceCS1	CCAAGAGTACCAAGGGCCAG	GCAGGCCCAAGGTAAGAACT	279	58
AceCS2	GTGGCAACCGGTGAAAACTC	CCTCCCATGCTTAGCCACAA	247	60
cACH (Acot12)	CCACCACCTTGGAGAAGATAAA	CACCGAGCAGGTGATGTAAT	215	62

2.4.8 Acetyl CoA assays

Acetyl CoA was assayed using an Acetyl-Coenzyme A Assay Kit (Sigma-Aldrich cat. # MAK039) according to manufacturer's instruction. Samples were isolated from fresh cell pellets,

lysed, and protein was quantified using a Pierce™ BCA Protein Assay Kit (Thermo-Fisher). Samples were deproteinized by adding 2 µl 1N perchloric acid/mg protein, and the resulting supernatant was neutralized by adding 3M $KHCO_3$. Standards were quantified on a 0-1 nmol scale, and 50 µl of sample was added to each well. The plate was read on a SpectraMax M2 Fluorescence Plate Reader and normalized to protein content. Analysis was performed using a one-way ANOVA and a *post-hoc* Bonferroni test of comparisons. Similar results were obtained when cells were simultaneously lysed and de-proteinated or when lysates were incubated on ice for prolonged periods. Thus results were not influenced by exogenous reactions that differentially depleted cells of AcCoA.

3.0 C-MYC AND AMPK CONTROL CELLULAR ENERGY LEVELS BY COOPERATIVELY REGULATING MITOCHONDRIAL STRUCTURE AND FUNCTION

3.1 INTRODUCTION

c-Myc (Myc) oncoprotein de-regulation occurs in a substantial fraction of human cancers and alters numerous transformation-associated phenotypes [14, 129-131]. Myc over-expression exerts marked effects on proliferation, survival, differentiation and biomass accumulation as a result of global changes in the expression of RNAs regulated by all 3 RNA polymerases [14, 23, 36, 132, 133]. Together, these changes reflect Myc's role as a general transcription factor that broadly modulates the levels of most, if not all, genes [134-137]. The molecular mechanisms by which Myc mediates these effects on transcription are varied and highly dependent upon the degree of Myc over-expression, the identity of various co-factors and the type of cell in which Myc de-regulation occurs [36, 136, 138, 139].

Metabolic changes are among the most universal consequences of aberrant Myc expression [140]. Myc induces the majority of genes encoding glycolytic enzymes and thus is important for promoting the Warburg effect, defined as the persistence of glycolysis under aerobic conditions [19, 23]. Rather than being a result of defective mitochondrial function and confined to tumor cells as originally proposed [20] , the Warburg effect also occurs in rapidly

proliferating normal cells [19, 141]. It thus seems likely that the major purpose of the Warburg effect is to supply anabolic precursors such as ribose sugars, nucleotides and select amino acids whose production must be increased and carefully coordinated with the doubling of biomass that accompanies replication [19, 21].

In addition to enhancing glycolysis, Myc re-programs oxidative phosphorylation (Oxphos) and supports the structural and functional integrity of mitochondria and the electron transport chain (ETC) via the direct up-regulation of certain mitochondrial-specific transcription factors [4, 17]. This has the effect of increasing the production of ATP needed to support macromolecular synthesis during proliferation [4, 37, 140]. Concurrently, Myc promotes the uptake and β-oxidation of exogenous fatty acids, which serve as an alternate source of acetyl CoA that is otherwise provided in lower yield by the re-programmed glycolytic pathway [11, 142, 143]. The transport of glutamine and its conversion to glutamate and α-ketoglutarate are also under stringent positive Myc control and provide yet another source of TCA cycle intermediates [23, 140, 144]. In support of all the above findings, *myc-/-* fibroblasts show severe structural and functional ETC defects, low rates of glycolysis and Oxphos and profound ATP depletion [4].

The regulation of both anabolic and catabolic processes is also a property of AMP-activated protein kinase (AMPK), a Ser/Thr kinase that is activated in response to a decrease in the ATP: AMP ratio [73, 145, 146]. AMPK is a trimeric enzyme whose γ-regulatory subunit undergoes a conformational change upon binding AMP that allows phosphorylation of the α catalytic subunit's Thr_{172} residue by the upstream kinase and putative tumor suppressor LKB [73, 147, 148]. The consequences of this activating phosphorylation event include a general inhibition of energy-consuming processes such as protein and fatty acid synthesis and proliferation [73]

and an increase in energy-generating process such as glycolysis and Oxphos [73, 149, 150]. Collectively, these cooperate to ensure the timely restoration of a positive ATP: AMP balance and allow the resumption of proliferation. Thus AMPK and Myc appear to enhance energy-generating processes while simultaneously exerting opposing effects on energy-consuming processes. How these are regulated and coordinated remain largely unexplored.

We have recently observed that the ATP-depleted state of *myc-/-* fibroblasts is associated with chronic phosphorylation-dependent AMPK activation whereas Myc re-expression restores normal ATP levels and suppresses AMPK [11]. These observations suggest that Myc and AMPK engage in a form of cross-talk, the purpose of which is to optimize proliferation and energy production while balancing Oxphos and the Warburg effect. In the current work, we have investigated how and the extent to which such communication occurs as well as how compromising AMPK function affects Myc's metabolic phenotype.

3.2 RESULTS

3.2.1 AMPK is necessary for Myc-stimulated mitochondrial biogenesis and function

To investigate the role for AMPK in mediating mitochondrial structure and function in the basal state and in response to Myc activation, we stably expressed the MycER fusion protein [151]. In both cases, the cells were of identical size and grew at similar rates (not shown). In response to the estrogen analog 4-hydroxytamoxifen (4HT), both cell types increased their rates of glycolysis although basal levels were higher in KO cells (Fig.8*A* and Suppl. Fig. 25*A* and *B*). Cells had very

little glycolytic reserve when simulated by oligomycin (Suppl. Fig. 25*A* and *B*.), implying that all lines were operating at near maximal glycolytic capacity. In contrast, KO cells failed to up-regulate Oxphos in response to MycER activation (Fig. 8*B* and Suppl. Fig. 25*C* and *D*). Thus, at least in MEFs, basal levels of glycolysis and Myc's up-regulation of Oxphos are AMPK-dependent. Very little oxygen was consumed for non-mitochondrial respiration in any of the cell lines (Suppl. Fig. 25*C* and *D*), indicating that no respiration was occurring as a result of side reactions attributable to factors such as peroxisomal oxidation. The trends of Oxphos and glycolysis recorded for basal respiration (Fig. 8*A* and *B*) continued throughout the mitochondrial stress test (Suppl. Fig. 25).

To determine whether KO cells' failure to increase Oxphos in response to MycER activation was indicative of a more global degree of mitochondrial unresponsiveness, we quantified changes in mitochondrial mass and production of reactive oxygen species (ROS), both of which are normally increased by Myc over-expression [4, 17, 152]. MycER activation in WT cells was accompanied by a reproducible 20-30% increase in mitochondrial mass as evidenced by staining with both MitoTracker Green and Acridine orange 10-nonyl bromide (NAO) as well as by an increase in ROS [4, 11] (Fig. 8*C*). The likely mitochondrial origin of ROS was also confirmed by MitoSox staining, which detects superoxide (O_2^-). The marked attenuation or absence of these responses in KO cells indicated that, in addition to Oxphos, other Myc-regulated mitochondrial responses are also AMPK-dependent.

We assessed the bio-energetic consequences of the above differences by measuring ATP levels in WT and KO MEFs during the course of MycER activation and subsequent inactivation. Basal (day 0) ATP levels in KO MEFs were routinely 30-40% lower than those in WT MEFs (Suppl. Fig. 24*B*.). In both cases, ATP levels declined within 24 hr. of MycER activation,

remained low throughout the ensuing 4 days and then normalized within 48 hr. of 4HT removal. However, the degree of ATP depletion in KO MEFs was greater than in WT MEFs, particularly after accounting for the lower basal levels in the former cells (Fig. 8*D* and Suppl. Fig. 2*4B.*). Concurrent immuno-blotting performed on WT cells showed an inverse relationship between AMPK activation and ATP levels (Fig. 8*E*) as well as the persistence of AMPK activation for at least 4 additional days beyond the time at which ATP levels had returned to pre-treatment levels. This suggested that factors other than adenosine nucleotide levels might also be contributing to AMPK activation. Because ROS can also activate AMPK [153-156], we repeated the above experiment in the presence of the anti-oxidant N-acetylcysteine (NAC) at a concentration that reduced ROS in 4HT treated cells (Fig. 8*F*). Under these conditions, AMPK phosphorylation was markedly attenuated (Fig. 8*G*). AMPK's activation beyond the point of ATP normalization also correlated with the persistence of high ROS following 4HT removal (Fig. 8*H*). Thus, in the face of Myc deregulation in WT cells, the prolonged activation of AMPK is likely to be a consequence of both ATP depletion and the persistence of ROS.

ETC structure and function are highly Myc-responsive in *myc-/-* rat fibroblasts [4]. To determine whether these properties were also AMPK-dependent in MEFs, we used blue native gel electrophoresis (BNGE) to evaluate the integrity of each of the 4 multi-protein components of the ETC (Complexes I-IV) along with the monomeric and dimeric forms of Complex V (ATP synthase) termed V_m and V_d, respectively. BNGE can also resolve ETC "supercomplexes" (SCs), which are comprised primarily of higher order associations of Complexes I, III and IV in varying stoichiometries and are believed to promote more efficient ETC function [157, 158]. Individual BNGE components of Complexes I-V from WT and KO MEFs were similar in appearance and

did not change appreciably following Myc induction (Fig. 9*A*). In contrast, at least 5 SCs (SC_a-SC_e) and Complex V_d, readily seen in WT MEFs, were reduced or absent in KO cells (Fig. 9*A*).

Activity assays for individual complexes better emphasized the differences between WT and KO MEFs both prior to and following MycER activation (Fig. 9*B* and *C* & Suppl. Fig. 26). For example, neither Complex I nor Complex V_m activity was significantly altered under either condition whereas Complex V_d was virtually absent in KO cells regardless of MycER status. In contrast, Complex III activity was decreased in KO cells regardless of MycER status whereas Complex IV decreased only in response to MycER activation. Consistent differences were also observed in the enzymatic activities of several SC components (Fig. 9*B* and Suppl. Fig. 26).

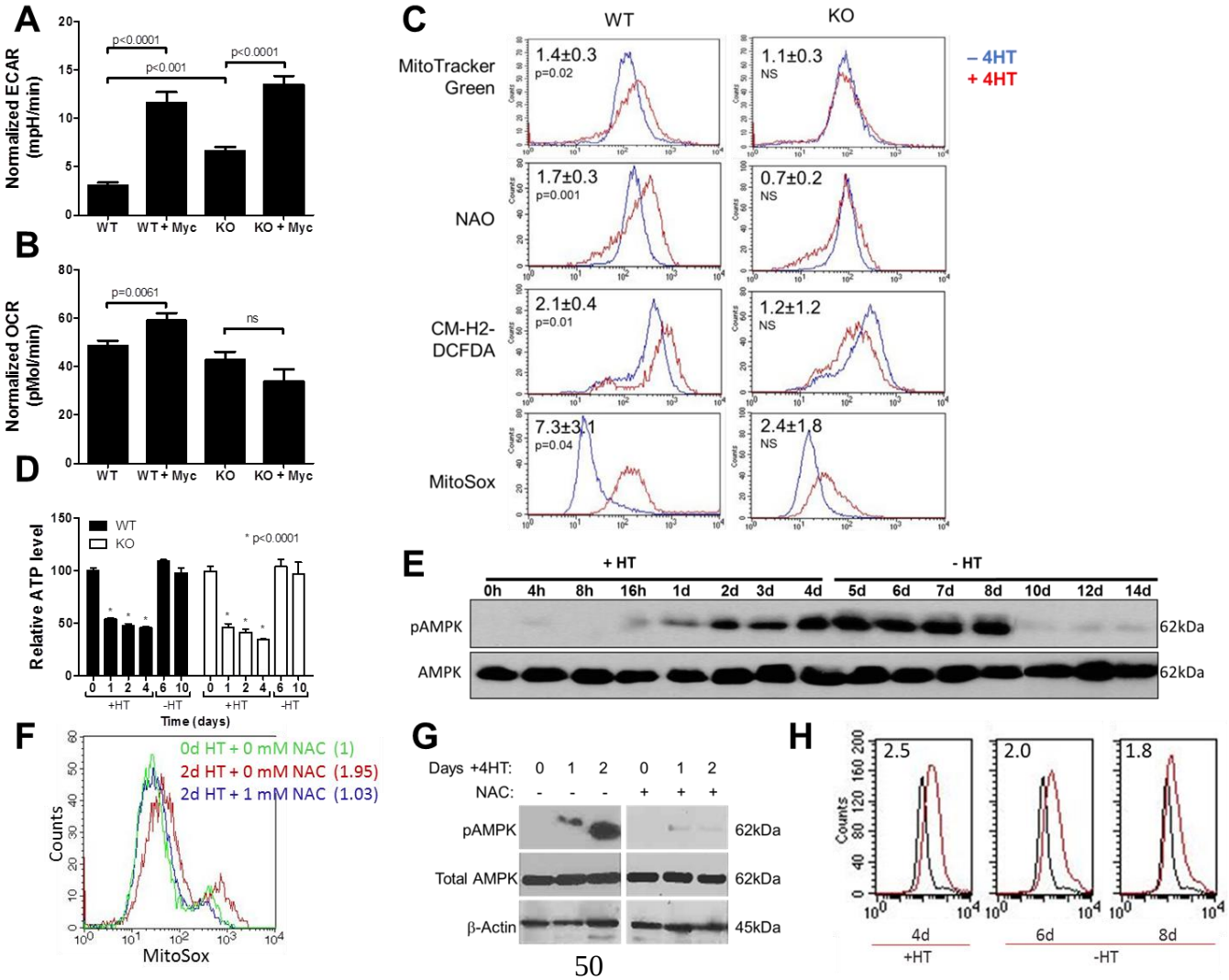

Figure 8: Energy-generating pathway responses to MycER activation. (A) Baseline glycolysis measurements normalized to cell number at conclusion of the experiment. WT and KO MEFs were either untreated or exposed to 4HT for 7 days to activate MycER (+Myc). Glycolysis was quantified by measuring extracellular acidification rates (ECAR). Bars represent the mean of quadruplicate measurements ± 1 standard error of the mean (SEM). (*A*) Baseline Oxphos measurements. Oxygen consumption rates (OCR) were simultaneously quantified on the same samples described in (*A*). See Suppl. Fig. 25 for additional details regarding the glycolytic and Oxphos responses of these cells. (*C*) Changes in mitochondrial mass and ROS production. Untreated or 4HT-treated (7 days) WT and KO cells were stained with MitoTracker Green or NAO to independently assess mitochondrial mass. In parallel experiments, cells were also stained with CM-H2-DCFDA to quantify total ROS production or with MitoSOX to specifically quantify the production of mitochondrial-derived superoxide. In all cases, typical flow diagrams are depicted. The numbers in the upper left portion of each panel indicate the mean ratios of fluorescence intensities between 4HT-treated and control, untreated cells from at least 4 independent experiments ± 1 SEM (*D*) ATP levels in response to MycER activation and inactivation. ATP levels were measured at baseline (Suppl. Fig. 24), after the indicated periods of exposure to 4HT (+) and its subsequent removal (-). Each value shown depicts the mean of quadruplicate samples ± 1 SEM. Basal (day 0) ATP levels in untreated KO cells were routinely found to be 30-40% lower than those of their WT counterparts (Suppl. Fig. 24) but are normalized here to 100% in both cell types for easier comparison. After taking the day 0 differences into account, KO MEFs also showed significantly lower ATP levels on days +1-4 compared to their WT counterparts ($P < 0.02$) (Suppl. Fig. 24). (*E*) AMPK response to MycER activation/inactivation in WT MEFs. WT cells were exposed to 4HT for the indicated times. On day 4, 4HT was removed (-4HT) and cells continued to be cultured in its absence for an additional 6 days. Total AMPK and pAMPK were assessed by immunoblotting at the time points shown. (*F*) MitoSox staining as described in Fig. 1C after 2 days of 4HT treatment. In the concurrent presence of 1 mM NAC, no significant change in ROS was observed. (*G*) AMPK activation is suppressed by NAC. WT cells were exposed to 4HT in the absence or presence of 1 mM NAC. Total and phospho-AMPK were assessed by immuno-blotting as described for panel (*E*). (*H*) Persistence of ROS following MycER inactivation. WT cells were exposed to 4HT for 4 days at which point ROS were quantified using MitoSox as described in (*C*). 4HT was then removed with ROS levels again being determined 2 and 4 days later (days 6 and 8). Numbers in upper left corner indicate the ratio of mean fluorescence intensity of 4HT-treated (red curves) to non-4HT-treated MEFs (black curves).

Specifically, SC_a activity was lower in KO cells, irrespective of Myc's activation status, whereas changes in the remaining SCs were detected only in KO cells following MycER activation (Suppl. Fig. 26.). Complex II activity was slightly higher in KO cells but increased significantly following MycER activation whereas no change was evident in WT cells (Fig. 9*C*). Thus, while MycER activation had little to no discernible effect on the ETC enzymatic activity of WT cells, it had a pronounced effect in KO cells. This provided further evidence that AMPK is needed to maintain normal mitochondrial function both in the basal state and in response to Myc deregulation.

3.2.2 Transcriptional and enzymatic profiling reveals co-operativity between Myc and AMPK in modulating metabolic function

Given AMPK's influence on both basal and Myc-dependent mitochondrial functions, we performed a small-scale gene expression survey of WT and KO cells. We examined 30 transcripts whose encoded proteins comprise key elements of glycolysis, the TCA cycle and other pathways relevant to energy regulation and mitochondrial function. Significant differences were noted between WT and KO MEFs with 19 transcripts being relatively under-expressed in the latter cells, 3 over-expressed and 8 unchanged (Fig. 10*A* and Suppl. Fig. 27.). Following MycER activation, WT cells showed significant up-regulation of 19 transcripts and down-regulation of 9, in a pattern that generally correlated with the increased rates of glycolysis and Oxphos (Fig. 8*A* and *B*). In contrast, the transcriptional response to MycER activation in KO cells was markedly different with only 12 transcripts demonstrating any significant change (Fisher's Exact test, $P < 0.0001$). Moreover, 19 of the 28 Myc-responsive transcripts in WT cells

were expressed discordantly in KO cells. Particularly noteworthy examples included transcripts for glucose 6-phophatase (G6P); the M2 isoform of pyruvate kinase (PKM2); isocitrate dehydrogenase 2 (IDH2) and each of the 4 subunits of succinate dehydrogenase (SDHa-d), which comprise Complex II of the ETC. Collectively, these studies indicate that AMPK functions to coordinate the transcriptional activity of the majority of transcripts examined herein. both in their basal state and in response to MycER activation.

The actual enzymatic activities of several mitochondrial oxidoreductases encoded by the above transcripts were also discordant (Fig. 10*B*). For example, basal activity of NADH-dependent isocitrate dehydrogenase (IDH) was higher in WT cells and increased in response to Myc activation whereas it declined in KO cells. A different pattern was observed in the case of glycerol 3-phosphate dehydrogenase (G3PDH), which was lower in basal-state KO cells than in WT cells; it also failed to respond to Myc over-expression in contrast to WT cells where its activity declined. That not all enzymatic activities were altered as a consequence of the loss of AMPK was evidenced by malate dehydrogenase (MDH) levels, which were identical in basal-state WT and KO cells and decreased commensurately in response to Myc over-expression. As is commonly the case for many transcripts and their encoded proteins and for individual subunits of multi-protein complexes [159-165] the measured enzyme activities did not closely correlate with the relevant transcript levels shown in Fig. 10*A*. Collectively, these findings are consistent with those depicted in Fig. 9 and Suppl. Fig. 26 and support the notion that some TCA cycle enzymes rely upon AMPK either for their basal function or their proper response to Myc over-expression.

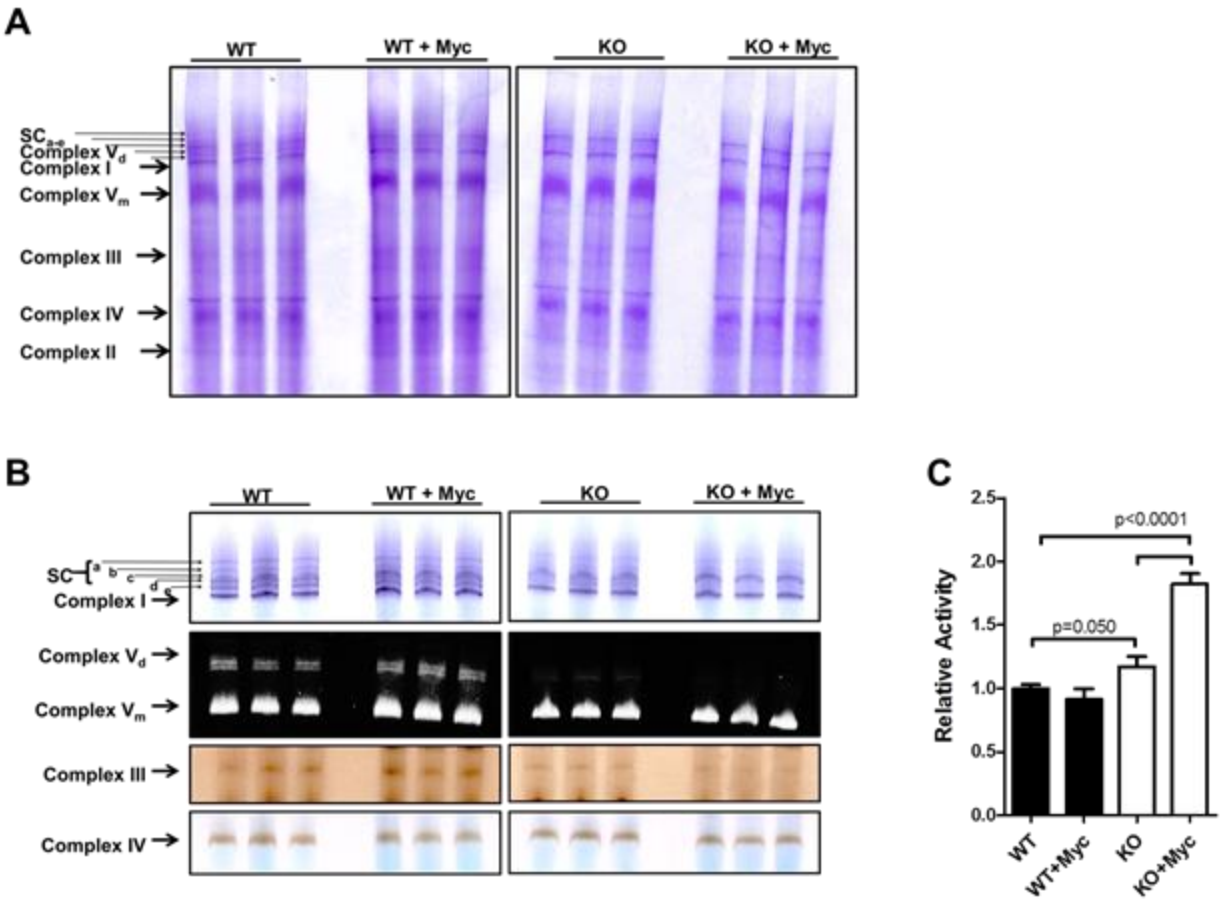

Figure 9: Structural and functional properties of ETCs complexes in WT and KO cells. (*A*) Analysis of ETC complexes by non-denaturing BNGE. Mitochondria were purified from triplicate cultures of the indicated cell types and resolved by BNGE. At least 5 individual supercomplexes (SCa-e) could be resolved. Note that Complex V (ATP synthase) is composed of both monomers (Vm) and dimers (Vd). (*B*) In situ enzymatic assays for Complex I (NADH ubiquinone oxidoreductase) plus supercomplexes, Complex Vm and Vd (ATPase), Complex III (decylubiquinol cytochrome c oxidoreductase) and Complex IV (Cytochrome c oxidase). Each assay was performed in triplicate on at least 2 occasions, with representative results being shown here (also see Suppl. Fig.26.). (*C*) Complex II (succinate dehydrogenase) activity was quantified on lysates prepared from purified mitochondria as its in situ assessment was found to be unreliable. The results shown in the histogram represent the mean of triplicate enzymatic determinations ± 1 SEM. See Suppl. Fig. 26 for quantification of all enzymatic measurements.

The above studies suggested that both AMPK and Myc might be controlling more proximal determinants of Oxphos. We therefore conducted a qRT-PCR-based survey for 20 known regulators of mitochondrial structure and function including those involved in DNA replication and transcriptional maintenance [166-169]. 13 of the tested transcripts were found to be differentially expressed between WT and KO cells, with 10 up-regulated in KO cells and 3 down-regulated (Fig. 10*C* and Suppl. Fig. 28). Following MycER activation, significant additional differences were noted. For example, in contrast to the up-regulation of 6 transcripts and the down regulation of 2 transcripts in WT cells in response to MycER activation, KO cells responded anomalously, with only 3 transcripts up-regulated and 9 down-regulated. Within these subsets of Myc-responsive transcripts, the largest differences in WT cells included a 2.4-fold increase in NSUN4 and a 4.6-fold increase in UCP2 whereas in KO cells, Mterf1 and UCP2 transcripts were reduced by 3.4- and 3.9-fold, respectively. These results indicate that AMPK and Myc cooperate to ensure the proper coordination of numerous factors that supervise mitochondrial-specific DNA replication and transcription.

Aiming to identify changes in the relative abundance of mitochondrial proteins between WT and KO MEFS both prior to and in response to de-regulated Myc over-expression, we applied a differential mass spectrometry (dMS) workflow to a set of enriched mitochondrial samples isolated from WT and KO cells either prior to or following an 8 day period of Myc activation [170, 171]. We reliably identified and quantified the relative abundance of 345 mitochondrial proteins as annotated in the DAVID Bioinformatic Database and/or the Mouse MitoCarta Inventory of Mammalian Mitochondrial Genes. High-resolution liquid-chromatography Fourier transformed mass spectrometry was used to detect these proteins by

comparing the relative intensity of individual high-resolution isotope distributions across each of the analyzed samples (S6 Fig.). We observed a 24% higher average intensity of all mitochondrial peptides in KO samples both with and without Myc over-expression 2-way analysis of variance (ANOVA) p value of 0.002 compared to WT samples, despite the overall abundance of non-mitochondrial proteins being otherwise identical. This may be caused by a slightly higher purity of mitochondria in the former samples.

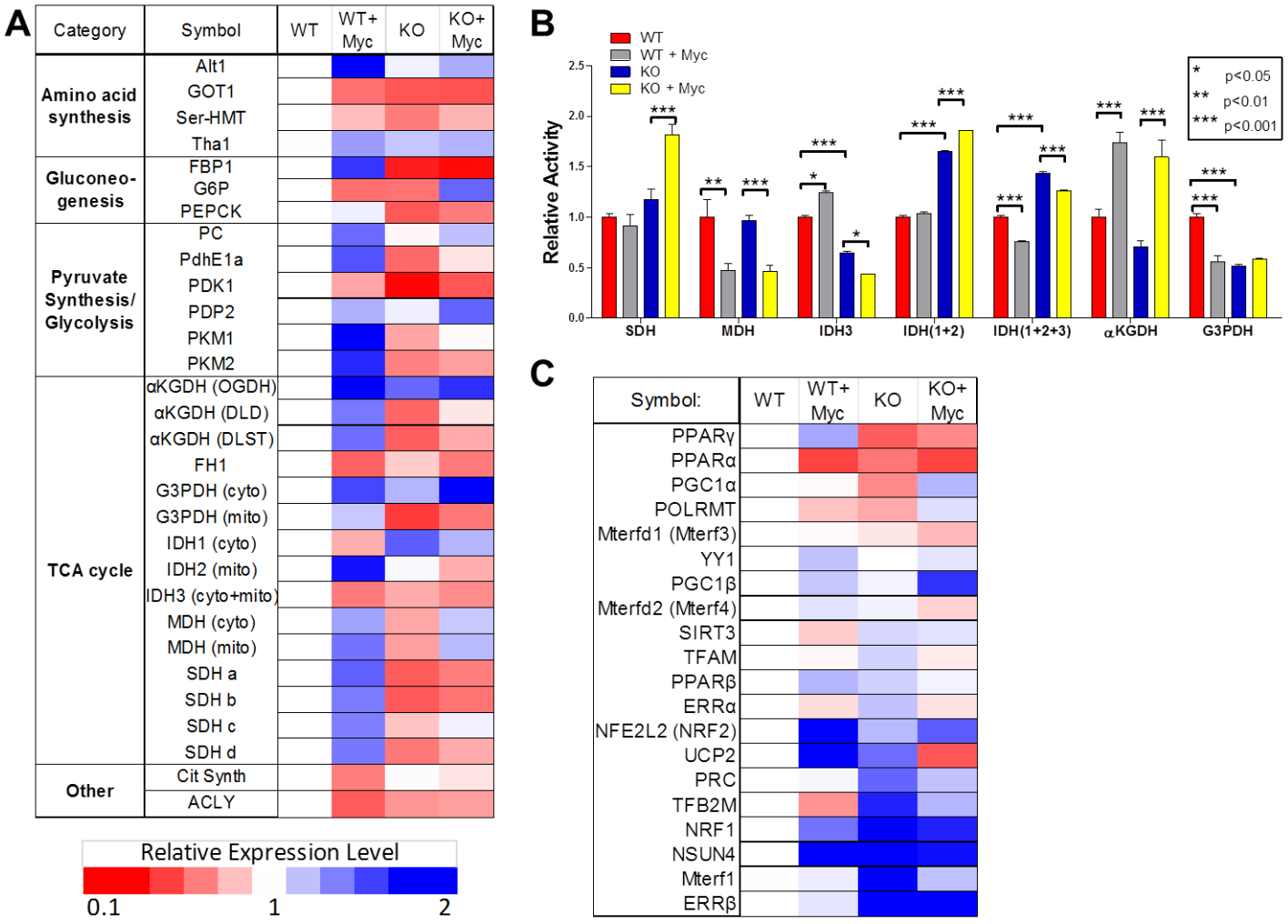

Figure 10: Transcriptional and enzymatic differences between WT and KO MEFs. (*A*) Transcriptional profiling. Real-time qRT-PCR was performed in triplicate for each of the indicated transcripts. The levels of each transcript determined in WT cells were arbitrarily set to 1 as indicated by the white boxes. See Suppl. Fig. 27. for the actual numerical values and p values for individual determinations. (*B*) Functional assays for oxidoreductases. Each bar represents the mean of biological triplicate determinations ± 1 SEM performed on purified mitochondrial lysates. Note that the results for SDH are the same as those presented in Fig. 9*C*. (*C*) qRT-PCR profiling of transcripts involved in the regulation of mitochondrial DNA replication and maintenance, transcription and function. Analyses were performed as described for (*A*). See Suppl. Fig. 28 for the actual numerical differences and p values for individual determinations.

It could also be due to a slightly greater overall mitochondrial mass in KO cells, although this was not observed by staining with NAO or MitoTracker dyes (Fig. 8*C*).

3.2.3 Differences in mitochondrial proteomes of WT and KO MEFs

Using a conservative q-value cutoff of 0.05, we determined the abundance of 28 proteins to be significantly different between WT and KO MEFs prior to MycER activation with 22 being more abundant in WT cells and 6 more abundant in KO cells (Fig. 11*A* and *C*, red circle). Following 8 days of MycER activation, 31 mitochondrial proteins were altered in WT cells, with 17 up-regulated and 14 down-regulated (Fig. 11*B* and *C*, green circle). 8 of these (26%) were also members of the group depicted in Fig. 11*A* that were thus also AMPK-responsive (Fig. 11*C*, yellow). In contrast, only 6 proteins were found to be Myc-responsive in KO MEFS (Fig. 11*D* and *C*, blue circle). Of these, Tamm41, Aldh1l2, and Clic4 were also influenced by Myc in WT cells (Fig. 11*C*, cyan). The response of 8 proteins to Myc over-expression was also found to be

discordant and having a significant "interaction effect" (Fig. 11*E*), with 5 of them (Prdx4, Sqrdl, Slc16a1, Clic4 and Ptrf) changing their abundance in opposite directions in WT vs. KO cells, and the other 3 (Cyb5a, Echs1, and Slc25a13) only being affected by Myc over-expression in WT cells. Together, these findings indicate that approximately 15% of evaluable mitochondrial proteins (i.e. 51 of 345) can be conservatively described as being regulated by AMPK and/or Myc and that much of the long-term mitochondrial proteomic adaptation to Myc deregulation is AMPK-dependent.

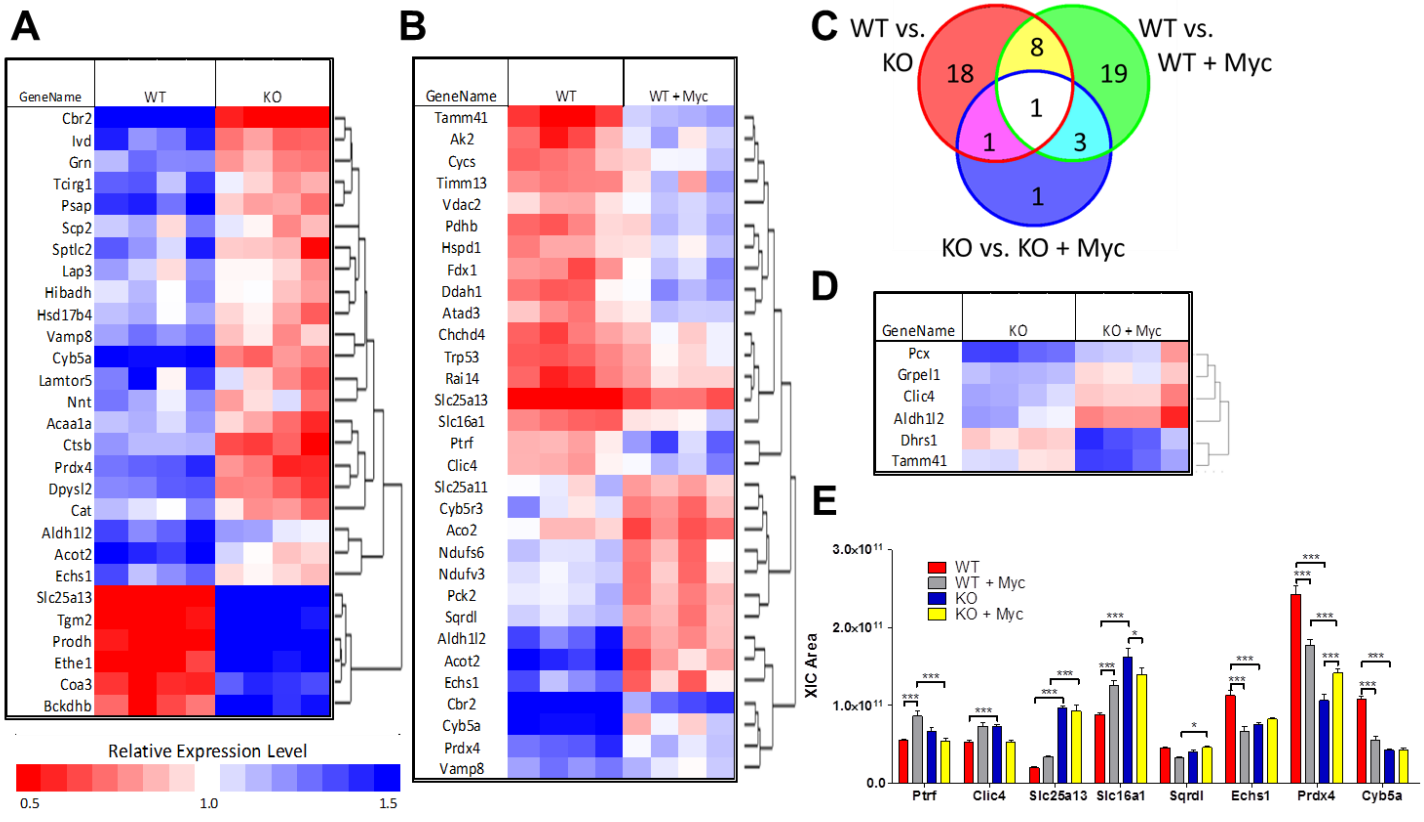

Figure 11: Mitochondrial proteomic profiling. LC-MS/MS reliably identified and quantified 345 proteins with mitochondrial localization from representative peptides in each of the 4 experimental groups. (*A*) Differential protein expression between WT and KO MEFs prior to MycER activation. (*B*) Differential protein expression in WT MEFs prior to or following an 8 day period of MycER activation. (*C*) Venn diagram of protein overlap between WT and KO MEFs, WT vs. WT+Myc and KO versus KO+Myc. Each of the protein subsets within these 3 groups are enclosed by red, green and blue circles and correspond to the proteins denoted in panels (*A*), (*B*), and (*D*), respectively. All proteins were selected by a conservative q-value of <0.05 by 2-way analysis of variance (two way ANOVA). (*D*) Differential protein expression in KO MEFs prior to or following 8 days of Myc over-expression. (*E*) Quantification of 8 proteins that showed a significant interaction effect by both AMPK and Myc overexpression.

3.2.4 Differential redox states of WT and KO cells

The differential activities of the ETC, mitochondrial dehydrogenases and the glycerol phosphate shunt (represented by G3PDH), as well as altered ROS production, might be expected to exert distinct effects on the redox states of WT and KO cells [172-175]. We tested this directly by stably targeting a redox-sensitive form of green fluorescent protein (roGFP2) [176, 177] to either the cytoplasm or mitochondrial matrix of WT or KO cells (Fig. 12*A*). In control experiments, exposure of roGFP-expressing WT or KO cells to H_2O_2 markedly increased the ratio of oxidized:reduced roGFP, irrespective of its subcellular location (i.e. roGFP-cyto versus roGFP-mito) whereas treatment of the same cells with DTT alone or with H_2O_2 followed by DTT shifted the ratio to that of a more reduced state (Fig. 12*B* and *C* and data not shown). The

responses of WT and KO cells to these extreme stresses were indistinguishable (not shown) and defined the limits within which supra-physiologic changes in the redox state can occur.

Quantification of oxidized and reduced roGFP2 in the mitochondrial and cytoplasm of WT and KO cells prior to or following MycER activation for 24 hr. showed both compartments to be relatively reduced (Fig. 12*C*) and in agreement with previous findings in other cell types [176, 178-180] However, in the basal state, KO cells showed a 28% greater degree of cytoplasmic oxidation ($p<0.001$) and a 6% greater degree of mitochondrial oxidation than WT cells ($p<0.001$). MycER activation in WT cells led to a further 9% increase in cytoplasmic oxidation ($p=0.0004$) and an 8% increase in mitochondrial reduction ($p<0.0001$). Finally, although an identical 9% increase in oxidation occurred in the cytoplasm of KO cells following MycER activation ($p=0.002$), no change occurred in their mitochondrial redox state ($p=0.2$). These results are consistent with those of our preceding studies indicating that AMPK and Myc cooperate to promote mitochondrial biogenesis and function. They further indicate that mitochondrial structural and functional alterations mediated by Myc de-regulation are associated with significant differences in the redox state of the mitochondrial matrix.

3.2.5 AMPK influences Myc-mediated re-programming of steady-state metabolites

We used high performance liquid chromatography-electrospray ionization tandem mass spectrometry (HPLC-ESI-MS/MS) to quantify steady state levels of a select group of metabolites in WT and KO cells prior to or following MycER activation. The metabolites were chosen to reflect relevant glycolytic and TCA cycle intermediates, anabolic substrates and determinants of cellular redox and energy status. Significant differences were seen between WT and KO cells

prior to MycER activation with the most striking being the generally lower levels of glycolytic substrates and higher levels of TCA cycle substrates in KO cells (Fig. 13*A*). This suggested that the higher glycolytic rate of KO cells (Fig. 5*A*) might be responsible for depleting some of the intermediates in this pathway whereas defects in the ETC might allow a buildup of TCA intermediates. Higher levels of nucleosides and deoxynucleosides in KO cells were consistent with the previously report of AMPK being a negative regulator of the Warburg effect [79], which could also explain the relative depletion of glycolytic substrates if they were being shunted into Warburg-related pathways. The modestly higher levels of AMP and ADP in WT cells in response to MycER activation, together with reduced ATP levels (Fig. 8*D* and Suppl. Fig. 24*B*), is likely sufficient to account for any activation of AMPK that is not otherwise attributable to ROS (Fig. 8*E*). In contrast, the even higher levels of AMP in KO cells, both prior to and following MycER activation, can likely be explained by the inability to normalize ATP and AMP in AMPK's absence.

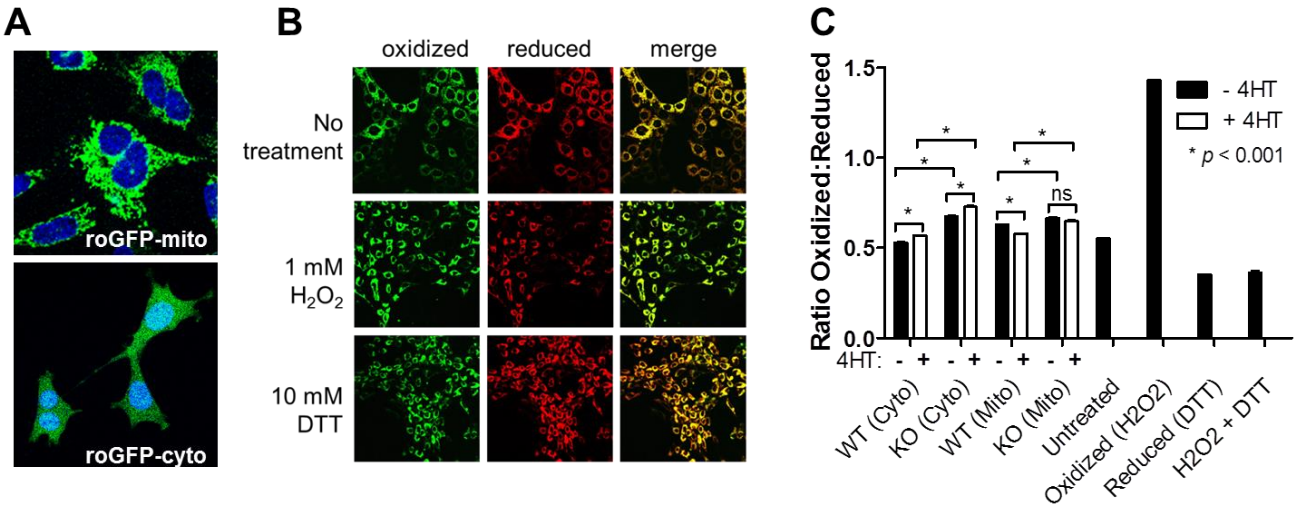

Figure 12: Redox states in cytoplasmic and mitochondrial compartments of WT and KO MEFs. (*A*) Live cell confocal images of WT MEFs stably expressing roGFP-mito and roGFP-cyto demonstrating specific mitochondrial and cytoplasmic localization, respectively. Nuclear counter-staining was with Hoechst 3334. (*B*) Live cell confocal microscopy of KO MEFs expressing roGFP-mito. Cells were untreated or exposed to 1 mM H2O2 or 10 mM DTT for 30 min prior to obtaining images. (*C*) Quantification of redox differences between WT and KO MEFs. Monolayer cultures were grown for 24 hr. in the absence or presence of 4HT. Flow cytometry was then used to quantify the mean fluorescence ratios of oxidized and reduced roGFP. Each bar represents the average ± 1 SEM of mean fluorescence intensities obtained from 3 independent plates of cells. *= P<0.001. Similar results were independently obtained in 2 repeat experiments as well as in 2 experiments performed following a longer period of MycER activation (7 days, not shown). The 4 bars on the right represent control experiments in which WT cells expressing roGFP-cyto were exposed under the conditions described in (*B*). These values define the maximal possible degree of oxidation or reduction capable of being achieved under the most extreme conditions.

patterns. Most notably WT cells showed an overall reduction of TCA cycle intermediates that most likely reflected their rapid consumption in response to increased mitochondrial mass and metabolic activity (Figs. 8*B and C*) and/or a reduction of acetyl CoA entering the TCA pathway, perhaps as a result of the Warburg effect as noted above. In contrast, changes in TCA cycle intermediate levels were less pronounced in KO cells following MycER activation, which was again consistent with their generalized mitochondrial unresponsiveness (Figs. 8*A and C*). Despite differences in the basal glycolytic intermediate content of WT and KO cells, the redistribution of these molecules was somewhat similar in response to MycER activation, with the exception of fructose-1,6-bisphospate. For example, both cell types showed significant increases in intracellular glucose content, likely reflecting the known propensity for Myc to increase glucose transport [19, 23]. Phosphoenolpyruvate (PEP) was also markedly increased in both cell lines

(Fig. 13*A*). Other notable differences included a generalized decrease in the free amino acid content of WT cells in contrast to either no change or an increase in KO cells. Both cell types also up-regulated nucleoside and deoxynucleoside pools in response to MycER activation. Finally, and consistent with their more highly oxidized cytoplasm (Fig. 12*C*), KO cells contained higher levels of glutathione disulfide (GSSG), which is the oxidized form of glutathione (GSH) [181]. Moreover, both cell types increased their GSSG:GSH ratio in response to Myc activation in a manner that closely mirrored the accompanying changes in cytoplasmic roGFP fluorescence (Fig. 13*C*).

To investigate potential mechanism(s) underlying some of the differences in metabolite distribution between WT and KO cells, we next examined pyruvate dehydrogenase (PDH) and pyruvate kinase (PK). These enzymes are notable for catalyzing 2 of the 3 irreversible steps in glycolysis (ΔG = -7.5kcal each) and are subject to complex and multi-factorial positive and negative regulation (Fig. 13*B*) [26, 182, 183]. For example, in addition to modifications such as acetylation and oxidation and feedback regulation by adenosine nucleotides, PDH is also tightly controlled post-translationally by the inhibitory Ser/Thr kinase pyruvate dehydrogenase 1 (PDK1) and the stimulatory phosphatase pyruvate dehydrogenase phosphatase 2 (PDP2) both of which regulate the level of Ser_{293} phosphorylation of the PDH E1 subunit (PDHE) [116, 184]. PK activity is typically regulated by changes in the abundance of its PKM1 and PKM2 isoforms, with the expression of the latter tending to correlate with high rates of proliferation [26, 182]. This, together with the significantly higher K_m of PKM2 is believed to account for the accumulation of substrates upstream of PEP that drive the Warburg effect and limit the availability of glycolytically-derived acetyl CoA for usage by the TCA cycle [26, 185]. Additionally, both PK isoforms are also subject to multiple and non-mutually exclusive types of

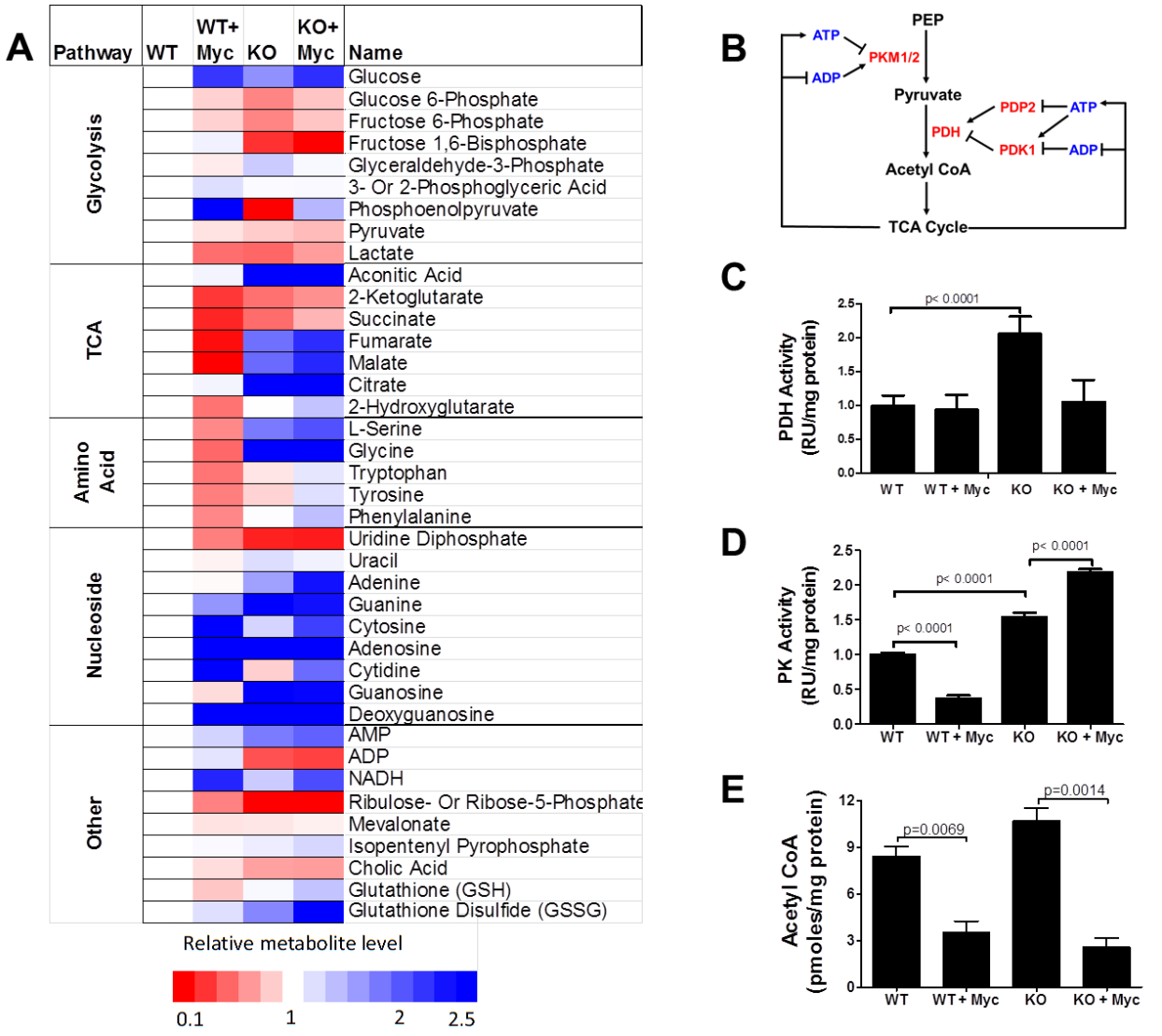

Figure 13: Metabolite profiling of WT and KO MEFs. (*A*) HPLC-ESI-MS/MS quantification of select metabolites in MEFs prior to or following MycER activation for 8 days. Each box represents the average of biological quadruplicate samples. Levels of each depicted metabolite were arbitrarily set to 1 in WT cells (white boxes). (*B*) Enzymatic and metabolite feedback control of PDH and PK. Note the control of the former by the stimulatory phosphatase PDP2 and the inhibitory kinase PDK1 as well as additional indirect and direct control of PDH and PK, respectively by ATP and ADP. PDH and PK enzyme activities (*C* and *D*, respectively) and acetyl CoA assays (*E*) were performed on whole cell extracts as previously described in Chapter 2.

post-translational modification; allosteric feedback by metabolites such as ATP, ADP and fructose-1,6,-bi-phosphate; and changes in enzyme dimer: tetramer ratios [29, 186].

Immunoblotting of WT and KO cell extracts both prior to and after MycER activation showed minimal changes in protein levels of PDHE, PKM1 and PKM2 (Suppl. Fig. 30.). A reduced amount of pPDHE1 was observed in KO cells although it did not change appreciably in response to MycER activation. Decreases in PDK1 and increases in PDP2 occurred in WT and KO cells following MycER activation.

Changes in the enzymatic activities of PDH and PK were more revealing. As seen in Fig. 13*C*, PDH activity was significantly higher in KO cells but only in the basal state. PK activity was also higher in KO cells, and increased even further in in KO cells in response to MycER activation, but decreased in WT cells after MycER activation (Fig. 13*D*). Together, these results are consistent with the idea that Myc and AMPK cooperatively regulate the switch between glycolysis and Oxphos by coordinating the activities of two critical and irreversible glycolytic steps that are important for determining the availability of acetyl CoA and its use by the TCA cycle. Interestingly, despite the above-noted differences in PDH and PK activities between WT and KO cells, the absolute abundance of acetyl CoA, either in the basal state or in response to MycER activation was quite similar in WT and KO cells (Fig. 13*E*).

3.3 DISCUSSION

3.3.1 Mitochondrial responses to Myc over-expression are AMPK-dependent

Considerable evidence supports the idea that Myc and AMPK influence similar cellular and biochemical functions although via different pathways and often for different purposes (Fig. 14). For example, both promote glucose uptake, glycolysis, mitochondrial biogenesis and Oxphos [4, 17, 23, 73, 145, 146, 149, 150]. In response to Myc over-expression, these activities are believed to provide the crucial anabolic precursors and ATP needed to support the highly energy-consuming process of biomass accumulation [19, 21]. In fact, much of the increased glycolytic flux mediated by Myc over-expression is currently viewed as being directed towards promoting the Warburg effect and anabolism while being diverted away from mitochondrial consumption (Fig. 14 and [23, 38, 141]). Similarly, TCA cycle intermediates, some of which originate from extra-glycolytic sources such as glutaminolysis and fatty acid β-oxidation, may also be directed into non-mitochondrial biosynthetic pathways in a Myc-dependent manner [11, 23, 37]. Moreover, Myc's enhancement of ETC activity increases ATP production and its rate of turnover to support anabolism and proliferation [4]. In contrast, AMPK activation occurs in response to critical energy shortages, which suppress energy-consuming processes while activating energy-generating ones [73]. Thus AMPK activation opposes the Warburg effect thereby reducing the flow of glycolytic substrates into anabolic pathways and maximizing their eventual conversion into acetyl CoA for utilization by the TCA cycle [73, 79]. The cross talk between Myc and AMPK is readily apparent in *myc-/-* fibroblasts, which constitutively express high levels of

phosphorylated AMPK as a consequence of their being unable to restore their ATP deficit by up-regulating glycolysis or Oxphos [11].

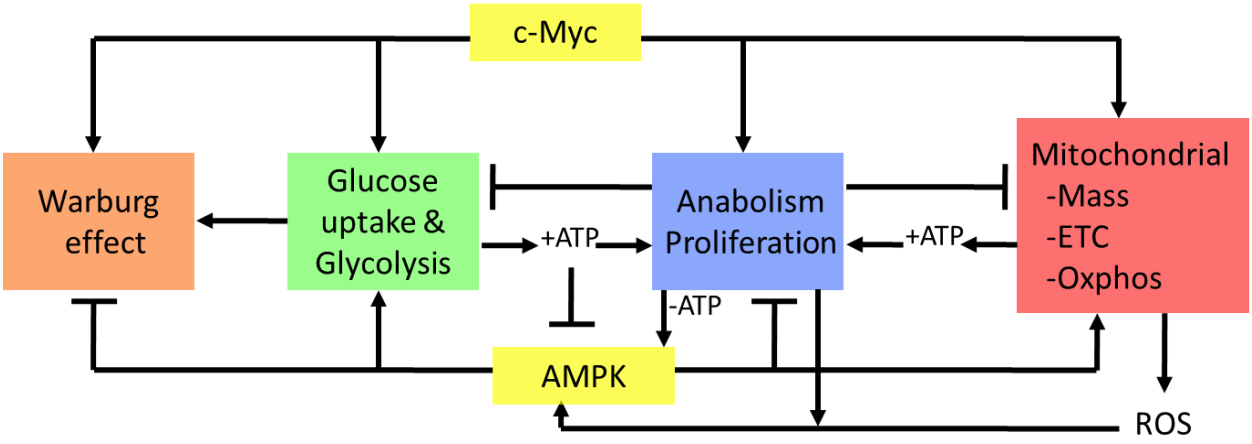

Figure 14: Model depicting the relationship between Myc and AMPK (yellow boxes) demonstrating their influence over common metabolic functions, although sometimes in opposite ways and for different purposes. Communication between Myc and AMPK may occur via at least 2 distinct and semi-autonomous routes with different initiating events and consequences. The first involves the activation of AMPK via Myc-mediated depletion of cellular ATP stores arising as a consequence of energy-consuming anabolic processes such as proliferation (-ATP, blue box) (Fig. 8*D* and Chapter 2). The second involves AMPK activation via ROS generated from increases in mitochondrial metabolism or cytoplasmic signaling pathways. It is notable that, in the first case, AMPK activation is dependent upon ATP depletion whereas, in the second case, AMPK activation occurs regardless of ATP status. AMPK activation via ROS can thus anticipate impending ATP depletion and prevent or limit this by down-regulating ATP dependent processes. In the face of a pre-existing ATP deficit, other functions of AMPK such as the promotion of proliferative arrest might tend to override the effects of Myc over-expression. In contrast, activation of AMPK by ROS might reinforce an already highly proliferative and ATP-replete state by promoting pro-anabolic functions such as glycolysis and Oxphos without necessarily compromising proliferation.

The failure of KO cells to increase Oxphos in response to MycER activation, while retaining a relatively normal glycolytic response (Figs. 1*A* and *B*), appears to be the result of a

more generalized mitochondrial dysfunction that includes an inability to accrete mass, to generate ROS, to maintain normal levels of TCA cycle intermediates and to properly regulate ETC function (Figs. 1*C*, 2 and 3). Perhaps not surprisingly, these abnormalities were collectively associated with lower levels of ATP and higher levels of AMP, both in the basal state and in response to MycER activation (Fig. 8*D* and 13*A*, & Suppl. Fig. 24). The increased basal glycolytic rate of KO cells (Fig. 8*A*), may therefore only reflect a partially effective compensatory mechanism aimed at correcting their relative energy deficit (Fig. 8*D* and Suppl. Fig. 24*B*). Because Myc's promotion of the pro-anabolic and proliferative states is tightly coupled to increased mitochondrial mass and function [4], it seems possible that the previously reported transformation-resistance of AMPK-deficient cells is a consequence of their ATP deficit and/or their mitochondrial unresponsiveness, despite their ability to up-regulate aerobic glycolysis (Fig. 8*A*) [79, 187-189]. This idea has particular appeal given that numerous proliferative signaling pathways converge upon Myc whose uninterrupted expression is critical for maintaining tumor cell proliferation *in vivo* [122, 190, 191]. Thus, the seemingly paradoxical finding that AMPK suppression enhances proliferation yet confers transformation-resistance [187-189] can perhaps best be explained by postulating that the relative importance of AMPK on metabolism and proliferation may vary depending on Myc's level of expression and/or deregulation. Over-expression of Myc might therefore cooperate with AMPK's tendency to enhance glycolysis and Oxphos while simultaneously overriding its suppression of proliferation and the Warburg effect. This could be particularly useful under the most highly proliferative conditions where high anabolic demands could compromise and perhaps outstrip ATP stores (Fig. 8*E*). AMPK activation might then cooperate with Myc to enhance both glycolysis and Oxphos without exerting deleterious effects on proliferation and its reliance on the Warburg

effect. The relative resistance of AMPK-depleted cells to transformation could therefore reflect the cooperative nature of AMPK and Myc on these metabolic pathways.

Our transcriptional, proteomic and functional profiling underscores the significant differences that distinguish WT and KO cells both in the basal state and in response to Myc de-regulation (Fig. 10 and 11). Indeed, we note that more genes serving as regulators of mitochondrial-specific functions such as DNA replication, maintenance of genomic integrity and transcription were found to be AMPK-responsive than Myc-responsive (13 of 20 vs. 8 of 20) (Fig. 10*C*). It seems plausible that the widespread abnormalities in mitochondrial protein abundance and function described here are the ultimate consequence of this aberrant transcriptional regulation. Both the AMPK α1 and α2 subunits have been noted to localize to the nucleus as well as to the cytoplasm and a direct role for AMPK in transcriptional regulation has been suggested [192-194]. Moreover, a number of transcription factors, including PGC-1α and the carbohydrate response element binding protein, chREBP, which cooperates with Myc to regulate certain glucose-responsive genes [195] have been identified as putative AMPK targets [196-199]. Thus it is feasible that AMPK also alters many of the genes described here indirectly by virtue of its effects on key transcription factors many if not all of which are also direct Myc targets. Indeed, we note that several of the mitochondrial-related transcripts studied in Fig. 10*C* such as PPARγ, POLRMT, SIRT3, and UCP2 are completely discordant with respect to their Myc responsiveness in WT and KO cells. The unresponsiveness of KO cell mitochondria appears to reflect a generalized loss of normal coordination among these various factors that is apparent both in their basal state and in response to Myc de-regulation. Obvious targets for AMPK-mediated post-translational modification include any of the large number of members

that comprise the chromatin-modifying and transcriptional-enhancing protein complex that assembles in response to DNA binding by Myc [200, 201].

3.3.2 Co-operativity between Myc and AMPK in determining cellular redox state

Maintaining a reduced intracellular environment is believed to protect against excessive oxidation of free thiols and other groups, particularly those residing within the catalytic domains of critical enzymes [176]. Our finding that both cytoplasmic and mitochondrial compartments, particularly the former, were more oxidized in KO cells under basal conditions supports the idea that redox regulation is an important, although likely indirect, AMPK function. The additional observation that cytoplasmic oxidation increased equivalently in WT and KO cells in response to MycER activation suggests that AMPK is less important in this compartment for regulating this balance following sudden oxidative stress. That WT mitochondria became more reduced following MycER activation further indicates that the cytoplasmic and mitochondrial compartments are under distinct forms of redox regulation. Multiple, non-mutually exclusive mechanisms could explain these findings including differences in the levels of various factors that maintain the reduced state such as thioredoxins, manganese superoxide dismutase, peroxiredoxins and the NAD+/NADH ratio [202-204]. The failure of mitochondria to significantly alter their redox state following MycER activation likely reflects their general unresponsiveness as discussed above.

The inter-membrane space is one source of ROS, which arise primarily as a consequence of electron leakage across Complexes I and III of the ETC [205, 206]. Myc-mediated enhancement of Oxphos may increase the absolute amount of this leakage without compromising

ETC efficiency or integrity. The mitochondrial matrix is a second source of ROS, which originate from qualitative defects in ETC function as occurs in patients with respiratory chain mutations [206-208]. The compartmentalization of ROS from these two sources might well have different effects on the redox state, with the former source tending to contribute more to cytoplasmic oxidation and the latter to mitochondrial. MycER activation likely favors the generation of ROS via the first mechanism, and such ROS might be less able to oxidize roGFP residing in the matrix.

3.3.3 Changes in PK and PDH as a potential mechanism for metabolite differences between WT and KO MEFs

In response to MycER activation, WT cells underwent a redistribution of metabolic substrates that included the accumulation of selective glycolytic intermediates and a depletion of TCA cycle intermediates (Fig. 13*A*). One explanation for these findings is an increased reliance on the Warburg effect, which is often accompanied by a shift from the M1 to the M2 PK isoform. The latter possesses a lower affinity for PEP thus slowing its conversion to pyruvate and allowing more time for the accumulation of upstream substrates and their diversion into anabolic pathways [19, 182, 183, 185, 186]. Although we did not detect significant changes in the PKM1:PKM2 ratio upon MycER activation in WT cells (Suppl. Fig. 30), we did observe a decrease in total PK activity (Fig. 13*D*). This by itself could explain the accumulation of substrates upstream of PEP thereby limiting the conversion of pyruvate to acetyl CoA. It could also account for the observed depletion of TCA cycle intermediates in response to the Myc-mediated increase in Oxphos (Fig. 13*A*). A second possibility is that the enhanced glycolysis

mediated by MycER activation in WT cells supplies sufficient levels of substrates for both the Warburg effect and Oxphos. This could explain the increased production of lactate and accompanying extracellular acidification in response to MycER (Fig. 8*A*). Taken together, increased glycolysis, an overall buildup of intermediates due to reduced PK, combined with increased mitochondrial activity and a depletion of TCA cycle substrates, could explain many, if not all, of the metabolite shifts detected in WT cells in response to Myc activation. However, this change is not without its energetic costs as evidenced by the accompanying chronic ATP depletion, higher levels of AMP and AMPK-activation (Fig. 8*D* and *E* and 13*A*).

KO cells in their basal state were relatively depleted of glycolytic substrates and oversupplied with TCA cycle intermediates compared to WT cells (Fig. 13*A*). Although the activities of PK and PDH were substantially different between these 2 cell lines (Fig. 13*C* and *D*), the fact that levels of PEP, pyruvate and AcCoA were actually quite similar (Fig. 13*A* and *E*) argues against the idea that significant changes in any of these could account for the differential levels and distribution of downstream TCA cycle substrates. Rather, the accumulation of TCA cycle intermediates most likely reflects the consequences of the loss of AMPK in these cells as manifested by their inability to properly coordinate the mitochondrial response. The ultimate result is even lower levels of ATP and higher levels of AMP in KO cells both in the resting state and in response to MycER activation (Fig. 8*D* and 12*A* & Suppl. Fig. 24).

3.3.4 Cross-talk between Myc and AMPK

The wide-ranging differences between WT and KO cells in response to MycER activation reported here demonstrate that Myc and AMPK likely engage in a complex cross-talk, the

presumed purpose of which is to correctly balance anabolic and proliferative needs with cellular energy levels (Fig. 14). The need for maintaining this balance is most dramatically illustrated by the rapid and dramatic reduction of ATP levels that follow MycER activation in WT cells and by the even steeper decline in KO cells (Fig. 8*D* and Suppl. Fig. 24). This ATP-mediated cross-talk between AMPK and Myc has been previously demonstrated in *myc-/-* rat fibroblasts in which AMPK is constitutively activated as a result of the inability to maintain normal levels of ATP due to the overall failure of Myc-dependent glycolysis and Oxphos [4, 11]. Thus, balancing ATP production and AMPK activation and with anabolic demands is a process that occurs in response to both Myc over- and under-expression.

Other potential mediators of the cross-talk between Myc and AMPK, that are largely independent of but linked to ATP levels, are ROS which, in the examples provided here, contribute extensively to AMPK activation (Fig. 8*G*). ROS are well-known second messengers that are rapidly generated in response to many different growth stimuli and the large increase in ETC function that accompanies Myc over-expression [4, 152, 209, 210]. Their ability to maintain AMPK in an active state, even beyond the point at which ATP levels have normalized (Fig. 8*E-H*) suggests that ROS might serve to limit growth factor-mediated proliferation at a point before which ATP levels are compromised and might also serve to more rapidly restore ATP levels to normal following a proliferative signal.

In retrospect, a close relationship between Myc and AMPK might have been anticipated given their well-known regulation of a variety of similar processes as noted above. A similar relationship has also been previously suggested by Liu *et al.* [80] who showed that ARK5, an upstream regulator of AMPK, could also affect several cellular functions that are relevant to Myc. These included the ability of ARK5 to protect against Myc-mediated apoptosis, to increase

oxygen consumption, to negatively regulate cell size and to promote cell cycle progression. However, many of the consequence of ARK5 suppression in cancer cells were not observed in the current study. Perhaps most importantly, and unlike the case with AMPK described here, the depletion of ARK5 in transformed cells had little influence on the expression of Myc target genes [80]. Taken together, these observations suggest that, while ARK5 and AMPK operate within the same pathway, their communication with Myc may occur by distinct mechanisms, may be cell-type specific and may serve distinct purposes.

3.4 EXPERIMENTAL PROCEDURES

3.4.1 Cell culture

SV40 T-antigen-immortalized *ampk+/+* and *ampk-/-* MEFs, the latter bearing a double knockout of the α1 and α2 subunits of AMPK, were a kind gift from Dr. Benoit Viollet (Institut Cochin, Université Paris Descartes) and Dr. Keith Laderoute (Discovery Technologies, SRI International) [211, 212] and were generated as described by Laderoute *et al.* [189]. Both cell lines were transduced with a pBabePuro retroviral vector encoding a Myc-estrogen receptor (MycER) fusion protein [151]. Stable clones of each AMPK genotype (hereafter referred to as WT or KO) were selected in 1 μg/ml of puromycin, pooled, and used for all subsequent experiments. Both WT and KO cells expressed equivalent levels of MycER (Suppl. Fig. 24*A*). All cell lines were maintained in puromycin-containing Dulbecco's-modified Eagle's minimal essential medium (D-MEM) supplemented with 10% heat-inactivated fetal bovine serum (FBS), L-glutamine and

penicillin/streptomycin as previously described [4]. Unless otherwise stated, MycER was activated by adding 4-hydroxytamoxifen (4HT) to cells for 7-9 days at a final concentration of 250 nM before performing any assessments. All recombinant DNA and retroviral and lentiviral work was approved by the University of Pittsburgh Recombinant DNA and Institutional Biosafety Committees and, in the latter cases, was performed under BSL2+ conditions.

3.4.2 Quantification of glycolysis, Oxphos and ATP levels

All experiments were performed on an XF24 Extracellular Flux Analyzer (Seahorse Bioscience, Billirica, MA) as previously described [4, 11]. O_2 consumption rate (OCR) and proton production, expressed as the extracellular acidification rate (ECAR), were quantified in unbuffered D-MEM containing 8.3 g of glucose- and pyruvate-free DMEM (Sigma) supplemented with 31 mM NaCl, 2 mM glutamine, 42.3 µM phenol red, and 25 mM glucose, pH 7.4 to obtain baseline metabolic levels. A mitochondrial stress-test was applied by adding 1 µM oligomycin, 0.3 µM FCCP, 100 mM 2-deoxyglucose (2-DG), and 1 µM rotenone. Each measurement point was performed in quadruplicate and experiments were repeated at least 3 times with similar results and normalized to cell number at the conclusion of the experiment. Relative effects were expressed as areas under the curve measurements that were generated by the manufacturer's software.

ATP assays were performed on 20,000–30,000 cells seeded in 96 well plates the day before and were performed in quadruplicate wells using the ATPlite Luminescence Assay System (Perkin Elmer, Waltham, MA) as instructed by the manufacturer. Results were normalized to total protein levels, which were determined on separate sets of identical wells.

3.4.3 Measurements of mitochondrial mass and reactive oxygen species (ROS)

Mitochondrial mass was determined as previously described [4, 11]. Monolayers were stained at 37C for 45 min in fresh D-MEM containing 20 nM of acridine orange 10-nonyl bromide (NAO), 0.5 mM of MitoTracker Green, 10 µM of CM-H2-DCFDA or 5 µM of MitoSox (all from Invitrogen, Carlsbad, CA)) and then analyzed using a FACStar flow cytometer (Becton-Dickinson Biosciences, San Jose, CA). Analyses were performed using BD FACSDiva Software as previously described [4].

3.4.4 Blue native gel electrophoresis (BNGE) and electron transport chain (ETC) enzyme assays

Samples were prepared for BNGE as previously described with some modifications [4]. Cells were suspended in 0.5 ml of ice cold HB buffer (50 mM KPO_4, pH=7.4; 1mM EDTA; 2.5% glycerol; 250 mM sucrose) containing protease inhibitor cocktail (Sigma-Aldrich, St. Louis, MO), disrupted on ice with a dounce homogenizer (Isobiotec, Heidelberg, Germany) and enriched for mitochondria by differential centrifugation. The pellet was washed twice with HB buffer and re-suspended in the same buffer at a final protein concentration of 2-5 mg/ml. To achieve optimal solubility of mitochondrial super-complexes/complexes, the digitonin concentration was optimized so that 8 mg of digitonin was added per mg of protein in HB buffer without EDTA. Following a 20 min incubation on ice, a Coomassie blue solution (5% Coomassie blue G250 in 750 mM 6-aminocaproic acid) was added (1:30 v/v). The supernatant was then electrophoresed on a 3–12% Native PAGE Novex Bis-Tris gel (Invitrogen) at 80 V for

4 hours at 4C in the buffer provided by the supplier. 80 µg of protein for each sample was electrophoresed to resolve complexes. Following electrophoresis, gels were stained for 30 min with Bio-Safe Coomassie G250 (Bio-Rad, Hercules, CA). Gels were scanned and the images analyzed for relative band density using AlphaEaseFC 2200 scanner and AlphaEaseFC software.

In situ gel assays of individual ETC complex activities were performed as previously described for Complexes I (NADH ubiquinone oxidoreductase) and V (ATPase) [213]. Complex III (CIII) (decylubiquinol cytochrome c oxidoreductase) was assayed by incubating gels with CIII assay solution [214] overnight with mild agitation. In a separate reaction, Complex IV (CIV) (cytochrome c oxidase) was measured by incubating the gel in a solution containing 1 nM catalase, 10 mg cytochrome c and 750 mg sucrose in CIII assay buffer with mild agitation for 30 min. An optional wash in water at room temperature was employed for 24 hours to further sharpen the band patterns. Band intensities were quantified using NIH Image J software and were normalized with their corresponding bands on the Coomassie stained gel.

In situ assays for Complex II (CII) (succinate dehydrogenase) proved to be relatively insensitive and irreproducible. We therefore measured this activity on mitochondria purified as described above using a method from Munujos *et al*. [12] modified for a 96 well plate format. As a negative control, an inhibitor of CII (0.5 mM thenoyltrifluoro-acetone) was added to a separate set of samples. Activity was assessed at 500 nm for 1 hour every minute on a BMG LabTech FLUOstar Omega spectrophotometer. The ΔAbs_{340}/min was obtained using the maximum linear rate over a period of 20 min.

3.4.5 RNA extraction and real-time qRT-PCR analysis

Total RNA was extracted from logarithmically growing cells and purified using an RNAeasy Mini kit (Qiagen, Inc., Chatsworth, CA) as previously described [11]. qRT-PCR reactions were performed with a Power SYBR Green RNA-to-CT™ 1-Step Kit (Life Technologies/Thermo-Fisher, Inc.) with a StepOnePlus Real-Time PCR System (Applied Biosystems, Inc. Carlsbad, CA). All primers were synthesized by International DNA Technologies, Inc. (Coralville, IA). Reactions were optimized so that single bands of the predicted size were visualized following gel electrophoresis. The real-time PCR results were calculated as relative expression after normalization to the internal standard β_2 microglobulin using $\Delta\Delta$CTs compared to WT cells. Statistical analyses were performed using Student's t-test. All primer sequences and amplification conditions are listed in Table 4.

Table 4: qRT-PCR primers used in Chapter 3

Symbol	Description (mRNA)	Gen Bank ID	Forward Primer Sequence (5' → 3')	Reverse Primer Sequence (5' → 3')	Anneal Temp.	Product Length (bps)
ACLY	ATP citrate lyase	BC056378.1	ACCCTTTCACTGGGGATCACA	GACAGGGATCAGGATTTCCTTG	56	65
Alt1	Alanine Aminotransferase1	BK005127.1	TCCAGGCTTCAAGGAATGGAC	CAAGGCACGTTGCACGATG	55	113
Cit Synth	citrate synthase	BC029754.1	GGACAATTTTCCAACCAATCTGC	TCGGTTCATTCCCTCTGCATA	55	109
ERRα	estrogen related receptor, alpha	NM_007953	GCCTCCAATGAGTGTGAGATC	TTTGTACTTCTGCCGTCCG	60	138
ERRβ	estrogen related receptor, beta	NM_011934	CATGAAATGCCTCAAAGTGGG	AAATCGGCAGGTTCAGGTAG	60	125
FBP1	fructose 1,6-bisphosphatase 1	NM_019395	GACTGGGGATCAAGTAAAGAAGC	AGGTAGCGTAGGACGACTTCA	55	80
FH1	Fumerate Hydratase	NM_010209.2	GAATGGCAAGCCAAAATTCCTT	TCTTACGGTCTGAGCACCATAA	55	95
G3PDH (cyto)	cytosolic glycerol-3-phoshate dehydrogenase 1	NM_010271	ATGGCTGGCAAGAAAGTCTG	CCTGCATTGCTACCCACGAT	51	80
G3PDH (mito)	mitochondrial glycerol-3-phoshate dehydrogenase 1	U60987	ATGGCGTTTCAAAAGGCAGTG	ACGGAGGAGGTCCCAAAACAG	51	79
G6P	glucose-6-phosphatase (catalytic)	U00445.1	CGACTCGCTATCTCCAAGTGA	GGGCGTTGTCCAAACAGAAT	60	208

GOT1	asprate aminotransferase isoenzyme, glutamine oxaloacetate transaminase	J02623.1	GCGCCTCCATCAGTCTTTG	ATTCATCTGTGCGGTACGCTC	55	133
IDH1 (cyto)	isocitrate dehydrogenase - cytosolic	NM_001111320	ATGCAAGGAGATGAAATGACACG	GCATCACGATTCTCTATGCCTAA	55	116
IDH2 (mito)	isocitrate dehydrogenase 1 (NADP+) mitochondrial	U51167	AAGAGCCCTAACGGAACGAT	TCTTTGGGGTGAAGACCAAC	51	202
IDH3 (cyto+mito)	isocitrate dehydrogenase3 - mito, (NAD+), alpha	NM_029573	TGGGTGTCCAAGGTCTCTC	CTCCCACTGAATAGGTGCTTTG	55	177
MDH (cyto)	cytosolic malate dehydrogenase	NM_008618	GAACCAATCAGAGTCCTTGTGAC	GGCACAGTCTTGCAGTTCCA	51	177
MDH (mito)	mitochondrial malate dehydrogenase	NM_008617	GCAACCCCTTTCACTCCTG	TCTGGTCTCAATGTGACTCAGAT	51	112
Mterf1	Mitochondrial transcription termination factor 1a	NM_001013023.2	GTTCCTTTGCTCTGTTGGATTG	GAAAGCAGCCTCTCTCTTATGT	60	363
Mterfd1 (Mterf3)	MTERF domain containing 1	NM_025547.3	TCATCGTCAAGTTTCCACAGT	AGGTTTTGCTGGGTCATACTG	60	107
Mterfd2 (Mterf4)	MTERF domain containing 2	NM_178051.3	CAGATGCCCCACTGTTTTG	TGTGTCTCTGCTTGATCTTGG	60	146
NFE2L2 (NRF2)	Nuclear factor, erythroid derived 2, like 2	NM_010902.3	TCCCATTTGTAGATGACCATGAG	CCATGTCCTGCTCTATGCTG	60	150
NRF1	nuclear respiratory factor 1	NM_010938	AATGTCCGCAGTGATGTCC	GCCTGAGTTTGTGTTTGCTG	60	149
NSUN4	NOL1/NOP2/Sun domain family, member 4	NM_028142.4	CCAAGTCCGAGTTACCTCATG	TCTTCCTTGACCGCTGAAAG	60	149
PC	Pyruvate carboxylase	L09192.1	CTGAAGTTCCAAACAGTTCGAGG	CGCACGAAACACTCGGATG	55	162
PdhE1a	pyruvate dehydrogenase E1 alpha 1 (Pdha1), mitochondrial protein	NM_008810.2	GAAATGTGACCTTCATCGGCT	TGATCCGCCTTTAGCTCCATC	55	123
PDK1	Pyruvate dehydrogenase kinase, isoenzyme 1, mitochondrial	NM_172665	GGACTTCGGGTCAGTGAATGC	TCCTGAGAAGATTGTCGGGGA	56	122
PDP2	pyruvate dehydrogenase phosphatase regulatory subunit	NM_198308.1	AAGACAAAGGACTAGCCCAGG	GATAGGCCACGGATGTACCC	55	146
PEPCK	phosphoenolpyruvate carboxykinase 2, mitochondrial	NM_028994.2	ATGGCTGCTATGTACCTCCC	GCGCCACAAAGTCTCGAAC	55	148
PGC1α	peroxisome proliferative activated receptor, gamma, coactivator 1 alpha	NM_008904	CACCAAACCCACAGAAAACAG	GGGTCAGAGGAAGAGATAAAGTTG	60	125
PGC1β	peroxisome proliferative activated receptor, gamma, coactivator 1 beta	NM_133249	GGTGTTCGGTGAGATTGTAGAG	GTGATAAAACCGTGCTTCTGG	60	72
PKM1	Pyruvate Kinase, Muscle, isoform 1	NM_01253883	TTGTGCGAGCCTCCAGTC	ACTCCGTGAGAACTATCAAAGC	55	106
PKM2	Pyruvate Kinase, Muscle, isoform 2	NM_011099	TTGCAGCTATTCGAGGAACTCCG	CACGATAATGGCCCCACTGC	55	115
POLRMT	Polymerase (RNA) mitochondrial (DNA directed)	NM_172551	AGAAGCCCAACACTCTGAAG	ATGTGTCCAGAAGCAGTCG	60	146
PPARα	peroxisome proliferator activated receptor alpha	NM_011144	CATTTCCCTGTTTGTGGCTG	ATCTGGATGGTTGCTCTGC	60	133
PPARβ	peroxisome proliferator activator receptor delta	NM_011145	GGAAAAGTTTTGGCAGGAGC	TGTCTTCATCTGTCAGTGAGC	61	149
PPARγ	peroxisome proliferator activated receptor gamma	NM_011146	ATAGGTGTGATCTTAACTGCCG	CCAACAGCTTCTCCTTCTCG	60	147

PRC	peroxisome proliferative activated receptor, gamma, coactivator-related 1	NM_001081214	ACTCAGGCATTGACATTCCC	TTTCGCCAAGAGTGAGACAG	61	146
SDH a	Succinate dehydrogenase subunit A	NM_023281	GGAACACTCCAAAAACAGACCT	TCCACCACTGGGTATTGAGTAG	51	106
SDH b	Succinate dehydrogenase subunit B	NM_023374	ATTTACCGATGGGACCCAGAC	GTCCGCACTTATTCAGATCCAC	51	79
SDH c	Succinate dehydrogenase subunit C	NM_025321	GCTGCGTTCTTGCTGAGACACA	ATCTCCTCCTTAGCTGTGGTT	51	110
SDH d	Succinate dehydrogenase subunit D	NM_025848	TGGTCAGACCCGCTTATGTG	GAGCAGGGATTCAAGTACCCA	51	193
Ser-HMT	Serine Hydromethyltransferase	AF237702.1	CAGGGCTCTGTCTGATGCAC	CGTAACGCGCTCTTGTCAC	57	91
SIRT3	NAD-dependent deacetylase sirtuin-3, mitochondrial	NM_022433	CGGCTCTATACACAGAACATCG	CATCAGCCCATATGTCTTCCC	61	145
TFAM	Transcription factor A, mitochondrial	NM_009360	CACCCAGATGCAAAACTTTCAG	CTGCTCTTTATACTTGCTCACAG	58	147
TFB2M	Transcription factor B2, mitochondrial	NM_008249	ACCAAAACCCATCCCGTC	TCTGTAAGGGCTCCAAATGTG	60	141
Tha1	Threonine aldolase	NM_027919.4	CTCAGTGGTCTAGGAATTGGGC	GTCTTCGCCGTAATCATCGTC	55	137
UCP2	Mitochondrial Uncoupling Protein 2	NM_011671	GCATTGGCCTCTACGACTC	AAGCGGACCTTTACCACATC	60	145
YY1	YY1 transcription factor	NM_009537	GATACCTGGCATTGACCTCTC	ATAGCAGAGTTATCCCTGAACATC	60	147
αKGDH (DLD)	dihydrolipoamide dehydrogenase, mitochondrial protein	NM_007861.4	GAGCTGGAGTCGTGTGTACC	CCTATCACTGTCACGTCAGCC	55	138
αKGDH (DLST)	dihydrolipoamide S-succinyltransferase (E2 component of 2-oxo-glutarate)	NM_030225.4	GGAACTGCCCTCTAGGGAGA	GACGCTACCACTGTTAATGACC	55	101
αKGDH (OGDH)	alpha ketogluterate dehydrogenase	NM_001252282	AGGGCATATCAGATACGAGGG	CTGTGGATGAGATAATGTCAGCG	51	106

3.4.6 Immunoblotting

Blotting were performed as previously described [4, 11]. All relevant antibodies used are listed in Table 5.

Table 5: Antibodies used in Chapter 3

Name of antibody	**Description**	**Host Species**	**-**	**Vendor**	**Catalog no.**	**dilution**
AMP-dependent protein kinase alpha (AMPK)	Polyclonal	Rabbit	IgG	Cell Signaling	2532S	1:1000
pAMPK(Thr_{172}) (D79.5E)	Monoclonal	Rabbit	IgG	Cell Signaling	4188S	1:1000
Pyruvate dehydrogenase E1 subunit (PDH) (D6)	Monoclonal	Mouse	IgG2a	Santa Cruz	sc-377092	1:1000
pPDH E1 (Ser_{293})	Polyclonal	Rabbit	IgG	EMD	AP1062	1:4000

				Millipore		
Pyruvate dehydrogenase kinase (PDK1)	Monoclonal	Rabbit	IgG	Cell Signaling	3820S	1:1000
Pyruvate dehydrogenase phosphatase 2 (PDP2)	Polyclonal	Rabbit	IgG	Biovision	3944-200	1:500
Pyruvate kinase M1 isoform (PKM1)	Monoclonal	Rabbit	IgG	Cell Signaling	7067S	1:1000
Pyruvate kinase M2 isoform (PKM2)	Polyclonal	Rabbit	IgG	Cell Signaling	3198S	1:1000
β-actin	Monoclonal	Mouse	IgG2b	Cell Signaling	3700S	1:10000

3.4.7 Mitochondrial oxidoreductase assays

The assay for malic dehydrogenase (MDH) relied on the conversion of oxaloacetate (OAA) to malate coupled with NADH to NAD+, which was measured using Protocol SPOXAL01 (Sigma-Aldrich). The ΔAbs_{340}/min was obtained as described above.

α-ketoglutarate dehydrogenase (α-KGDH) was quantified by measuring the conversion of α-ketoglutaric acid (α-KG) to succinyl-CoA coupled to NAD+ conversion to NADH as described in Protocol SPKETO03 (Sigma-Aldrich). The ΔA_{340nm}/min was calculated over 15 min using the maximum linear rate.

Isocitrate dehydrogenase (IDH) activity was quantified on 10 µg of mitochondria using an IDH Activity Assay Kit according to the directions provided by the supplier (Sigma-Aldrich). Absorbance was measured at 37C at OD_{450nm} every 5 minutes over 2 hr. with a final reading taken at the plateau stage.

Glycerol 3-phosphate dehydrogenase (G3PDH) was assayed using a G3PDH Assay Kit (Abcam, Inc., Burlingame, CA) with 10 µg of mitochondria and quantified as recommended by the manufacturer. End point absorbance (Abs_{450}) was corrected for background controls. All enzyme assays were performed on at least triplicate samples

3.4.8 Enrichment and Tryptic Digestion of MEF Mitochondrial Proteins

16 MEF samples (4 each of WT, KO, WT+Myc and KO+Myc) were separately enriched for mitochondrial proteins from 10^7 cells prepared from individual plates as described for BNGE. Protein concentrations were determined using a BCA assay (Pierce, Inc., Rockford, IL). A pooled control sample was prepared by combining equal volumes of each individual sample and was used to monitor sample preparation variation. 22 aliquots (16 samples and 6 controls) containing 20 µg of total protein were spiked with 4 µl of 125 nM ovalbumin protein. In-solution trypsin digestion was carried out as described [215]. The resulting tryptic peptides were desalted with PepClean C-18 Spin Columns (Pierce) according to the manufacturer's protocol, vacuum-dried, and resuspended in 20 µl 0.1% formic acid.

3.4.9 LC-MS/MS Analysis

Tryptic digests were analyzed using high resolution liquid chromatography tandem accuracy mass spectrometer as previously described [216]. In brief, samples were loaded with a nanoAcquity autosampler (Waters, Waltham MA) onto a capillary sample trap column, separated using a reversed phase gradient on a commercial PicoChip nanospray C18 column (PicoChip) and electrospray ionization source (New Objective, Inc. Woburn MA). Mass analysis was performed on a hybrid electrosprayed into a LTQ/Orbitrap Velos hybrid mass spectrometer (Thermo Fisher). Data dependent acquisition consisted of cycles of a high resolution full scan FT mass spectrum followed by 13 MS/MS low resolution tandem mass spectra scans in the linear ion trap, with dynamic exclusion setting enabled to minimize redundant selection of precursor

ions previously selected for CID. High-resolution liquid chromatography mass spectrometry was used to measure the mass-to-charge ratio, retention time, and intensity of the isotopes for each identified peptide (for example, see Suppl. Fig.29). Custom differential mass spectrometry software (dMS 1.0, University of Pittsburgh and InfoClinika, Seattle WA) was used to align, integrate, and link the high resolution peak areas data to the protein identification results from a COMET to the tandem MS sequence database search results [217]. In total, detection of 414,655 isotope distributions, 9,397 peptide sequences, and 1929 protein identifications were obtained from this data set (available upon request).

3.4.10 Selection of Mitochondrial Proteotypic Peptides

Intensities of a single representative peptide were used as surrogate markers for relative abundance of each protein. Proteotypic representative peptides were selected based upon their signal intensities and their correlation with other peptides originating from the same protein. Proteins with a single identified peptide sequence or with poor concordance among identified peptides were excluded from further analysis. For the remaining proteins, peptides with the highest signal intensities (average of all samples) among those with good correlation with other peptides from the same protein (mean Pearson's correlation coefficient >0.5) were selected as representative peptides. A total of 345 peptides belonging to proteins annotated as having evidence of mitochondrial localization in the David (http://david.abcc.ncifcrf.gov/) Bioinformatics Database and/or mouse MitoCarta Inventory (http://www.broadinstitute.org/pubs/MitoCarta/mouse.mitocarta.html) were selected and their high resolution peak area extracted using dMS software were used for statistical analysis.

3.4.11 Statistical Analysis

Two way ANOVA was used to determine the influence of AMPK genotype and Myc over-expression on the abundance of mitochondrial proteins, and also to determine whether there was any significant interaction effect between AMPK genotype and Myc over-expression (i.e. whether a protein's response to Myc was discordant between WT and KO cells). Features were selected based on a q value (false discovery rate) cutoff of 0.05. Myc over-expression did not affect the overall abundance of mitochondrial proteins (p values for student's t test comparison of WT vs. WT + Myc and KO vs. KO + Myc were 0.870 and 0.761 respectively). However, we did observe a 24% higher average intensity of all mitochondrial peptides in KO samples both with and without Myc over-expression (two-way analysis of variance [ANOVA] p value of 0.002) despite the overall intensities of non-mitochondrial proteins being otherwise identical. This could be due to a slightly greater overall mitochondrial mass in KO cells although this was not confirmed by staining with NAO or MitoTracker dyes (Fig. 8*C*). To reduce the potential effect of bias due to slightly higher amounts of mitochondrial proteins in the KO samples, proteins with greater abundance in KO but with fold change less than 2.6 (twice the fold change of overall mitochondrial abundance in KO samples) were not considered for the main effect of genotype.

3.4.12 Expression of roGFP2

roGFP2 was a generous gift from Dr. Michael Palladino (The Univ. of Pittsburgh). Compared to GFP, roGFP2 contains several amino acid substitutions, including S147C and Q204C, which

allow the molecule to form stable intra-molecular disulfide bonds in reduced environments [176]. Oxidation of these residues alters the tertiary structure of the protein as well as the intensity of 510 nm light emitted following alternating excitation at 410 nm and 474 nm [180].

We used standard molecular biology techniques to insert roGFP coding sequences into the pDsRed2-Mito vector (Clontech, Inc., Mountain View, CA) from which the DsRed insert had been excised. This step placed the roGFP coding sequence downstream from and in-frame with the mitochondrial targeting signal peptide from subunit VIII of the human cytochrome c oxidase ETC subunit (roGFP-mito). To generate a cytoplasmically-localized roGFP2 vector (roGFP-cyto), the roGFP-mito vector was digested with NheI and BamHI to excise the mitochondrial signal peptide and the subsequently blunt-ended vector was self-ligated. The coding region of each vector was then amplified by PCR and cloned directionally into the pLenti6/V5-TOPO lentiviral vector (Life Technologies, Inc.). After packaging in 293FT cells, WT and KO MEFs were transduced with each vector and selected in 1 μg/ml of blasticidin. Pooled blasticidin-resistant clones were then further selected by fluorescence-activated cell sorting in order to purify the brightest population, which were used for all subsequent experiments.

3.4.13 Confocal microscopy and flow cytometry of roGFP-mito- and roGFP-cyto-targeted cells

WT and KO cells stably expressing roGFP-cyto and roGFP-mito were grown overnight in glass bottom 6 well plates. Fresh medium lacking or containing 4HT was then added for an additional 24 hr. Confocal images of live cells were obtained with a confocal laser scanning microscope (LSM710; Zeiss) using a 20x/0.8 M27 Plan-Apochromat objective and a 31 μm pinhole with the

following excitation/emission wavelength (λex/em) settings: λex/em 405/495-575 for oxidized roGFP, λex/em 488/495–575 for reduced roGFP. To quantify changes in the cellular redox states, analyses were performed by flow cytometry on a BDFACS Aria II SORP using BD FACSDiva Software and ratios were calculated using FlowJo software. Spectra were collected using a violet laser with 405 nm excitation, emission collected using a 525/50 bandpass filter and 488 nm excitation was collected using an emission bandpass of 520/50. Control experiments to determine maximal responses to oxidized and reduced environments were performed by adding H_2O_2 or DTT to final concentrations of 1 mM or 10 mM, respectively for 30 min prior to flow cytometry. A third sample was treated with H_2O_2 for 30 min followed by the addition of DTT for an additional 30 min and then analyzed. In all cases, biological triplicates were assessed for each group and each experiment was repeated at least twice. Results were expressed as the mean ratio of oxidized: reduced fluorescent roGFP based on changes in emission spectra.

3.4.14 High performance liquid chromatography-electrospray ionization tandem mass spectrometry (HPLC-ESI-MS/MS)

Analyses were conducted on a Q Exactive mass spectrometer with on-line separation by Dionex Ultimate 3000 HPLC (both from Thermo Fisher, San Jose, CA). For untargeted quantification of polar metabolites, ~10^9 cells were extracted in 80% methanol at 0^oC and then incubated at -20 °C for 1 h. Thermo SIEVE (Thermo Fisher) was used for peak alignment and integration of MS results to derive the relative abundance of individual metabolites. For ATP analysis,10^9 cells were extracted at 0^0 C in 15% trichloroacetic acid (TCA) containing ([$^{13}C_{10}$,$^{15}N_1$]ATP) as an internal standard. An aliquot of the clarified sample was then directly injected. Quantification

was performed by integrating the extracted ion chromatograms of each metabolite, which were then compared with a standard curve.

For the analysis of polar metabolites, lysates from sub-confluent cell cultures were prepared as described above, clarified by centrifugation, and the supernatants were placed in autosampler vials. HPLC-ESI-MS/MS was performed on a Q Exactive mass spectrometer (Thermo Fisher) with on-line separation by Dionex Ultimate 3000 HPLC (Thermo Fisher). HPLC was performed as described by Paredes *et al.* [218], with some modification: column, Luna NH_2, 3 μm, 2 x 150 mm (Phenomenex, Inc., Torrance, CA); mobile phase A, 5% acetonitrile in water with 20 mM ammonium acetate and 20 mM ammonium hydroxide, pH 9.45; mobile phase B, acetonitrile; flow rate, 300 μL/min; gradient, 85%-1% B over 10 minutes and held at 1% B for 10 minutes. Full scan mass spectra were acquired in the orbitrap using negative ion detection over a range of m/z 100 – 800 at 70,000 resolution (m/z 300). Metabolite identification was based on the metabolite accurate mass (± 5 ppm), manual interpretation of the MS/MS fragment patterns, and agreement with the HPLC retention time of authentic standards. Thermo SIEVE was again used to process raw data files in order to quantify metabolites of interest. Peak alignment and integration were performed and relative abundances of each metabolite were generated among different samples.

Nucleotides were quantified from cell lysates prepared as described above. Cell pellets were extracted at 4° C with 15% TCA containing $^{13}C,^{15}N$-ATP as the internal standard, and then neutralized with a mixture of trioctylamine and 1,1,2-trichlorotrifluoroethane. LC-MS analyses were performed on a Q Exactive mass spectrometer with on-line separation using Dionex Ultimate 3000 HPLC (both from Thermo Fisher). HPLC conditions similar to those detailed in Zhou *et al.* [219], with some exceptions: Waters XTerra-MS C18 column (3.5 μm, 2.1 x

150mm); mobile phase A, 5 mM hexylamine and 0.5% diethylamine in water, pH10; mobile phase B, 50% acetonitrile in water; flow rate, 400 μL/min; gradient, 1%-20% B over 10 minutes and followed by 20%-30%B over 5 minutes. Full scan mass spectra were acquired in the orbitrap using negative ion detection over a range of m/z 300-800 at 70,000 resolution (m/z 300). Identification of metabolites was based on the metabolite accurate mass (± 5 ppm) and agreement with HPLC retention times of standards. Quantification was achieved by integrating the extracted ion chromatograms of individual metabolites and compared with the appropriate standard curves.

3.4.15 Pyruvate dehydrogenase (PDH), pyruvate kinase (PK) assays, and acetyl CoA assays

PDH activity was quantified using the PDH Enzyme Activity Microplate Assay Kit according to the directions provided by the supplier (MitoSciences, Eugene, OR). Triplicate samples were loaded at 1 mg/well, measured kinetically over 30 min and the rates were determined as changes in OD (ΔOD) over time.

PK activity was determined using a modified protocol from Worthington Biochemical Corp (Lakewood, NJ) in which the conversion of phospho(enol)pyruvate (PEP) to pyruvate by PK is coupled to the conversion of lactate to pyruvate and the generation of NAD+. 1 plate of semi-confluent cells was trypsinized and resuspended in 50 mM imidazole HCl buffer, pH 7.6 containing 12 mM KCl and 62 mM MgSO4 at 10^6 cells/ml. 100 μl of cells were dispensed into individual wells of a 96 well plate containing a reaction solution whose final components consisted of 1.36 mM ADP, 1.36 mM PEP, 0.4 mM NADH and 40-45 U of lactate

dehydrogenase in imidazole buffer to a final volume of 200 µl. NADH conversion to NAD+ was measured at 340 nm for 15 min and the rate was determined by ΔAbs_{340}/min from quadruplicate reactions.

Acetyl CoA was assayed using an Acetyl Coenzyme A assay kit and was performed as recommended by the supplier (Sigma-Aldrich). Samples were prepared as described by Edmunds *et al.* [11]. Triplicate samples were compared to a 1 nmol standard curve using a SpectraMax M2 fluorescence plate reader and analyzed by Students's t-test.

4.0 ABNORMAL LIPID PROCESSING BUT NORMAL LONG-TERM REPOPULATION POTENTIAL OF *MYC-/-* HEPATOCYTES

4.1 INTRODUCTION

A direct role for the c-Myc (Myc) oncoprotein in promoting and/or sustaining neoplastic growth was first demonstrated over 35 years ago [220]. This has been subsequently supported by studies documenting recurrent *MYCC* de-regulation in

human tumors, from animal models of Myc over-expression and from demonstrations that Myc silencing in these models promotes tumor regression [221, 222]. Although Myc supervises many of the pathways that are commonly perturbed in cancer such as those regulating differentiation, proliferation, survival and metabolism [15, 16], its precise role in these processes and its function(s) in normal cells have been somewhat more controversial and, at times, subject to conflicting experimental outcomes.

A requirement for Myc is well-established in the developing mouse where *myc-/-* embryonic lethality occurs at E9.5-10.5 as a result of placental insufficiency and cardiac and neural tube defects [223]. Postnatally, Myc silencing is compatible with long-term survival and is associated with only mild and reversible toxicities in proliferative tissues such as the bone marrow and gastrointestinal track [86]. Moreover, haplo-insufficiency of Myc actually slows the onset of numerous age-related pathologies and prolongs life span by approximately 15% [78]. In

contrast, the *in vitro* proliferation of primary murine embryonic fibroblasts declines progressively as Myc levels are reduced [84]. Thus, the consequences of Myc loss in normal cells appear to be more tissue- and context-dependent and variable than in transformed cells [84].

Myc's presumptive role in hepatic regeneration rests in part on the observation that it is induced within minutes of partial hepatectomy and is silenced following restoration of normal liver mass [224]. However, the actual requirement for Myc in this process has varied among different studies which have not always assessed identical parameters [87, 89, 225]. These reports also relied exclusively on hepatic regeneration following PH, which occurs over a relatively short time frame, requires <2 population doublings by the remaining hepatocytes and can also be influenced by the deletion of Myc in cells other than hepatocytes [89]. For these reasons, we sought here to assess Myc's role in hepatocyte proliferation by utilizing a novel mouse model of liver regeneration that imposes fewer restrictions on hepatocyte replication.

Type I hereditary tyrosinemia is a metabolic disorder caused by defective production of fumarylacetoacetate hydrolase (FAH), which catalyzes the final step in hepatic tyrosine catabolism. In HT, the toxic upstream metabolites fumaryl- and maleyl-acetoacetate accumulate and cause liver failure [226]. Deletion of the murine *fah* gene faithfully mimics the human disease [227]. Hepatocyte death in *fah*-/- animals can be prevented with the drug 2-(2-nitro-4-trifluoro-methyl-benzoyl)-1,3-cyclo-hexanedione (NTBC), which inhibits p-hydroxyphenylpyruvate dioxygenase, a more proximal enzyme that catalyzes the second step in the tyrosine catabolic pathway [227]. Alternatively, *fah*-/- animals can be rescued by the intrasplenic injection of *fah*+/+ hepatocytes, which migrate to the recipient liver, expand 50-100-fold over several weeks-months and partially replace the defective parenchyma [228, 229].

Here, we studied livers or purified hepatocytes from mice bearing "floxed" *myc* alleles (hereafter referred to as WT mice) or from littermates expressing albumin promoter-driven Cre recombinase in which both *myc* alleles are deleted perinatally (KO mice). We report heretofore unappreciated phenotypes and gene expression differences in KO hepatocytes both prior to and following transplant into *fah-/-* recipients. We also show WT and KO hepatocytes to be equally proficient at long-term repopulation of *fah-/-* livers. The ability of WT and KO hepatocytes to proliferate identically under highly demanding conditions may explain why a more global long-term silencing of Myc is associated with only mild side effects or may even be beneficial [78]. Oncogene "addiction", a frequent feature of Myc-over-expressing cancers [230], may thus impose unique cellular changes that are necessary for maintaining transformed but not normal states of proliferation.

4.2 RESULTS

4.2.1 Characterization of livers and hepatocytes from WT and KO mice

We first verified excision of $myc^{fl/fl}$ alleles from purified KO hepatocytes (Suppl. Fig. 31*A*-*E*). RNAseq from the same cell populations further confirmed a >90% reduction in the number of reads across exons 2 and 3 relative to those from WT hepatocytes (Suppl. Fig. 31*F*).

Although body weights of WT and KO mice were indistinguishable (not shown), liver:total body weight ratios differed, being lower in young ($\leq$1 month) KO animals and higher in older ($\geq$3 months) animals (Suppl. Fig. 32*A*). This was not associated with any differences in

liver histology as assessed by hematoxylin and eosin (H&E) staining (Suppl. Fig. 32*B*). WT and KO hepatocyte sizes were also similar (Suppl. Fig. 32*C*) indicating that, as previously reported, KO livers contain fewer rather than smaller hepatocytes to account for their reduced mass [78, 84]. We discuss below possible reasons for the larger liver:body mass ratio of older KO mice.

myc-/- rat fibroblasts have dysfunctional mitochondria and a profound energy deficit [4, 11]. To rectify this, they up-regulate pyruvate dehydrogenase (PDH), presumably to maximize pyruvate conversion to acetyl CoA [11]. They also constitutively up-regulate AMP-activated protein kinase (AMPK), which responds to reduced ATP:AMP ratios by down-regulating energy-consuming processes and up-regulating energy-generating ones as fatty acid β-oxidation (FAO) [11]. WT and KO livers showed no significant differences in any of these properties except for increased rates of FAO (Suppl. Fig. 32*D-H*).

Finally, we noted that, while Myc alters the susceptibility to multiple intrinsic and environmental pro-apoptotic factors [14, 231] no evidence for an increased level of apoptosis in KO livers was observed (Suppl. Fig. 32*I*).

4.2.2 Differences in metabolism and mitochondrial function of KO mice

KO mice have increased oxygen consumption, carbon dioxide production and heat generation (Fig. 15) particularly when maintained on a high fat diet. These studies suggested that the increased metabolism of KO mice is due to abnormalities in lipid metabolism.

In addition to altering cellular metabolism, Myc also affects mitochondrial structure and function[4, 11, 69]. Blue native gel electrophoresis (BNGE) showed no significant differences in electron transport chain (ETC) complexes I-IV and Complex V of WT and KO hepatocytes

(Suppl. Fig. 33). However, higher ATPase activity of Complex V (V_m and V_d) was noted in KO livers (Suppl. Fig. 33*H* and *I*).

Respirometry measurements showed O_2 flux of WT and KO liver mitochondria to be low but otherwise equivalent prior to and after priming with the Complex I substrates glutamine, pyruvate and malate (G,M,P) (Fig. 16*A*). However, the magnitude of O_2 flux change in response to ADP was less pronounced in KO mitochondria (Fig. 16*A* and *B*), indicating that they reduced molecular oxygen to water via complex IV less efficiently. The provision of succinate resulted in additional but similarly unequal increases in O_2 flux. This indicated that the ability of Complex II (succinate dehydrogenase [SDH]) to drive additional electron flow was unable to compensate for the Complex I defect of KO mitochondria (Fig. 16*A* and *C*).

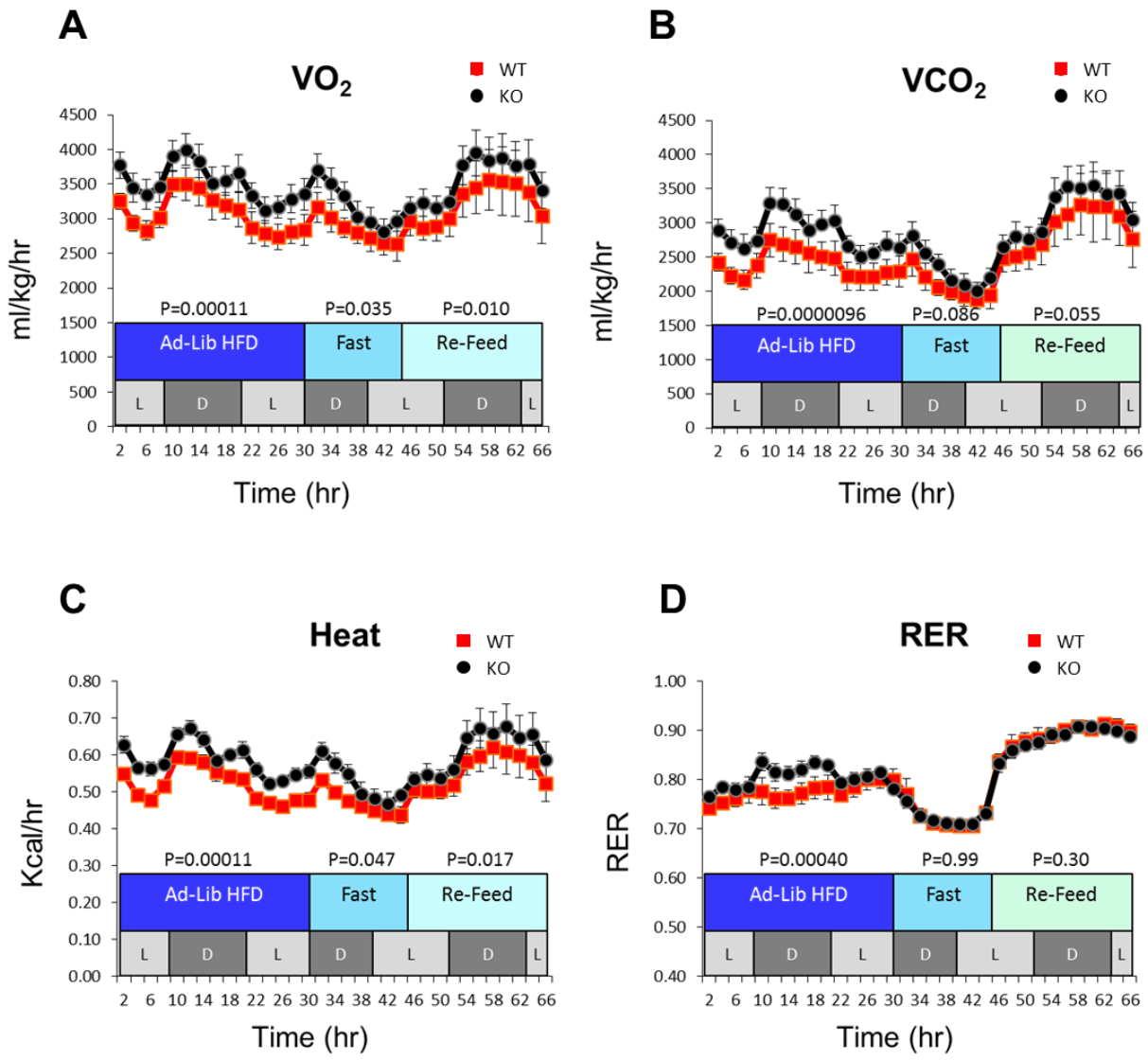

Figure 15: Increased metabolic activity of KO mice. Mice were maintained in metabolic cages that quantified (*A*) oxygen consumption rate (VO2), (*B*) carbon dioxide production rate (VCO2), (*C*) heat production, and (*D*) respiratory exchange ratio (RER). Mice of similar weights were initially maintained on an ad lib high-fat diet followed by a period of fasting and subsequent re-feeding with standard chow plus 5% glucose-containing water over the course of the experiment. L and D indicates cyclic periods of light and dark. Other monitoring showed no differences in the overall activity, food consumption, total fat mass or glucose tolerance between groups of WT and KO mice (not shown).

We also quantified the activities of several mitochondrial dehydrogenases other than Complex II (Suppl. Fig. 33*E*) which donate electrons to the ETC [232]. WT and KO liver-derived mitochondria had equal levels of isocitrate dehydrogenases (IDH) 1-3, malate dehydrogenase (MDH) and glycerol 3-phosphate dehydrogenase (G3PDH) (Fig. 16*D-F)*. Taken together we conclude that, while KO liver mitochondria have defects in Oxphos, they are not severe enough to compromise ATP production.

We next employed a recently described targeted proteomics assay using liquid chromatography-tandem mass spectrometry to assess the relative abundance of the 93 known subunits of the ETC plus an additional 46 mitochondrial metabolism-related proteins [232]. Based on a p-value cut-off of 0.05, none of the quantified proteins exhibited statistically significant differences between the two groups (data not shown).

Next, an unbiased mass spectrometry-based approach was used to compare the relative abundance of proteins comprising ~30% of the mitochondrial proteome [232]. In total, 2439 peptide ions (features) were matched to 377 mitochondrial proteins. Using a Student's t-test with a cut off of $p<0.05$, we again found there to be no significant differences between WT and KO livers with respect to the relative amounts of any of these proteins (data not shown). Together with the results shown in Suppl. Fig. 33, we conclude there to be no major quantitative differences in the composition of the mitochondrial proteomes of WT and KO hepatocytes.

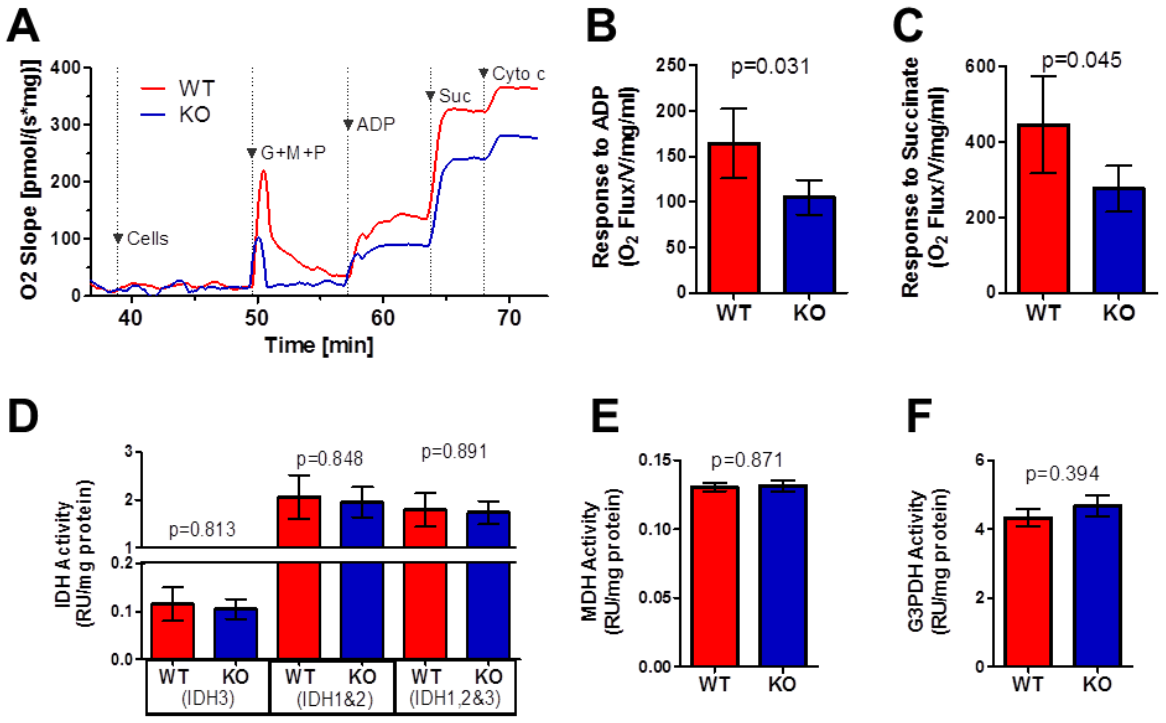

Figure 16: ETC function of WT and KO livers. (*A*) Typical respirometry profiles from WT and KO liver homogenates. Arrowheads indicate the time of addition of glutamine, malate and pyruvate (G,M,P), ADP and succinate (Suc). WT and KO liver preparations were simultaneously assayed in parallel. Cytochrome c was added to test mitochondrial outer membrane integrity. Note that the large, spike in O_2 flux seen upon adding G,M,P is an artifact resulting from injecting a large volume of diluted substrates and transiently disturbing the O2 concentration. (*B*) Graphic representation of the ADP responses in mitochondria prepared from 7 sets of WT and KO livers assayed as shown in (*A*). (*C*) Graphic representation of succinate responses. The results in (*A*)-(*C*) were adjusted to account for minor differences in total protein concentrations. (*D-F*) Assays of selective TCA cycle dehydrogenases, including: NAD+- and NADP+-dependent IDHs (IDH3 and IDH1+2) (*D*); MDH (*E*) and G3PDH (*F*) See Suppl. Fig. 33*E* for similar assays performed for SDH (Complex II).

4.2.3 RNAseq analysis of WT and KO hepatocytes

We performed RNAseq on hepatocytes from WT and KO animals of comparable ages (ca. 17-18 weeks). After adjusting for false discovery rate (FDR), we identified 102 transcript differences, 35 of which were up-regulated in KO hepatocytes and 67 of which were down-regulated (q values <0.05, Fig. 17*A*). The largest subset was comprised of 12 of the ~103 member cytochrome p450 (cyp450) family (Fig. 17*B*) [233]. Re-evaluation of our data identified 11 additional members that were initially excluded for not meeting false discovery rate (FDR) criteria but which still demonstrated significant differences between the two groups ($p<0.05$) (Fig. 17*B*). 15 of the 23 differentially expressed cyp450 transcripts (62%) were encoded by the CLAN2 family whose 37 members are particularly relevant for the regulation of sterol, bile acid and eicosinoid metabolism [233].

In keeping with Myc's role in regulating ribosomal biogenesis [234], 12 of the ~80 known transcripts (~15%) encoding ribosomal proteins were down-regulated in KO hepatocytes (Fig. 17*C*). Thus, Myc maintains normal levels of a subset of ribosomal protein transcripts.

Ingenuity Pathway Analysis of all differentially expressed transcripts of significance ($p<0.05$) identified specific functional classes of genes that were not necessarily fully represented in Fig. 17*A*. Of 642 pathways queried, 5 of the top 7 involved the regulation of cholesterol, sterol or bile acid synthesis (Fig. 17*D* and *E*). The remaining 2 related to farnesoid X receptor (FXR)- and the liver X receptor (LXR) or their regulation by lipopolysaccharide and/or interleukin 1, which are also activated by oxysterols and bile acids [235]. Thus, KO hepatocytes also up-regulate multiple pathways involved directly in sterol and bile acid bio-synthesis.

A

B

Gene Symbol	p-value	q-value (for FDR)	WT 1	WT 2	WT 3	WT 4	KO 1	KO 2	KO 3	KO 4
Cyp3A59	0.000	0.009								
Cyp3A25	0.001	0.057								
Cyp3A11	0.007	0.314								
Cyp2D12 *	0.000	0.009								
Cyp4A12A	0.012	0.424								
Cyp21A1	0.005	0.227								
Cyp2D37-Ps *	0.004	0.200								
Cyp2J9 *	0.010	0.372								
Cyp2D40 *	0.038	0.789								
Cyp2A22 *	0.036	0.783								
Cyp4A31	0.005	0.245								
Cyp2C37 *	0.009	0.361								
Cyp2C44 *	0.005	0.245								
Cyp2A4 *	0.000	0.009								
Cyp51	0.000	0.022								
Cyp2C50 *	0.000	0.009								
Cyp2B10 *	0.000	0.009								
Cyp2C54 *	0.000	0.009								
Cyp2C68 *	0.000	0.009								
Cyp7A1	0.000	0.009								
Cyp2C67 *	0.000	0.009								
Cyp2C40 *	0.000	0.009								
Cyp2C69 *	0.000	0.009								

C

Gene Symbol	p-value	q-value (for FDR)	WT 1	WT 2	WT 3	WT 4	KO 1	KO 2	KO 3	KO 4
RPL12	0.000	0.015								
RPL13	0.036	0.779								
RPL23	0.049	0.856								
RPL37	0.019	0.561								
RPL10A	0.003	0.166								
RPL18A	0.043	0.819								
RPS7	0.045	0.832								
RPS8	0.019	0.559								
RPS12	0.004	0.205								
RPS20	0.047	0.842								
RPS15A	0.043	0.820								
RPSA	0.018	0.541								

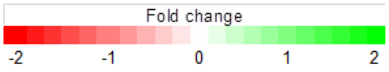

D

Gene Symbol	p-value	q-value (for FDR)	WT 1	WT 2	WT 3	WT 4	KO 1	KO 2	KO 3	KO 4
SAA1	0.000	0.009								
FABP4	0.000	0.009								
SLC10A2	0.000	0.027								
IDI1	0.000	0.009								
PPARGC1A	0.000	0.009								
FABP5	0.000	0.009								
MSMO1	0.000	0.009								
ALAS1	0.000	0.009								
SQLE	0.000	0.022								
SULT1B1	0.001	0.054								
MGST3	0.008	0.326								
FOXA3	0.002	0.135								
FDPS	0.009	0.361								
PKLR	0.008	0.339								
SC5D	0.006	0.265								
FABP2	0.020	0.575								
TNFRSF1B	0.016	0.514								
NSDHL	0.039	0.793								
Gstm3	0.008	0.328								
PON1	0.038	0.789								
SERPINF2	0.042	0.810								
HSD17B7	0.044	0.827								
FOXO1	0.046	0.838								
APOF	0.048	0.847								
C4A	0.026	0.647								
SERPINA1	0.018	0.554								
SLC22A7	0.020	0.577								
ABCG5	0.030	0.715								
MLXIPL	0.008	0.326								
ABCG8	0.040	0.794								

E

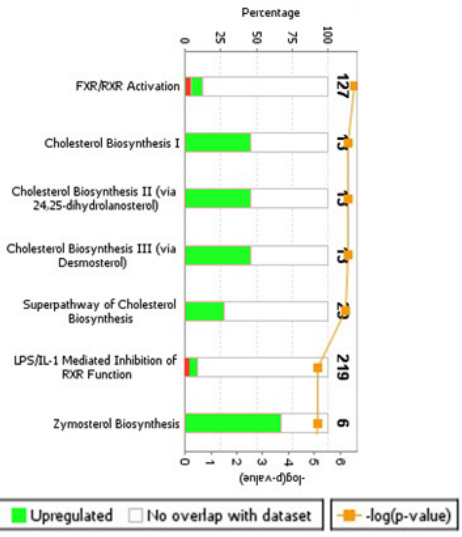

Figure 17: Transcript differences between WT and KO hepatocytes. (*A*) RNAseq results from 4 individual sets each of WT and KO hepatocytes. The 102 differentially expressed transcripts with adjusted FDR q<0.05 are shown. (*B*) Differences in cyp450 member transcript expression between WT and KO hepatocytes. Those with q<0.05 were taken from A whereas the others represent significant differences at the level of p<0.05 among other members of the cyp450 family. Those encoding members of the CLAN 2 family are indicated by asterisks. (*C*) Differentially expressed transcripts encoding ribosomal proteins (p<0.05) are listed. RPL12 is from (*A*). (*D*) Differential gene expression profiling of genes involved in the top 7 deregulated pathways identified by Ingenuity Pathway Analysis. Note that the cyp450 members shown in (*B*) are not repeated here but were included and found to be significant in the pathway analysis of cholesterol metabolism. (*E*) The top 7 classifications of all significantly deregulated (p<0.05) transcripts according to their involvement in specific pathways based on Ingenuity profiling. The top axis represents the percentage of genes comprising that pathway whose transcripts were differentially expressed between WT and KO hepatocytes. Green bars indicate transcripts that were up-regulated in KO hepatocytes and red bars indicate down-regulated transcripts. Some transcripts are included in more than one pathway. Orange circles indicate the log10 p value indicating the probability that the differentially expressed transcripts within a specific pathway would have been selected randomly. Numbers on the right indicate the number of transcripts assigned to the indicated pathway.

WT and KO hepatocytes did not differentially express genes potentially capable of complementing the loss of Myc such as N-Myc and L-Myc and non-Myc family-related genes such as Myct1, HMG-IY and serine hydroxymethyltransferase [236, 237] (Suppl. Fig. 34*A*). Transcripts encoding the "Mlx family" of bHLH-ZIP transcription factors were also unchanged save for a modest (~30%) decrease in those encoding Mlxip1/MondoB/ChREBP in KO cells [41], which was not manifested at the protein level (Suppl. Fig. 34*B*).

4.2.4 Abnormal regulation of triglycerides and sterols in KO livers

Myc inhibition *in vitro* increases FAO and neutral lipid storage [11, 69], which is consistent with the increased FAO rate in KO livers (Suppl. Fig. 32*H*). Our RNAseq results and the fact that lipid droplets also contain cholesterol suggested that sterol and/or bile acid metabolism might be compromised in KO hepatocytes particularly since bile acids derive from sterols and can regulate sterol and triglyceride biosynthetic pathways [238]. Indeed, livers of fasted KO mice contained higher triglyceride levels as well as more numerous and larger neutral lipid droplets (Suppl. Fig. 35*A* and *B* and 35*A* and *B*). A trend toward lower fasting cholesterol levels was also noted and increased significantly following re-feeding (Suppl. Fig. 35*C*). KO hepatocytes also contained significantly higher levels of transcripts for squalene epoxidase (SQLE), sterol C-4 methyloxidase (SC4MOL), 3β-hydroxysteroid dehydrogenase (NSDHL) and sterol C-5 desaturase (SC5DL) [1.7-fold, 2.0-fold, 1.3-fold and 1.4-fold, respectively (Suppl. Fig. 35*D*)]. However, profiling a series of intermediates in the biosynthetic pathway leading from lanosterol to cholesterol and including the bile acid intermediate cholestanol showed no differences between WT and KO mice when adjusted either to total protein or total sterol content (Suppl. Fig. 35*E* and *F*).

Bile acids consist of conjugates between taurine or glycine and cholic or chenodeoxycholic acid [239]. When measured in the livers of non-fasted animals, secondary bile acids, which are formed within the small intestine by the action of enteric bacteria, make a larger contribution to the total bile acid pool. Therefore, we measured total bile acid levels in the livers of fasted WT and KO mice. As seen in Suppl. Fig. 35*G*, no significant differences were observed.

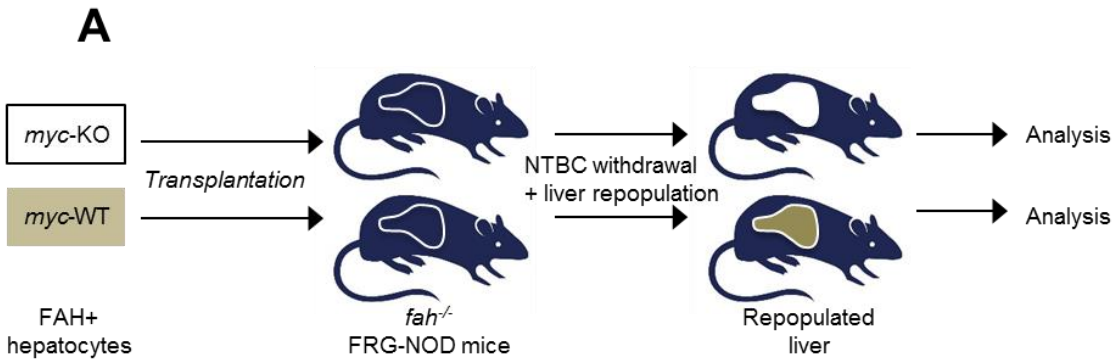
A
myc-KO
myc-WT
Transplantation
FAH+
hepatocytes
fah-/-
FRG-NOD mice
NTBC withdrawal
+ liver repopulation
Repopulated
liver
Analysis
Analysis

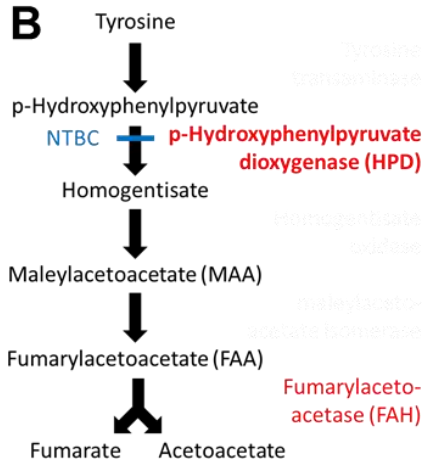
B
Tyrosine
p-Hydroxyphenylpyruvate
NTBC
p-Hydroxyphenylpyruvate
dioxygenase (HPD)
Homogentisate
Maleylacetoacetate (MAA)
Fumarylacetoacetate (FAA)
Fumarylaceto-
acetase (FAH)
Fumarate
Acetoacetate

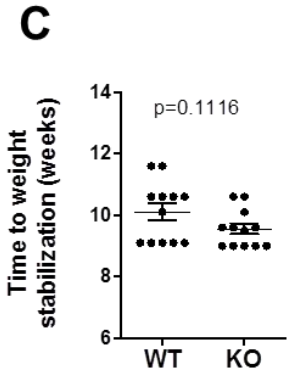
C
Time to weight
stabilization (weeks)
p=0.1116
14
12
10
8
6
WT
KO

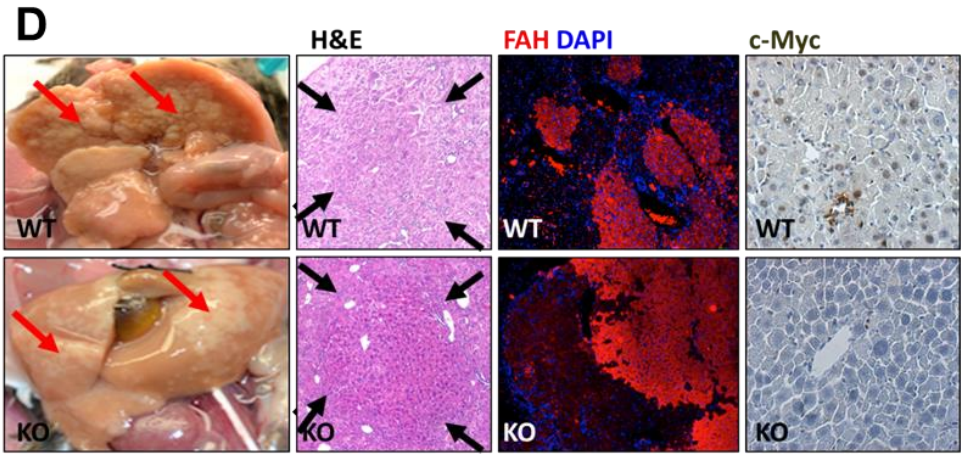
D
H&E
FAH DAPI
c-Myc
WT
WT
WT
WT
KO
KO
KO
KO

Figure 18: Rescue of FGR-NOD mice with fah+/+ WT and KO hepatocytes occurs at equivalent rates. (*A*) Schematic for repopulating fah-/- NOD-SCID mice with WT or KO donor fah+/+ hepatocytes (*B*) Pathway of hepatic tyrosine catabolism. FAH's absence causes accumulation of the toxic upstream intermediates maleyl- and fumarylacetoacetate. Animals can be rescued by blocking the more proximal enzyme hydroxyphenylpyruvate dioxygenase with NTBC or by transplanting fah+/+ hepatocytes. (*C*) 3x105 hepatocyes from WT or KO mice (both fah+/+) were inoculated intraspenically into recipient fah-/- FRG-NOD mice. 4 days later, NTBC cycling began until body weight stabilized at >100% of the pre-transplant weight. No differences were seen in the times needed to achieve NTBC independence and body weight stabilization. (*D*) Gross appearance of recipient FRG-NOD livers 12-14 wks after transplantation of WT or KO hepatocytes. Livers have been flushed with PBS to facilitate visualization of regenerating nodules (arrows). H&E staining of post-transplant livers showing regenerating nodules of donor cells (arrows). FAH immuno-staining of donor-derived fah+/+ nodules (red) in recipient fah-/- FRG-NOD mice. Note the lack of staining of adjacent, fah-/- recipient hepatocytes. Tissues were counterstained with DAPI (blue). Myc immuno-staining of regenerating hepatic nodules. Numerous representative Myc-positive nuclei in a regenerating nodule following transplantation with WT hepatocytes are shown in the top panel. Note the absence of Myc in a similar nodule repopulated with KO hepatocytes (lower panel).

4.2.5 WT and KO hepatocytes have equivalent repopulation capacity

Mice with tyrosinemia can be rescued by the intrasplenic injection of FAH+ donor hepatocytes, particularly when performed in immune-compromised *fah-/-* FRG-NOD recipients [240]. This approach therefore provides a superior alternative to PH as the transplanted hepatocytes are subject to a more intense and prolonged replicative stress.

We injected FRG-NOD mice with $3x10^5$ WT or KO hepatocytes and withdrew NTBC 4d post-transplant to facilitate recipient liver repopulation (Fig. 18*A* and *B*). Because NTBC discontinuation is associated with weight loss, it was re-initiated whenever body weights

dropped by >20% and discontinued permanently when weights stabilized at ≥100% of pre-transplant values. The time needed to permanently re-establish pre-transplant weights was similar in the two groups suggesting that WT and KO hepatocytes possessed equal repopulation potential (Fig. 18*C*). This was supported by the presence of numerous macroscopic and microscopic foci of regenerating hepatocytes in both groups of animals (Fig. 18*D*) and by extensive focal FAH immuno-positivity (Fig. 18*D*, FAH). Additional immuno-histochemical staining showed Myc-positive hepatocytes only in regenerating nodules derived from WT donors (Fig. 18*D*, c-Myc). Thus, hepatic parenchyma regeneration by KO hepatocytes could not be explained by the selective expansion of cells with non-excised *myc* loci.

Quantification of $fah^{+/+}$ and $fah^{-/-}$ alleles in hepatocytes isolated from repopulated livers established that $fah^{+/+}$ donor cells comprised ~40-50% of the entire hepatocyte population (Fig. 19*A* and *B*). This was confirmed using the PCR-based strategy shown in Suppl. Fig. 31*B* and *C* (black and blue arrows) to amplify different sized segments of donor and recipient *myc* loci.

A more sensitive quantification of proliferative potential was obtained with a competitive re-population assay performed ~18 weeks after transplanting a mixed population of WT and KO donor hepatocytes (Fig. 19*D*). PCR of *fah* alleles (Fig. 19*A*) again indicated transplant efficiency to be ~40% (not shown). PCR for *myc* alleles (Suppl. Fig. 31*A*-*C*) showed that, on average, their individual contributions precisely reflected those of the input populations (Fig. 19*E*). KO hepatocytes therefore are not at a proliferative disadvantage even when competing directly with their WT counterparts.

4.2.6 Abnormal neutral lipid storage following transplantation with KO hepatocytes

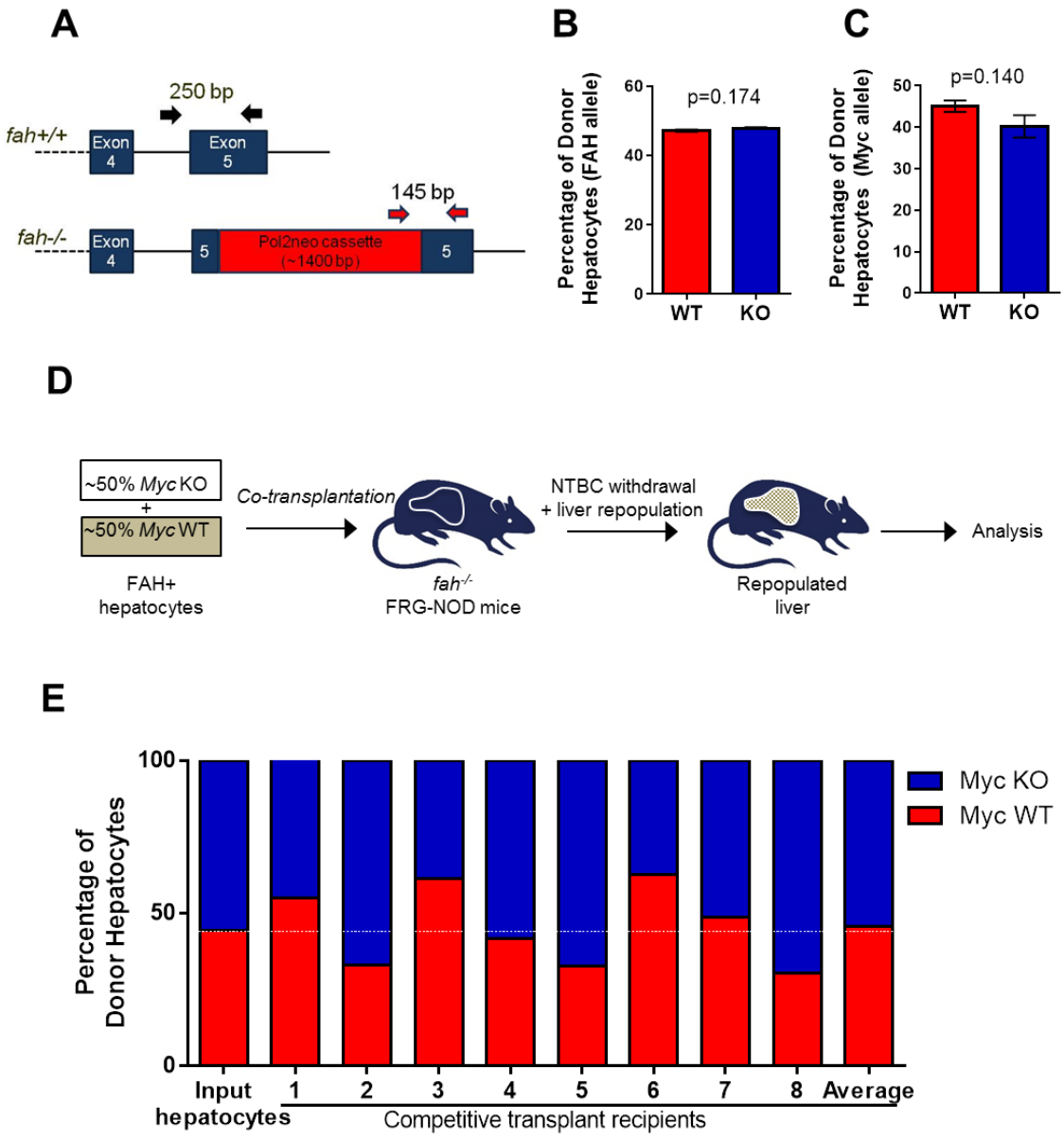

Figure 19: WT and KO hepatocytes are equally proficient at re-populating the hepatic parenchyma. (*A*) PCR-based strategy to distinguish fah+/+ donor and fah-/- recipient alleles. (*B*) Hepatocytes were isolated from 11 recipient animals 17-18 wks after transplanting with WT or KO hepatocytes and ~6 wks after NTBC discontinuation. PCR of fah alleles showed no difference in the contribution of WT and KO myc alleles to the

repopulated liver. (*C*) The strategy depicted in Suppl. Fig. 30*B* and *C* (black and blue arrows) was used to amplify the myc alleles from the same hepatocyte samples used in (*B*). (*D*) Schematic for competitive transplants of Myc WT and KO hepatocytes. (*E*) 8 FRG-NOD mice were transplanted with a ~1:1 mixture of 1.5x105 hepatocytes each from WT and KO donors (input) and allowed to achieve NTBC independence. Following repopulation, PCR quantification of fah alleles again showed that the donor populations comprised ~40% of the total hepatocyte mass (not shown). This was confirmed by amplification of the three myc alleles. Shown here is the proportion of the donor population in each animal that was comprised of Myc WT and KO donor hepatocytes. Note that the average allelic composition of this group was identical to that of the input population. Each set of PCR reactions was performed in triplicate for each population of hepatocytes.

The proliferative stress imposed on donor hepatocytes might exaggerate previously identified abnormalities or reveal new ones. Consistent with this, ORO staining and triglyceride levels were again more pronounced in recipient livers transplanted with KO hepatocytes, with much of the stored lipid now being extracellular (Fig. 20*A* and *B*). Interestingly, whereas the overall total number of lipid droplets/cell fell in transplanted KO hepatocytes, their average size increased, as well as the overall cellular area occupied by lipid. These findings suggested that, following transplantation, the lipid droplets of KO hepatocytes increase in size by fusing with pre-existing droplets (compare Suppl. Fig. 36*A* and *B* to *C* and *D*).

As was the case pre-transplant (Suppl. Fig. 35*E*), sterol intermediates in recipients reconstituted with WT or KO hepatocytes were similar when normalized to protein content (Fig. 20*C*) but differed when each analog, including the bile acid intermediate cholestanol, was expressed relative to the total sterol content (Fig. 20*D*). Bile acid levels were also similar in the two groups (Fig. 20*E*). These findings show that abnormalities in sterol biosynthetic pathways,

initially identified in pre-transplant hepatocytes only by transcriptional profiling (Fig. 17*E*) become more pronounced following transplantation.

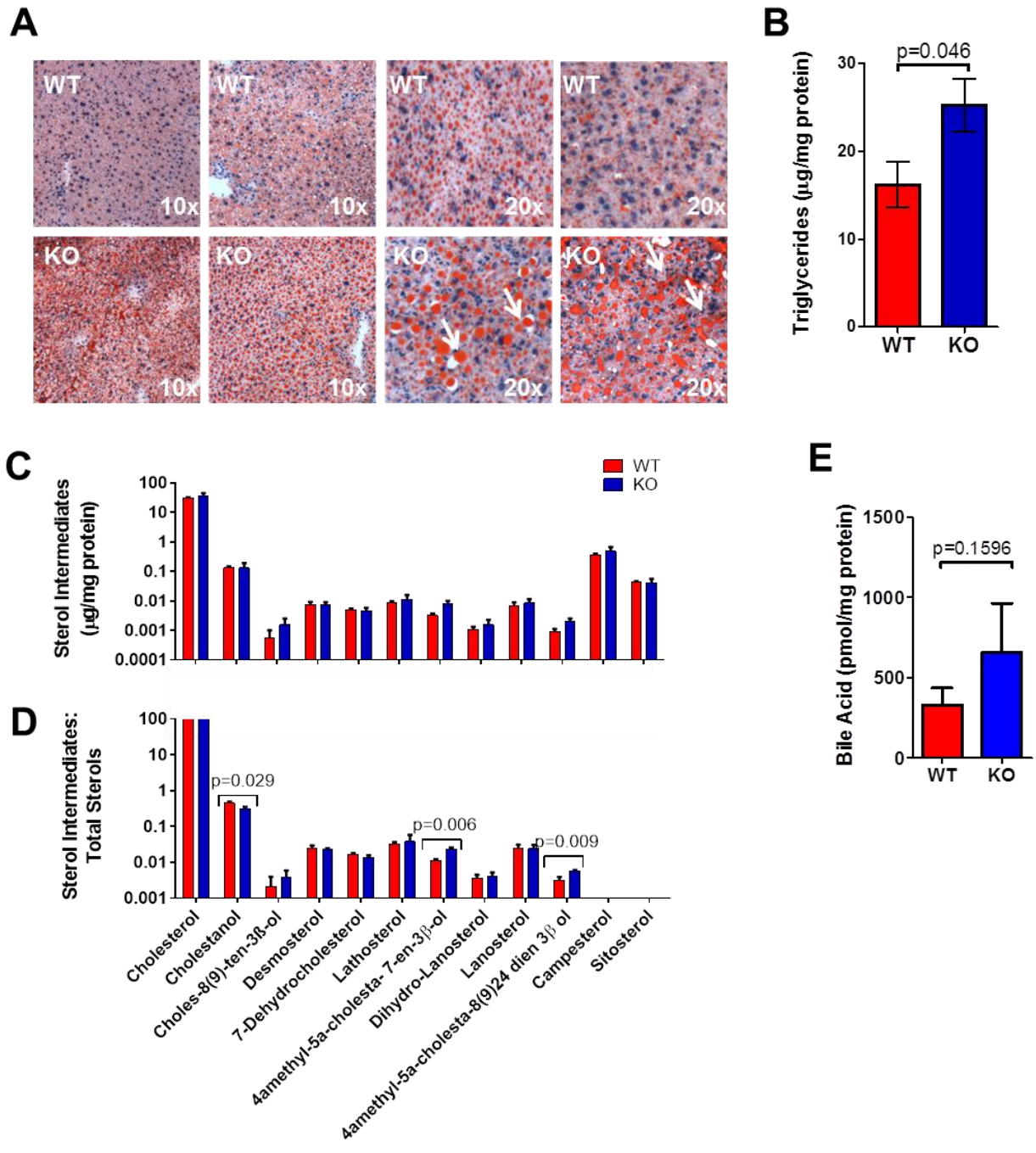

Figure 20: Hepatic repopulation enhances the defective handling of lipids in KO hepatocytes. (*A*) ORO-stained liver sections showing increased neutral lipid accumulation following transplant of KO hepatocytes. The last 2 panels are higher power magnifications that demonstrate not only the overall increased lipid content in KO hepatocytes but the larger size of their lipid droplets and extracellular lipid deposits. See Suppl. Fig. 36*C* and *D* for quantification of lipid droplet numbers and sizes. (*B*) Quantification of total triglyceride levels in mouse livers. Triglyceride assays were performed as described for Suppl. Fig. 35*B*. (*C*) Liver sterol levels adjusted to protein content. Assays were performed as described for Suppl. Fig. 35*E*. (*D*) Data from C expressed as a fraction of total sterol content as described in Suppl. Fig. 35*F*. (*E*) No differences in the total bile acid of WT and KO transplanted liver, performed as described in Suppl. Fig. 35*G*.

4.2.7 Transcriptional profiling of post-transplant hepatocytes

Post-transplant transcriptional profiling is complicated given that isolated hepatocytes are a mixed population of donor and recipient cells (Fig. 19*B* and *C*) that could potentially mask anything other than the most striking differences between donor hepatocytes. Any differences that are observed also cannot necessarily be attributed with certainty to the donor population. Nevertheless, with these caveats in mind, we repeated RNAseq on isolated liver cell populations from a small number of recipient mice ~18-19 weeks post-transplant. Unlike the limited number of transcript differences between pre-transplant hepatocytes (Fig. 17*A*), we documented 1784 differences ($q<0.05$) in the post-transplant setting (Fig. 21*A*). Gene ontology analysis revealed that the 3 groups involving the greatest number of common function transcripts related to energy production, metabolism and ribosomal proteins. The first included 19 of the 44 known subunits of Complex I and Park7/DJ-1, which plays a role in mitochondrial fission and Complex I stabilization [241]. All these transcripts were down-regulated in the livers of mice repopulated with KO hepatocytes (Fig. 21*B*). The second group contained 20 transcripts encoding subunits of

various ATPases, 7 of which encoded components of Complex V (Fig. 21*C*). These were down-regulated in the livers of mice repopulated with KO hepatocytes whereas 10 of the remaining 13 were up-regulated. The third group was comprised of transcripts encoding 61 members of both large and small ribosomal subunits, all of which were down-regulated (Fig. 21*D*). This group contained all 6 small ribosomal subunit transcripts previously identified as being down-regulated in KO hepatocytes (Fig. 17*C*). 6 of the 10 most highly altered pathways discovered through Ingenuity Pathway Analysis, all of which were up-regulated in recipient livers transplanted with KO hepatocytes, pertained to some aspect of acute or chronic inflammation or healing, including the induction of fibrosis, leukocyte and IL-8 signaling, phagocytosis and modulation of the complement system, (Fig. 21*E* and Suppl. Table 8). This strongly correlated with increased immuno-histochemical staining for the pan-leukocyte cell surface marker CD45 and for 4-hydroxynonenol, a byproduct of lipid peroxidation (Fig. 21*F* and Suppl. Fig. 37).

The remaining 4 pathways were related by virtue of the central role of mTOR in nutrient-sensitive control over protein translation and mitochondrial oxidative function, although mTOR also plays a central role immune modulation [242]. The most conservative interpretation of these results is that the livers of mice, otherwise equally repopulated with WT or KO hepatocytes, nevertheless vary considerably in their gene expression profiles, with the latter showing an up-regulation of transcripts involved in pro-inflammatory pathways and a down-regulation of transcripts regulating mitochondrial function and protein translation.

A

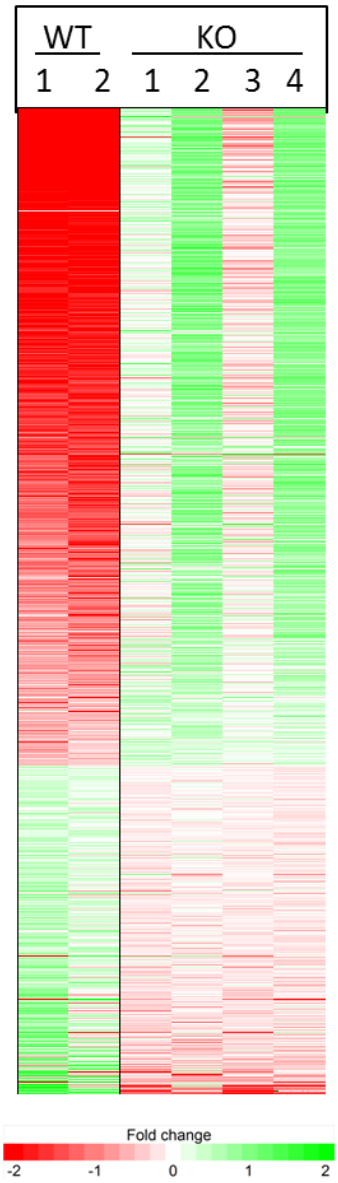

B

Gene Symbol	p-value	q-value (for FDR)	WT 1	WT 2	KO 1	KO 2	KO 3	KO 4
Ndufa2	0.000	0.006						
Ndufa1	0.002	0.017						
Ndufa11	0.003	0.025						
Ndufb7	0.003	0.026						
Ndufa3	0.006	0.042						
Ndufa5	0.007	0.051						
Ndufs6	0.006	0.042						
Ndufs4	0.011	0.067						
Ndufb5	0.014	0.079						
Ndufs2	0.022	0.110						
Ndufb3	0.014	0.080						
Ndufb10	0.018	0.097						
Ndufb6	0.022	0.108						
Park7	0.032	0.143						
Ndufb8	0.033	0.144						
Ndufb4	0.030	0.134						
Ndufa7	0.032	0.142						
Ndufa12	0.035	0.149						
Ndufa6	0.037	0.156						
Ndufa8	0.039	0.160						

C

Gene Symbol		p-value	q-value (for FDR)	WT 1	WT 2	KO 1	KO 2	KO 3	KO 4
Atp5l	*	0.000	0.003						
Atp5e	*	0.001	0.014						
Atp5g2	*	0.003	0.026						
Atp6v0b		0.004	0.031						
Atp5g3	*	0.028	0.128						
Atp13a1		0.014	0.078						
Atp5h	*	0.022	0.111						
Atp5k	*	0.040	0.162						
Atp5j2	*	0.045	0.176						
Atp6v1f		0.038	0.158						
Atp6v1a		0.010	0.062						
Atp13a2		0.010	0.061						
Atp7a		0.037	0.155						
Atp7b		0.001	0.013						
Atp2b2		0.002	0.021						
Atp8a1		0.002	0.016						
Atp6v0d2		0.000	0.001						
Atp6v0e2		0.001	0.008						
Atp8b2		0.001	0.014						
Atp2b4		0.000	0.001						

D

Gene Symbol	p-value	Adjusted p-value (for FDR)	WT 1	WT 2	KO 1	KO 2	KO 3	KO 4
Rps27A	0.0001	0.0011						
Rpl41	0.0001	0.0011						
Rps12	0.0001	0.0011						
Rpl35A	0.0001	0.0011						
Rps21	0.0001	0.0011						
Rpl38	0.0004	0.0057						
Rpl37A	0.0001	0.0011						
Rpl13A	0.0001	0.0019						
Rplp2	0.0001	0.0011						
Rps24	0.0003	0.0046						
Rpl12	0.0002	0.0034						
Rps18	0.0004	0.0051						
Rpl27A	0.0003	0.0040						
Rpl17	0.0003	0.0046						
Rps9	0.0005	0.0062						
Rps14	0.0002	0.0034						
Rpl27	0.0002	0.0027						
Rpl36A	0.0002	0.0034						
Rpl8	0.0005	0.0062						
Rpl9	0.0007	0.0082						
Rps5	0.0004	0.0051						
Rps19	0.0006	0.0073						
Rplp1	0.0004	0.0057						
Rps8	0.0007	0.0082						
Rpl36	0.0003	0.0040						
Rpl35	0.0002	0.0034						
Rps10	0.0005	0.0062						
Rps13	0.0005	0.0062						
Rps6	0.0023	0.0216						
Rpl10A	0.0011	0.0123						
Rps15A	0.0005	0.0062						
Rpl7A	0.0023	0.0212						
Rps20	0.0008	0.0097						
Rpl18A	0.0018	0.0176						
Rps16	0.0009	0.0102						
Rpl37	0.0009	0.0106						
Rps7	0.0019	0.0183						
Rpl23	0.0030	0.0261						
Rps23	0.0033	0.0283						
Rpl36Al	0.0022	0.0205						
Rpl24	0.0022	0.0209						
Rplp0	0.0061	0.0443						
Rpl32	0.0027	0.0245						
Rps25	0.0033	0.0283						
Rpl39	0.0020	0.0194						
Rpl28	0.0054	0.0403						
Rpl5	0.0087	0.0563						
Rps17	0.0076	0.0512						
Rps3	0.0103	0.0635						
Rpl14	0.0091	0.0581						
Rpl23A	0.0135	0.0773						
Rps26	0.0074	0.0503						
Rps2	0.0274	0.1274						
Rpl6	0.0176	0.0935						
Rps4X	0.0205	0.1043						
Rpl22	0.0089	0.0570						
Rpl7	0.0255	0.1217						
Rpl11	0.0193	0.0998						
Rpl29	0.0215	0.1077						
Rps11	0.0265	0.1247						
Rpl21	0.0466	0.1807						

E

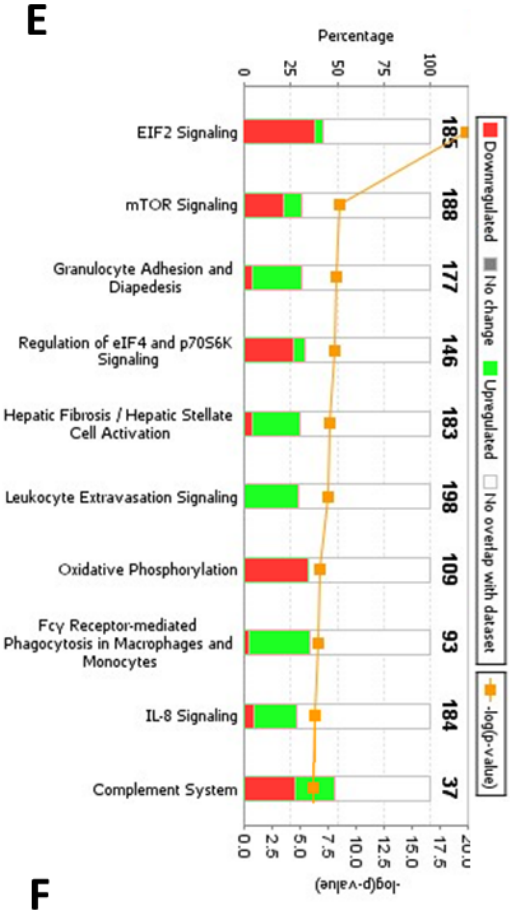

F

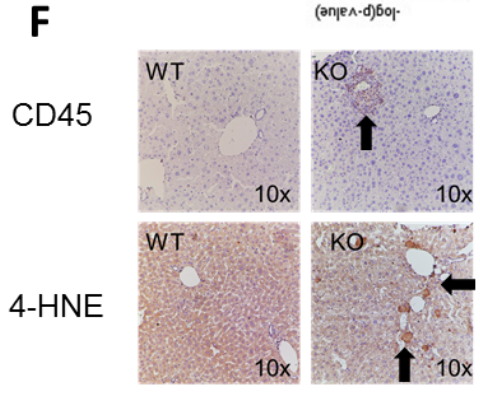

Figure 21: Transcriptional profiling of post-transplant hepatocytes. (*A*) RNAseq results for all 1784 differentially expressed transcripts with q values <0.05. (*B-D*) Gene ontology profiling for transcripts involved in common functions identified 20 encoding components of Complex I, 20 encoding various ATPases and 61 encoding ribosomal components. (*E*) Ingenuity Pathway Analysis depicting the most de-regulated functionally related groups of transcripts shown in A. Green bars and red bars indicate transcripts that are up-regulated and down-regulated, respectively in cells isolated from animals transplanted with KO hepatocytes. Transcripts levels from these top 10 pathways are represented in Suppl. Table 8.

4.3 DISCUSSION

Previous studies on Myc's role in hepatic function have produced conflicting or inconclusive results. For example, Baena *et al.* noted increased nuclear pyknosis and apoptosis in KO hepatocytes and a disorganized hepatic parenchyma with whereas Sanders *et al.* found no differences [87, 89]. Sanders *et al.* observed identical liver:body weight ratios in WT and KO mice whereas Qu *et al.* found them to be somewhat reduced in KO mice and Baena found them to be increased [87, 89, 225]. Only Sanders *et al.* reported liver weights following PH and found them to be similar in WT and KO mice [87]. Potential explanations for the discrepancies among these studies include variable efficiencies of *myc* gene knockout, excision of *myc* from cells other than hepatocytes and differences in animals' ages when various phenotypes were assessed.

Like Qu et al. [225], we found lower liver:body weight ratios in young KO mice (Suppl. Fig. 32*A*). Since WT and KO hepatocytes were of equivalent size (Suppl. Fig. 32*C*), the most likely explanation is that KO livers contained smaller numbers of normal-sized cells as

previously described [78, 84]. The larger livers of older KO mice (Suppl. Fig. 31*A*) likely reflects their age-related lipid accumulation (Suppl. Fig. 35 and 36*A* and *B*).

Increased VO_2 by hemizygous (*myc*+/-) mice has been attributed to a higher surface area:body mass ratio and/or to the increased activity and caloric intake of older animals [78]. These physical differences, as well as the global nature of the *myc*+/- state, precluded a more definitive explanation for the higher VO_2. In our KO mice, increased VO_2 and VCO_2 were not associated with differences in weight, caloric intake or activity compared to WT mice (Fig. 15 and data not shown). Thus, although the KO metabolic phenotype is solely attributable to the loss of Myc in hepatocytes, we cannot state unequivocally that the liver is the actual site of the abnormal gas exchange. Indeed, an interesting observation was that despite increased VO_2 and CO_2 in KO animals, there was no difference in RER (calculated as the ratio of VCO_2/VO_2) indicating that fuel utilization was unchanged during fasting and re-feeding in the whole animal.

The more pronounced metabolic abnormalities of KO mice maintained on a high fat diet is likely related to their higher rate of hepatic FAO (Suppl. Fig. 32*H*) This is reminiscent of metabolic changes observed in hearts of obese and/or diabetic mice where reduced glucose uptake is offset by an imbalanced increase in fatty acid uptake and utilization, with the former exceeding the latter and the difference being stored as neutral lipid [243]. FAO is associated with more efficient production of TCA-cycle-derived NADH and FADH2, higher oxygen consumption and increased reactive oxygen species (ROS) production, which can cause mitochondrial uncoupling [244]. The greater activity of Complex V in KO liver mitochondria (Suppl. Fig. 32*H* and *I*) may therefore represent a successful compensatory mechanism to maintain normal ATP levels in the face of an excess reliance on FAO during a time of excessive ETC stress or compromise.

The abnormalities in fatty acid metabolism in KO mouse livers also bear similarity to those observed in *myc*-/- fibroblasts [4, 11]. That KO hepatocytes did not activate AMPK however, suggests that, while energetically stressed, they maintain normal energy supplies, perhaps by optimizing their excessive reliance on FAO. This successful adaptation could be the result of less severe mitochondrial structural abnormalities than occur in *myc*-/- fibroblasts [4] (no significant changes in proteomics data [not shown] and Suppl. Fig. 33) and/or the higher Complex V activity (Suppl. Fig. 33*H* and *I*) [245]. It remains unclear why hepatocytes are so much less reliant on Myc than fibroblasts for maintaining mitochondrial integrity.

Unlike cell lines in which Myc over-expression affects hundreds-thousands of genes [18] KO hepatocytes had relatively few transcriptional changes (Fig. 17*A*). This may reflect the relatively low expression levels of Myc in the largely quiescent WT hepatocyte population and/or its otherwise normal regulation in the former cells. Transcript differences included those encoding some of the same ribosomal proteins reported by others as being affected by Myc over-expression [87, 234]. However, the most striking differences involved pathways pertaining to sterol and bile acid biosynthesis. Cyp450 family members, which also play important roles in steroidogenesis and bile acid production, were also highly de-regulated[233, 246] (Fig. 17*E*). Interestingly, 2 of the 7 most de-regulated pathways involved LXRs and FXRs, which are activated by oxysterol and bile acid metabolism, respectively [247]. LXRs and FXRs may also regulate fatty acid and glucose metabolism, both of which are also Myc-responsive [15, 235]. The lipid storage defects of KO livers thus appear to be the result of both increased fatty acid uptake [11, 69] and defective steroidogenesis. The ongoing accumulation of these in lipid droplets likely accounts for the age-related increase KO liver size (Suppl. Fig. 16*A*) [248].

Our studies on the repopulation potential of WT and KO hepatocytes capitalized on the fact that they expand 50-100-fold following transplantation [227, 240] thus providing a more demanding and prolonged proliferative stress than afforded by PH [224, 240]. This model also allows a more accurate evaluation of intrinsic hepatocyte proliferative capacity given that it assesses re-population rather than regeneration which is more dependent on contributions from liver cells other than hepatocytes [224]. That the transplanted fraction remains constant at ~40% over time (Fig. 19*B* and *C*) probably reflects the ability of donor cells to fully assume the disposal of toxic tyrosine catabolites, thus eliminating any further selective pressure. Collectively, these studies provide what we feel to be unequivocal proof that Myc is dispensable for hepatic repopulation, even under the most challenging circumstances.

Despite the equivalent repopulation potential of WT and KO hepatocytes (Fig. 19), we observed marked differences in the post-transplant setting including an exacerbation of the pre-existing lipid abnormalities. The lipid accumulation by KO livers is reminiscent of non-alcoholic fatty liver disease that commonly evolves to a more severe form termed non-alcoholic steatohepatitis [238, 249]. This progression is associated with increased oxidative stress, de-regulation of cyp450 genes and extracellular lipid accumulation leading to long-term inflammation, fibrosis and hepatic failure [90, 249]. The prominence of inflammation- and fibrosis-related pathways in the post-transplant setting (Fig. 21*E*) is consistent with such evolution and probably involves transcripts expressed by inflammatory cells that co-purify with KO hepatocytes (Fig. 21*F* and Suppl. Fig. 37). The widespread de-regulation of cyp450 genes in KO hepatocytes might further abet this pro-inflammatory environment by affecting arachidonate and eicosanoid metabolism [246].

Myc's dispensability for hepatocyte repopulation is consistent with some reports in other organ systems. For example, *myc* deletion during murine intestinal morphogenesis leads to an early but transient decline in the number of small intestinal crypts [85]. Long-term suppression of Myc in adult mice with a globally-expressed dominant-negative form of the protein is also associated with transient intestinal and hematopoietic phenotypes [86]. In contrast, *myc's* deletion from hematopoietic stem cells results in impaired hematopoietic renewal and a sustained reduction in both myeloid and lymphoid compartments [250]. The long-term survival and maintenance of normal tissues thus appears to be under distinct forms of Myc-directed control that in many cases are quite different than occur in tumors, which are commonly "addicted" to the oncoprotein [86, 221]. Clearly, it will important in future work to define the nature of these differences.

4.4 EXPERIMENTAL PROCEDURES

4.4.1 Animal studies

All animal work was conducted in conformity with the Public Health Service Policy on Humane Care and Use of Laboratory Animal Research (ILAR) Guide for Care and Use of Laboratory Animals. Experimental procedures were approved by the Institutional Animal Care and Use Committee at the University of Pittsburgh. C57BL6 c-Myc$^{fl/fl}$ (WT) mice were obtained as a gift from I. Moreno de Alboran [89, 222]. They were housed in a pathogen-free facility, maintained under standard conditions. Mice were fasted overnight before sacrifice unless otherwise noted.

Myc KO mice were generated by breeding a Cre-recombinase heterogeneous mouse with a WT control, and then genotyped for Cre-recombinase positivity. FRG-NOD mice (Yecuris, Inc., Tualatin, OR) [240, 251] were bred and maintained on 8mg/L NTBC (Yecuris) in the drinking water. At the time of sacrifice, mice were euthanized, and their livers were weighed and divided into small pieces for further analysis. Genomic DNA was tested for Myc WT and KO PCR products, from primers listed in Table 6.

Table 6: PCR primers used in Chapter 4

Transcript Name:	Forward Primer Sequence (5' → 3')	Reverse Primer Sequence (5' → 3')	Annealing Temp.	Product Length (bps)
Myc WT	GCCCCTGAATTGCTAGGAAGACTG	CCGACCGGGTCCGAGTCCCTATT	65	379 (wt/wt) 413 (fl/fl)
Myc KO	TCGCGCCCCTGAATTGCTAGGAA	TGCCCAGATAGGGAGCTGTGATACTT	65	666
FAH WT	TGAGAGGAGGGTACTGGCAGCTAC	TTGCCTCTGAACATAATGCCAAC	57	250
FAH Δ	GATTGGGAAGACAATAGCAGGC	TTGCCTCTGAACATAATGCCAAC	57	145

4.4.1.1 Metabolic cage studies

Mice were maintained on a diet comprised of 45 kcal% fat (D12451, Research Diets Inc., New Brunswick, NJ) for 22 weeks prior to performing metabolism studies (high fat diet). Mice were weighed every week and body composition was determined every four weeks in awake mice using EchoMRI (Echo Medical Systems, Houston, TX). Oxygen consumption (VO_2), respiratory exchange ratio (RER), and physical activity were determined using a Comprehensive Laboratory Animal Monitoring System (CLAMS, Columbus Instruments, Columbus, OH). Mice were fed-fasted-refed during the CLAMS monitoring. Re-feeding was with 5% glucose solution in addition to standard chow diet. The respiratory exchange ratio (RER) was defined as the ratio of

VCO_2/VO_2. Caloric value (CV) was calculated from the formula: CV = 3.815 + (1.232 x RER) and heat production was calculated from the formula: Heat = CV x VO_2.

4.4.1.2 Hepatocyte isolation

Hepatocytes were isolated as previously described using a two-step collagenase perfusion method [228]. PCR primers listed in Table 6 allowed us to distinguish *fah*$^{+/+}$ donor and *fah-/-* recipient alleles. Similarly, donor and recipient *myc* alleles could be distinguished by a similar PCR-based strategy (Suppl. Fig. 31*A*-*C*).

4.4.2 Histology and immunohistochemistry

H&E and ORO staining of paraffin-embedded sections were performed using standard histopathologic techniques. FAH immuno-staining was performed as previously reported[228]. Immuno-staining for Myc, CD45 and 4-HNE were performed under similar conditions (Table 7).

4.4.3 Assays for pyruvate dehydrogenase, ^{3}H-palmitate oxidation, acetyl CoA and ATP

PDH activity was quantified using the PDH Enzyme Activity Microplate Assay Kit according to the directions provided by the supplier (MitoSciences, Eugene, OR). Liver pieces were homogenized in PBS and protein concentrations were determined using a BCA assay (Pierce, Inc., Rockford, IL). The homogenate was solubilized in the detergent provided in the kit and processed according the manufacturer's protocol. Typically, 100 µg of extract was assayed

kinetically on a BMG LabTech FLUOstar Omega instrument for 30 minutes (Cary, NC). The kinetic rates were determined as change in OD over time.

For ^{3}H-palmitate oxidation, fresh tissue was finely minced and added to SET buffer (0.25 M sucrose, 10 mM Tris, 1 mM EDTA at pH 7.4) containing 1 mM carnitine plus with 0.5 µCi BSA-bound [9.10-^{3}H(N)]-palmitate (sp. act. = 32 mCi/mmol) (Perkin-Elmer, Waltham, MA). The mixture was incubated at 37C for 1 hour, then homogenized and subject to organic extraction as previously described [11]. Total protein content was determined using the BCA reagent.

To measure Acetyl CoA, a pulverized piece of flash frozen tissue was solubilized in ice cold lysis buffer (20 mM Tris, pH 7.5; 150 mM NaCl; 1 mM EDTA; 1 mM EGTA; 1% Triton X-100; 2.5 mM sodium pyrophosphate; 1 mM β-glycerolphosphate; 1 mM Na3VO4; 1 µg/ml Leupeptin and 1 mM PMSF). The assay was then carried out according to manufacturer's instructions using an Acetyl-Coenzyme A Assay Kit (Sigma-Aldrich cat. # MAK039).

ATP assays were performed by lysing tissues with 10% trichloroacetic acid to inactivate ATPases, and then diluting the samples 1:50 with PBS. 100 µl of this was mixed with 50 µl of ATPlite mammalian cell lysis solution in quadruplicate in 96 well plates. The remainder of the assay was carried out according to the manufacturer's instructions using the ATPlite^{TM} Luminescence Assay System (Perkin Elmer, Waltham, MA). Results were normalized to total protein levels, which were determined on separate sets of identical wells.

4.4.4 Immuno-blotting

Immuno-blotting was performed essentially as described previously using whole liver lysates [11, 232]. Antibodies used are listed in Table 7.

Table 7: Antibodies used in Chapter 4

Name of antibody	Vendor	Catalog no.	Dilution	Secondary
AMP-dependent protein kinase (AMPK)	Cell Signaling	2532S	1:1000	Rabbit
pAMPK(Thr172)	Cell Signaling	4188S	1:1000	Rabbit
β-actin	Cell Signaling	3700S	1:10000	Mouse
FAH	Gift from Markus Grompe		1:500	Rabbit
c-Myc	Epitomics	1472-1	1:500	Rabbit
Caspase-3	Cell Signaling	9662S	1:2000	Rabbit
L-Myc (C-20)	Santa Cruz	sc-790	1:500	Rabbit
N-Myc	Santa Cruz	SC-791	1:1000	Rabbit
ChREBP	Abcam	ab157155	1:2000	Rabbit
GAPDH	Sigma	G8795	1:20,000	Mouse
4-HNE	EMD Millipore	393207	1:2,000	Rabbit
CD-45	Santa Cruz	sc-53665	1:100	Rat

4.4.5 BNGE of mitochondrial proteins and assays for ETC function

BNGE and enzymatic assays for ETC Complexes I, III, IV and V as well as supercomplexes comprised primarily of Complexes I, III and V were performed as previously described [4, 232].

4.4.6 Quantification of oxidative phosphorylation

These studies were performed on an Oroboros Oxygraph 2k instrument (Oroboros Instruments,Innsbruck, Austria). Homogenates were prepared from fresh liver tissue as described in the protocol provided by the vendor (MiPNet17.02). Oxygen consumption was measured in MiR05 medium (0.5 mM EGTA, 3 mM $MgCl_2$, 60 mM K-lactobionate, 20 mM taurine, 10 mM KH_2PO_4, 20 mM HEPES, 110 mM Sucrose, and 1 g/L bovine serum albumin) at 37^{o}C Substrates added throughout the experiment included those for Complex I (glutamate [10mM], malate [1mM], pyruvate [5mM]), complex II (succinate [10mM]), Complex V (ADP [4mM]) and cytochrome C (10 µM) to assess outer mitochondrial membrane integrity. O_2 consumption rates were normalized to total protein content.

4.4.7 Proteomic Mass Spectrometry

4.4.7.1 In solution trypsin digestion for mass spectrometry

For each digestion, 20 µg of mitochondria were re-suspended in 100 µl 50 mM NH4HCO3/0.02% ProteaseMAX™ Surfactant (Promega, Madison, WI). The mixture was then boiled for 10 min in the presence of 10 mM dithiothreitol and then alkylated by the addition of 45 mM iodoacetamide for 1 hr in the dark at room temperature). 0.5 µg of trypsin gold (Promega, Madison, WI) was then added and digestion was performed overnight at 37°C. The resulting tryptic peptides were de-salted using PepClean C-18 Spin Columns (Pierce, Inc., Rockford, IL), vacuum-dried, and re-suspended in 40 µl of 0.1% formic acid.

4.4.7.2 Targeted mass spectrometry assays for selected peptides

Selective/multiple reaction monitoring (SRM/MRM)-based targeted mass spectrometry was performed on a TSQ Quantum Ultra instrument (Thermo Fisher Scientific) coupled to a Thermo Fisher Nanoflow Dionex Ultimate 3000 liquid chromatography system. Nano-LC separations, each performed in duplicate, used an analytical C18 PicoChip™ columns packed with 10.5 cm Reprosil C18 3µm 120Å chromatography media with a 75 µm ID column and a 15 µm tip (New Objective, Inc., Woburn, MA). Mobile phase A consisted of 0.1% formic acid in HPLC water and mobile phase B consisted of 0.1% formic acid in 100% acetonitrile. 2 µg of tryptic peptides were loaded onto the column and washed with mobile phase A for 4min at 6 µl/min. The peptides were then eluted into the analytical C18 column at a flow rate of 300 nl/min with a gradient comprised of 0-5% solvent B for 4.5 min, 5-40% solvent B for 31.5 min, 40-95% solvent B for 4 min and 95% solvent B for 8 min. The collision energies were calculated using a linear equation CE =0.034 x m/z + 3.314. The full width at half maximum was set to be 0.7 Da for Q1 and Q3. The instrument was operated using scheduled SRM mode with 1 sec cycling time and 5 min retention time window. The majority of peptides had base peak widths of ~20 sec base and ~12 data points were acquired per chromatogram peak. Skyline software [252] was used to facilitate targeted SRM assay method development and data analyses. The transitions of the targeted peptides were originally selected based on mouse tandem spectrum library downloaded from PeptideAtlas (http://www.peptideatlas.org/) and subsequently optimized on the TSQ. All selected peptides and their corresponding SRM assay parameters are available upon requrest. Peak areas of all transitions for the same peptide were summed and the total peak area was used as metric for relative quantitation. Student's t test was applied to log-transformed total peak area to determine the significance of the differences between groups.

4.4.7.3 Unbiased label free mass spectrometry assays

2 µg of tryptic peptides per sample were analyzed with reverse-phased LC-MS/MS using a nanoflow LC (EASY-nLC II, Thermo Fisher) coupled online to LTQ/Orbitrap Velos Elite hybrid mass spectrometer (Thermo-Fisher). Mobile phases contained 0.1% formic acid in HPLC grade water for solvent A and 0.1% formic acid in 100% acetonitrile for solvent B. Peptides were first loaded onto a C-18 trap column (Thermo Fisher) and desalted on line for 6 µl solvent A. Peptides were then eluted onto a capillary column (75 µm inner diameter x 360 µm outer diameter x 15 cm long (Polymicro Technologies, Phoenix, AZ) slurry-packed-in-house with 5 µm particle size, 125 Å pore size C-18 silica-bonded stationary phase (Phenomenex, Torrance, CA) and resolved using a 100 min gradient at the flow rate of 0.2 µl/min (3-33% B for 90min, 33-80% B for 2min, constant at 80% B for 6min, and then 80-0% B for 2min). Eluted peptides were analyzed via electrospray ionization to the mass spectrometer. Data was collected in positive ionization mode, with FT MS1 AGC targets = 100,000, maximum injection time = 200 ms, spray voltage = 2.5 kV, capillary temperature = 325°C. Acquisition consisted of cycle of a full scan FT mass spectrum at a resolution of 60,000 and top 20 MS/MS spectra recorded sequentially on the most abundant ions on the ion trap.

Relative label free quantification of identified peptides/proteins was obtained MaxQuant software (version 1.5.1.0). Acquired MS/MS spectra were searched using the MaxQuant build-in Andromeda search engine against a mouse proteome downloaded from UniProt (http://www.uniprot.org/) together with a sequence database for frequently encountered contaminants with the following modifications: trypsin as the proteolytic enzyme, static carbamidomethylation of cysteine (+57.0214 Da), variable oxidization of methionine (+15.9949 Da) and variable acetylation of proteins' N-termini (+42.0106 Da). Mass tolerance was set to 20

ppm for initial search and 4.5 ppm for the main search for precursor ions, and 0.5 Da for fragment ions. Minimum peptide length was set to 7 amino acids and the false discovery rate (FDR) based on a target-decoy approach was set to 1%. The match between runs options was enabled with 2 min match time window and 20 min alignment window. The intensity values from MaxQuant output for identified peptides were used for relative quantitation across samples. Only peptides with non-zero intensity values in all samples were included for statistical test. Student's t test was applied to log-transformed intensities to identify peptides with significant difference between WT and KO. The linear step-up (LSU) [253] was used to compute FDR-adjusted p-values (q values) to account for multiple comparisons. Mitochondrial localization was confirmed by the David (http://david.abcc.ncifcrf.gov/) Bioinformatics Database and/or mouse MitoCarta Inventory (http://www.broadinstitute.org/pubs/MitoCarta/mouse.mitocarta.html). All selected peptides and their corresponding SRM assay parameters are available upon request.

4.4.8 RNAseq and analyses

Total RNAs were extracted from 10^7 isolated WT or KO hepatocytes using Qiagen RNeasy columns (Valencia, CA). Each RNA sample was assessed for quality and quantity using a Qubit 2.0 fluorometer and Agilent Bioanalyzer TapeStation 2200. The Sample preparation was replicated using Illumina TruSeq Stranded mRNA kit (San Diego, CA). mRNA was used to generate poly-A+ libraries using oligo-dT beads following 2 rounds of poly-A selection. Following this, RNA was fragmented to an average length of 260 nt by magnesium-catalyzed hydrolysis at 94^0C and then converted into cDNA by random priming. cDNA 3' ends were adenylated, followed by adaptor ligation and a 9-cycle PCR to enrich DNA fragments. cDNA

libraries were then validated using KAPA Biosystems (Wilmington, MA) primer premix kit with Illumina-compatible DNA primers on the Qubit 2.0 fluorometer and Tapestation 2200 systems described above. Libraries were diluted in 0.1% Tween 20 to concentrations of 2 nM for stabilization. The cDNA libraries were then pooled to final concentrations of 2.5 pM. Cluster generation and 75 bp paired-end single-indexed sequencing were performed with an Illumina NextSeq 500 sequencer. Sequence analysis was performed using mRNA-Seq for Differential Expression in Eukaryotes (Maverix Biomics, San Mateo, CA). Raw sequencing reads were quality checked for potential sequencing issues and contaminants using FastQC (Babraham Bioinformatics, Inc, Cambridge, UK.). Adapter sequences, primers, Ns, and reads with quality score below 28 were trimmed using fastq-mcf of ea-utils and PRINSEQ (http://prinseq.sourceforge. net/manual.html). Reads with a remaining length of less than 20 bp after trimming were discarded. Paired end reads were mapped to the mouse genome (m10) using TopHat (http://ccb.jhu.edu/software/tophat/index.shtml) in a strand specific manner. Read coverage on forward and reverse strands for genome browser visualization was computed using SAMtools, BEDtools, and UCSC Genome Browser utilities. Pairwise differential expression was quantified using Cuffdiff and DESeq [254, 255]. Cufflinks was used to determine FPKM levels for each gene from the TopHat alignment and was used as input for Cuffdiff. Significant differentially expressed genes were determined by adjusted P-value with a threshold of 0.05. DESeq was utilized for raw read counts, which were calculated by HTSeq based on the TopHat alignment (http://www-huber.embl.de/users /anders) /HTSeq/doc/count.html. Read counts were then normalized across all samples and significant differentially expressed genes were determined by adjusted P-value with a threshold of 0.05 [253].

4.4.9 Hepatic triglyceride, sterol and bile acid quantification

Triglyceride content was determined on ~25 mg of flash-frozen tissue using the Infinity™ Triglycerides reagent (Thermo Scientific, USA) as previously described [256].

To determine serum and hepatic sterol levels, we used ion-ratio GC/MS on an Agilent 6390N/5973 GC/MS system as previously described [9] with modifications to the GC/MS method to include ions specific for principal post-squalene cholesterol precursors. Bile acids were quantified on frozen total liver tissue using a Mouse Total Bile Acids Assay kit (Crystal Chem, Downer's Grove, IL) using the suppliers' protocol.

5.0 CONCLUSIONS AND FUTURE DIRECTIONS

5.1 CONCLUSIONS

We hypothesized that loss of Myc might switch dependence from glucose to fatty acids. One of the major findings in the previous chapters is the role of Myc in the regulation of FAO and lipid accumulation. We have shown in two models of *myc* homozygous deletion, a rat *myc-/-* fibroblast cell line and *myc-/-* mouse liver homogenates, an increase in FAO, indicating that the loss of Myc changes the preferential fuel source from glucose and glutamine to fatty acids. That both glycolysis and Oxphos are Myc-driven as well is abundantly clear, as Myc over-expressing cells can increase both while Myc KO fibroblasts and hepatocytes have reduced capacity [4]. Surpassing demand by β-oxidation, the accumulation of intracellular lipids droplets also accompanies inhibition of Myc, as demonstrated in cancer cell lines or non-transformed cell lines and *in vivo* tissue (chapters 2 and 4 and [69, 72]). Because all of the Myc KO models demonstrated lipid congestion resulting from an imbalance between FAO and uptake, we can infer the means for sensing proper balance must be Myc regulated. The loss of Myc typically results in decreased respiratory chain capabilities that result in mitochondrial dysfunction, ATP deficit, activation of AMPK [4, 11, 72]. That Myc KO hepatocytes do not have activated AMPK or reduced ATP and acetyl CoA levels means *in vivo* loss by hepatocytes does not result in

severe energy crisis. Perhaps because the ETC default in mouse hepatocytes is not as severe, they are able to better cope metabolically with Myc loss.

In chapter 3, we examined the coordination between Myc-directed metabolism and AMPK, and how this would affect proliferation. AMPK was found to be unnecessary for the induction of Myc-driven proliferation in MEFs, but it does contribute to maintaining mitochondrial homeostasis. Crosstalk between Myc and AMPK balances Myc-driven anabolism with AMPK-driven catabolism, as illustrated in the dramatic drop of ATP levels in *ampk-/-* cells following the abrupt induction of Myc expression. That Myc activation leads to increased glycolysis and ROS production has been documented in many studies [22, 152], but that AMPK represses glycolysis and ROS production has been shown in cells with only Myc de-regulation. Loss of AMPK function may be more devastating in further progressed tumorigenesis with a variety of driver mutations.

Chapter 4 offered conclusive evidence that Myc is unnecessary for adult hepatic proliferation, during the course of a 50-100-fold expansion of transplanted Myc KO hepatocytes. The more intense proliferative stress imposed by this method compared to a 2/3rd partial hepatectomy is drastic. Interestingly, the fact that our assay was so specific to hepatocytes does not allow any conclusions to be made on any of the other liver cell types, such as biliary-specific regeneration [257]. Though there was no differential repopulation capacity, there was a huge disparity in the amount of stress and damage caused by the KO population, as shown by transcriptional differences, lipid droplet accumulation, inflammatory infiltrate, and lipid peroxidation. This is analogous to the human disease non-alcoholic fatty liver disease (NAFLD) which we hypothesize could worsen to non-alcoholic steatohepatitis (NASH) with increased stress common to the aging process.

5.2 FUTURE DIRECTIONS

5.2.1 What is the role of HIF2 and MONDOA/CHREPB in lipid accumulation occurring from loss of Myc?

A paper from Rankin *et al.* [258] found changes in lipid metabolism very similar to our Myc KO hepatocytes, including severe hepatic steatosis, caused by constitutive activation of hypoxia inducible factor 2 (HIF2). HIF2 has a stabilizing effect on the Myc-Max heterodimerization under normal conditions, by binding with Max and blocking interactions with Mad1, which can enhance transcription of target genes [2] and is expressed preferentially in the hepatic parenchyma [259]. HIF2 also regulates the Myc family of transcription factors by inducing Mxd2 transcription [1]. When Myc is absent or deregulated, the effect on HIF2 is unknown. RNA sequencing in proliferating, transplanted hepatocytes (though contaminated with an equal proportion of recipient tyrosinemic hepatocytes as described in chapter 4) found HIF2α (also known as EPAS1) to be 1.5-fold up-regulated by RNA sequencing in the Myc KO hepatocytes, while HIF2β (or ARNT2) was 5.2-fold up-regulated in KO hepatocytes. This implies that loss of Myc constitutively up-regulates HIF2 at the transcriptional level in proliferating hepatocytes (although we cannot state unequivocally that the transcripts are of donor cell origin).

To summarize the Myc family of transcription factors, Myc (and paralogs L-Myc and N-Myc) heterodimerize with obligate binding partner Max, another basic helix-loop-helix leucine zipper (bHLHLZ) protein (Figure 22A). The Mxd arm of the family include Mxd1-4, MNT, MGA, which also bind to Max and oppose Myc signaling, such as prompting cell cycle arrest and differentiation [41]. Mxd1&4 and MNT can also bind to MLX, which coordinates the

nutrient sensing arm of the Myc family. The nutrient sensing arm of the family include MondoA and MondoB, more commonly referred to as ChREBP. Loss of Myc in these proliferating hepatocytes keeps HIF2 from binding to Myc-Max dimers and instead allow Max:Mxd1 heterodimerization and HIF2 activation of Mxd2. (Figure 22B). De-regulation in the Myc family members could tip the balance between normal lipid regulation and increased lipid accumulation as regulated by the Myc family member MondoA (as described by [40, 41]). Several interesting questions arise from this, such as: 1) What are the proteins levels of HIF2, the Mxd proteins, MondoA and ChREBP in Myc-driven proliferation states?; 2) Does ChREBP play a similar role in lipid regulation, given that it is the predominant liver isoform and that it has been shown previously to preferentially regulate genes involved in carbohydrate and lipid metabolism [260]?; 3) Is HIF2 necessary for hepatic survival in proliferating *myc*-/- hepatocytes, and in what manner does it contribute to the steatosis found in both models of Myc loss and HIF2 constitutive activity?; and 4) Does HIF2 interact with MondoA or ChREBP, or perhaps control Max or Mlx dimerization in some way between the Mxd arm, which affects hepatic steatosis?

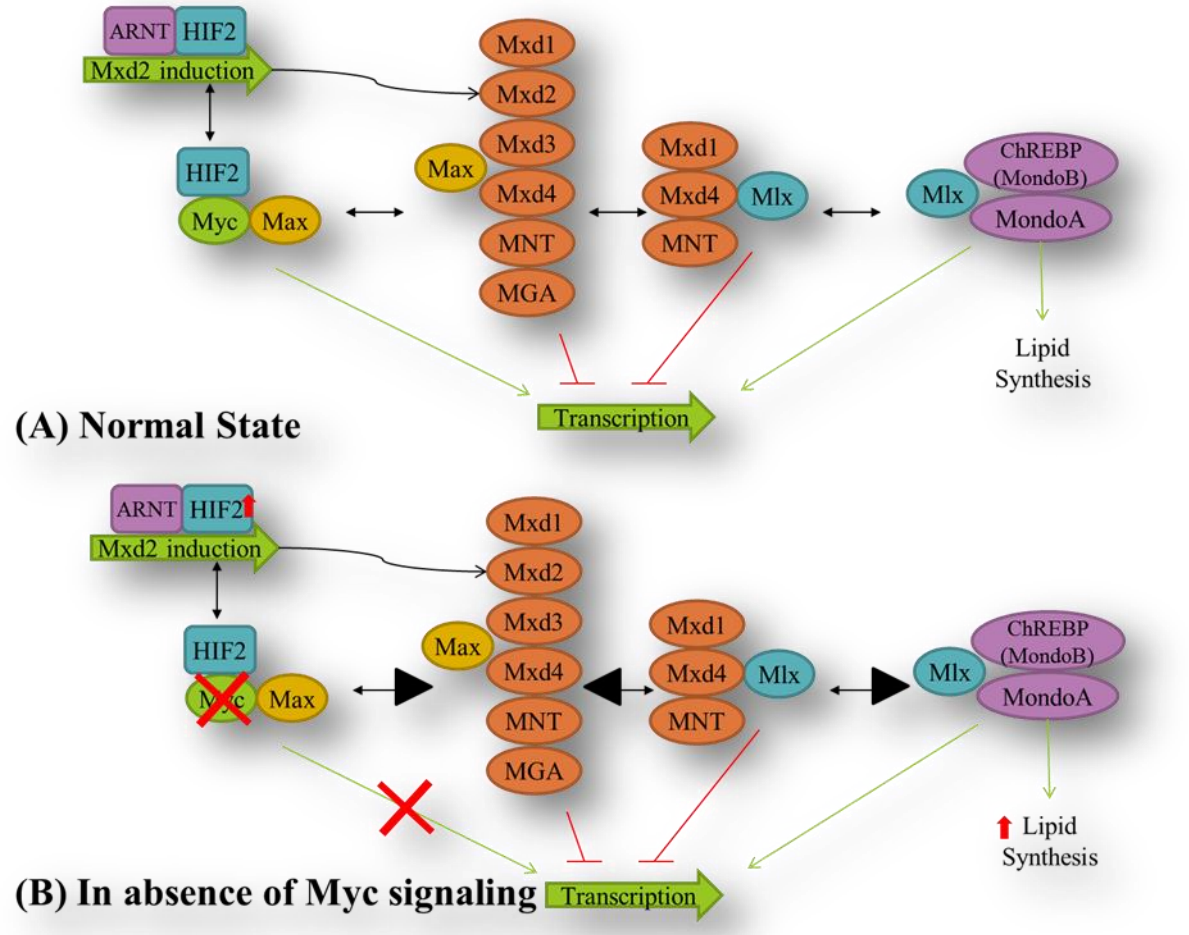

Figure 22: Role of HIF2 and Myc in Steatosis (A) Under normal, basal conditions, the Myc:Max heterodimer is stabilized by HIF2 [1, 2], which acts in balance with other Myc family members to coordinate transcription and appropriate lipid synthesis. (B) When Myc is absent, Max can bind preferentially to the Mxd arm, thus allowing Mlx:MondoA heterodimers to increase lipid synthesis.

5.2.2 How does lipid biosynthesis affect proliferation in Myc-driven cancers?

Lipid synthesis is critical for many tumors, including Myc-driven cancer [40, 261]. This is supported by slowed tumor growth after inhibiting key enzymes involved in lipid synthesis such

as ACCα, FASN, and stearoyl-CoA desaturase 1 (SCD1) [63, 64, 262]. Transcription factors that promote lipid biogenesis are considered good targets for cancer metabolism [263], and many of these are down regulated in *myc* hypomorphic mice, which also exhibit lower cholesterol and fibrosis levels than controls [78]. The accumulation of fat in Myc KO models comes from increased uptake, rather than increased synthesis (as shown in Chapter 2), and enhanced β-oxidation further limits synthesis (in an AMPK-dependent manner as described previously). It is possible that a therapeutic reduction of Myc might provide health benefits against diseases like non-alcoholic fatty liver disease or hepatocellular carcinoma, particularly when combined with therapeutic interventions like metformin. Metformin's mechanism of action involves the activation of AMPK, which can then drive FAO and Oxphos while simultaneously inhibiting fatty acid synthesis [264, 265]. Faubert *et al.* [79] found that loss of AMPK signaling cooperates with Myc to accelerate tumorigenesis, therefore, reversing both of these trends might dramatically reduce tumorigenesis. The reduction of Myc combined with AMPK activation would also combat cancers through one of the main mechanisms of Myc-driven cancers – an increase in fatty acid synthesis.

5.2.3 What is the effect of AMPK loss in Myc-driven tumors, and how does non-cannonical ROS activation contribute?

In chapter 3, we found the primary mechanisms of AMPK activation during Myc over-expression was the non-canonical activation by ROS, in addition to a reduction in cellular ATP (Figure 23A). Potential sources of ROS include the Myc activation of genes that elevate

oxidative metabolism thus ROS production, such as p53 [266], ornithine decarboxylase [267], TGF-α [268], or the fact that Myc increases Oxphos and thus increases the basal ROS produced in the ETC. The sustained phosphorylation of AMPK lasted 8 days after the removal of 4HT and 4 days beyond a restoration of ATP levels (Figure 23B). We also found ROS levels to remain elevated up to 8 days after 4HT removal, as measured by MitoSox staining and flow cytometry. Sustained phosphorylation of AMPK ceased after a corresponding reduction in ROS by the antioxidant N-acetyl Cysteine (NAC) (Figure 23C). Non-canonical activation by sustained ROS explains the delayed phosphorylation of AMPK when 4HT was removed.

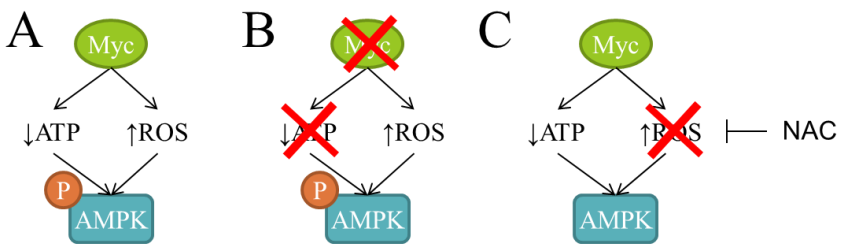

Figure 23: Activation of AMPK by Myc. (A) Myc induction promotes AMPK activation through an ATP poor and ROS rich environment. (B) When Myc signaling is removed, ATP levels return to normal almost immediately, but ROS levels remain high and AMPK stays activated. (C) When ROS signaling is perturbed by an antioxidant, N-Acetyl Cysteine (NAC), an ATP-poor conditions persists but AMPK is not activated.

Not as much is known about non-canonical modes of AMPK activation, so it is worthwhile to expand this model of Myc-directed activation and see if the ROS activation still occurs. A cancer cell line where Myc is a major driver of proliferation could be used to determine if tumorigenesis requires AMPK, either during initiation or for sustained proliferation. Going one step further, if AMPK is required, is initiation or proliferation inhibited if AMPK

activation is inhibited by reducing ROS levels? The activation of AMPK may or may not require reduced ATP or increased ROS, as determined by pharmacological inhibition of each.

APPENDIX A

SUPPLEMENTAL FIGURES

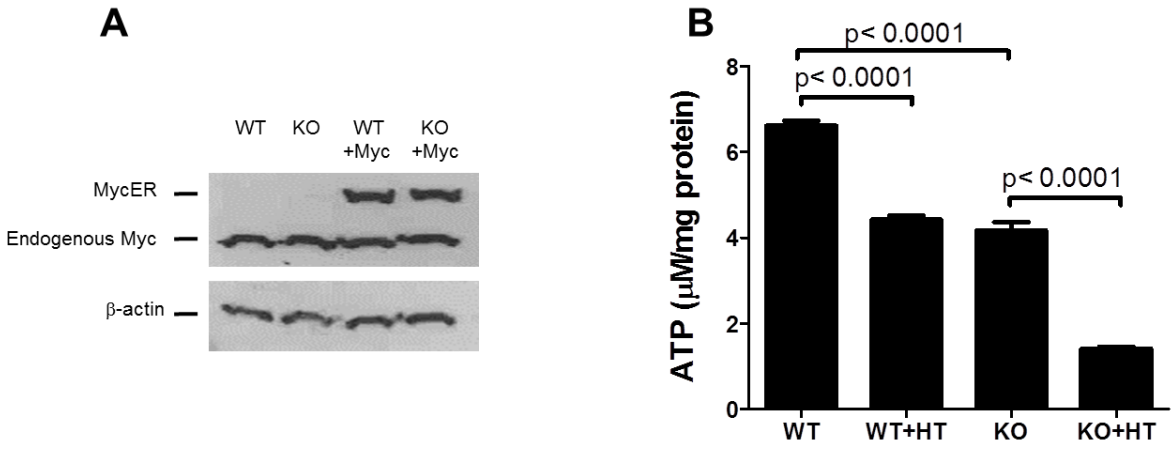

Figure 24: (*A*) Immunoblots of endogenous c-Myc and MycER in AMPK WT and KO MEFs before and after MycER transduction and β-actin loading control. Both proteins were detected with an anti-Myc antibody. (*B*) Baseline ATP levels in WT and KO cells. The results represent the data obtained in Fig. 15*D* plotted as absolute rather than relative ATP levels. Several repeat experiments showed ATP levels in KO cells to be reproducibly lower than WT cells by 30-40%.

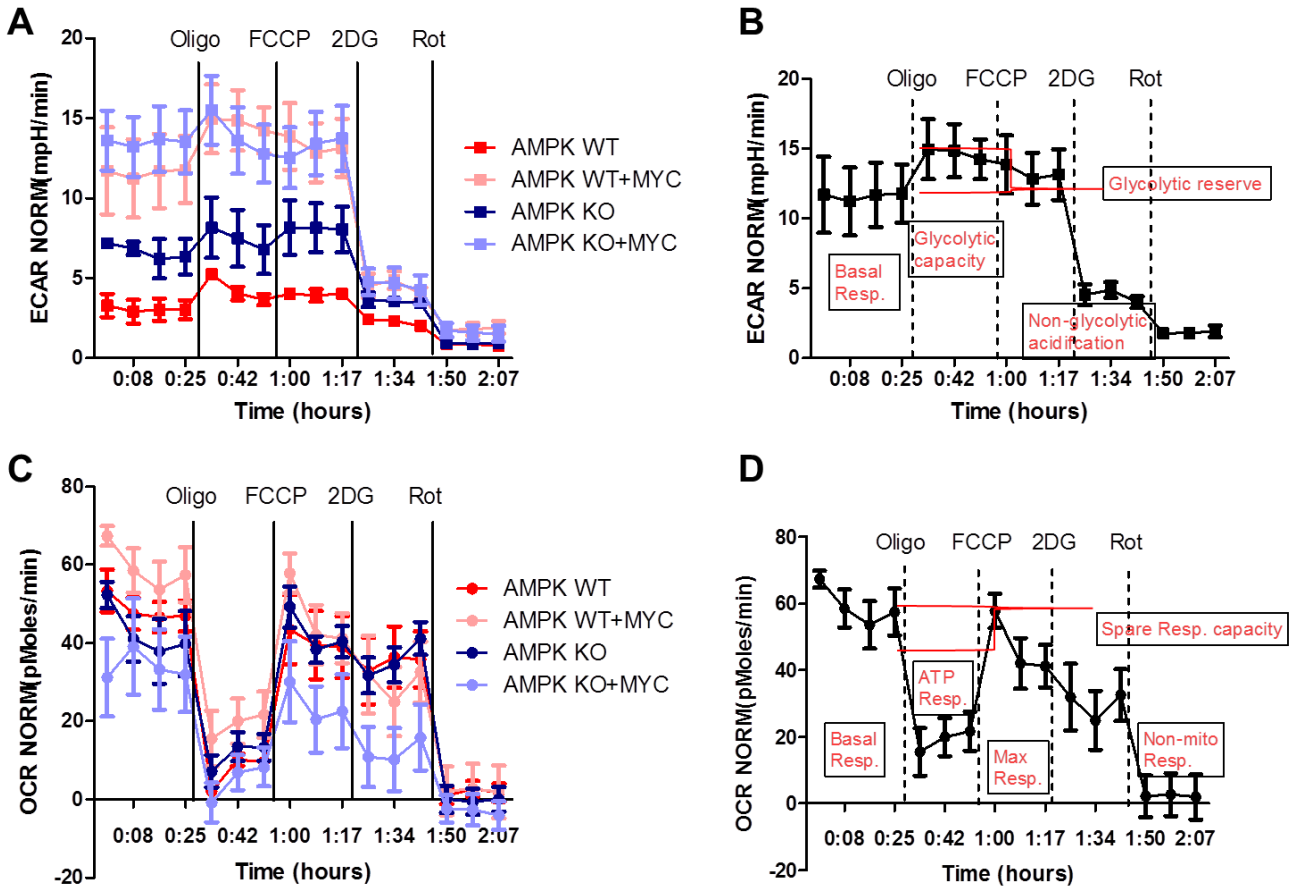

Figure 25: Seahorse Flux Analysis of Extracellular Acidification Rate (ECAR) and Oxygen Consumption Rate (OCR). Cells were plated and analyzed as described in Materials and Methods. (*A*) ECAR normalized to cell number at conclusion of the experiment, which includes the addition of 1 µM oligomycin (oligo, an inhibitor of Complex V [ATP synthase]), 0.3 µM carbonyl cyanide-p-trifluoromethoxyphenylhydrazone (FCCP, an uncoupling agent), 100 mM 2-Deoxy-D-glucose (2-DG, an inhibitor of glycolysis), and 1 µM rotenone (rot, a complex I inhibitor). Note that the addition of oligomycin is associated with a continued higher level of ECAR by both WT+Myc and KO+Myc cells, which is consistent with their overall rates of glycolysis being enhanced following MycER activation (*B*) Representation of basal respiration, glycolytic capacity, non-glycolytic acidification, and glycolytic reserve (differences in respiration after addition of oligomycin). (*C*) OCR normalized to cellular number at the conclusion of the experiment, including the same set of injections described in (*A*). (*D*) Representation of OCR basal respiration, ATP-dependent respiration, maximum respiration, non-mitochondrial respiration, and the spare respiratory capacity.

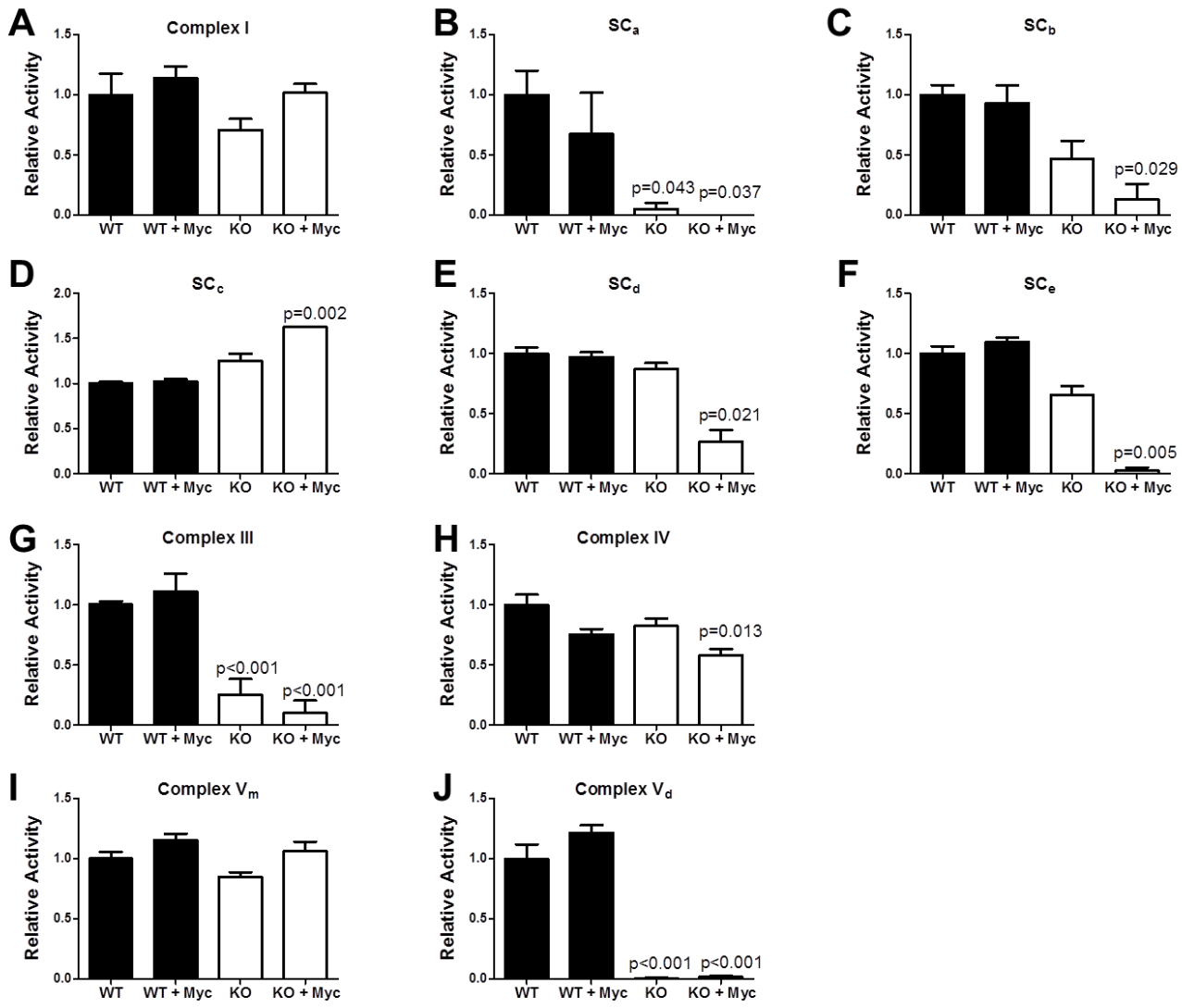

Figure 26: Quantification of the results shown in Fig. 9. In situ assays for each complex were performed on triplicate samples. Results are expressed as the mean ± 1 SEM after normalizing each sample's activity to the amount of protein present in the respective complex. This value in WT cells was arbitrarily set to 1 in all cases to allow for relative comparisons. Complex II could not be reliably assayed in situ and was therefore assayed in separate reactions and adjusted to total input mitochondrial protein content (see Fig. 9*C*). Significance was determined using the Students' t-test and all values are compared to WT cells.

Category	Symbol	WT	WT + Myc	KO	KO + Myc	P value (WT:WT+Myc)	P value (WT:KO)	P value (KO:KO+Myc)
Amino acid synthesis	Alt1	1.00	2.08	1.06	1.32	***	ns	ns
	GOT1	1.00	0.50	0.40	0.39	***	***	ns
	Ser-HMT	1.00	0.77	0.54	0.74	***	***	***
	Tha1	1.00	1.39	1.23	1.30	***	ns	ns
Gluconeo-genesis	FBP1	1.00	1.80	0.20	0.13	***	***	***
	G6P	1.00	0.49	0.51	1.60	***	***	***
	PEPCK	1.00	1.07	0.41	0.54	ns	***	ns
Pyruvate Synthesis/ Glycolysis	PC	1.00	1.59	0.97	1.25	***	ns	ns
	PdhE1a	1.00	1.67	0.47	0.90	***	***	***
	PDK1	1.00	0.68	0.12	0.40	***	***	ns
	PDP2	1.00	1.31	1.06	1.61	***	ns	***
	PKM1	1.00	2.01	0.68	0.99	***	***	*
	PKM2	1.00	1.85	0.56	0.67	***	***	ns
TCA cycle	αKGDH (OGDH)	1.00	2.14	1.60	1.82	***	***	ns
	αKGDH (DLD)	1.00	1.53	0.47	0.91	***	***	***
	αKGDH (DLST)	1.00	1.57	0.44	0.71	***	***	ns
	FH1	1.00	0.45	0.82	0.53	***	ns	***
	G3PDH (cyto)	1.00	1.73	1.29	2.03	***	**	***
	G3PDH (mito)	1.00	1.22	0.31	0.52	ns	***	ns
	IDH1 (cyto)	1.00	0.71	1.63	1.29	***	***	ns
	IDH2 (mito)	1.00	1.93	1.03	0.72	***	ns	*
	IDH3 (cyto+mito)	1.00	0.54	0.70	0.60	***	***	ns
	MDH (cyto)	1.00	1.37	0.69	1.22	***	**	***
	MDH (mito)	1.00	1.55	0.66	1.27	***	***	***
	SDH a	1.00	1.62	0.43	0.55	***	***	ns
	SDH b	1.00	1.52	0.41	0.51	***	***	ns
	SDH c	1.00	1.51	0.80	1.06	***	ns	ns
	SDH d	1.00	1.53	0.53	0.71	***	***	ns
Other	Cit Synth	1.00	0.54	1.01	0.91	***	ns	ns
	ACLY	1.00	0.43	0.63	0.66	***	***	ns

Figure 27: Quantification of real time qRT-PCR data depicted in Fig. 10*A*. The values presented were compared to average gene expression and normalized to β2 microglobulin gene expression. **** P < 0.0001, *** P < 0.001, ** P < 0.01, * P < 0.05.

Symbol	WT	WT + Myc	KO	KO + Myc	P value (WT:WT+Myc)	P value (WT:KO)	P value (KO:KO+Myc)
PPARγ	1.00	1.35	0.43	0.59	*	**	*
PPARα	1.00	0.33	0.52	0.34	**	**	ns
PGC1α	1.00	0.98	0.59	1.29	ns	****	****
POLRMT	1.00	0.78	0.70	1.13	ns	ns	ns
Mterfd1 (Mterf3)	1.00	0.98	0.91	0.75	ns	ns	*
YY1	1.00	1.24	1.00	1.10	ns	ns	ns
PGC1β	1.00	1.22	1.05	1.81	*	ns	*
Mterfd2 (Mterf4)	1.00	1.11	1.05	0.84	ns	ns	***
SIRT3	1.00	0.83	1.16	1.12	***	**	ns
TFAM	1.00	0.97	1.18	0.93	ns	**	**
PPARβ	1.00	1.29	1.18	1.05	**	*	*
ERRα	1.00	0.88	1.24	0.90	ns	*	***
NFE2L2 (NRF2)	1.00	2.16	1.28	1.65	**	ns	ns
UCP2	1.00	4.63	1.58	0.41	***	ns	**
PRC	1.00	1.04	1.61	1.24	ns	****	**
TFB2M	1.00	0.62	1.87	1.29	ns	*	*
NRF1	1.00	1.55	2.37	1.88	ns	**	ns
NSUN4	1.00	2.38	2.96	1.95	**	**	ns
Mterf1	1.00	1.08	4.19	1.25	ns	***	****
ERRβ	1.00	1.10	6.75	7.24	ns	*	ns

Figure 28: Quantification of real time qRT-PCR data depicted in Fig. 10*D*. The values presented were compared to average gene expression and normalized to β2 microglobulin gene expression. **** P < 0.0001, *** P < 0.001, ** P < 0.01, * P < 0.05.

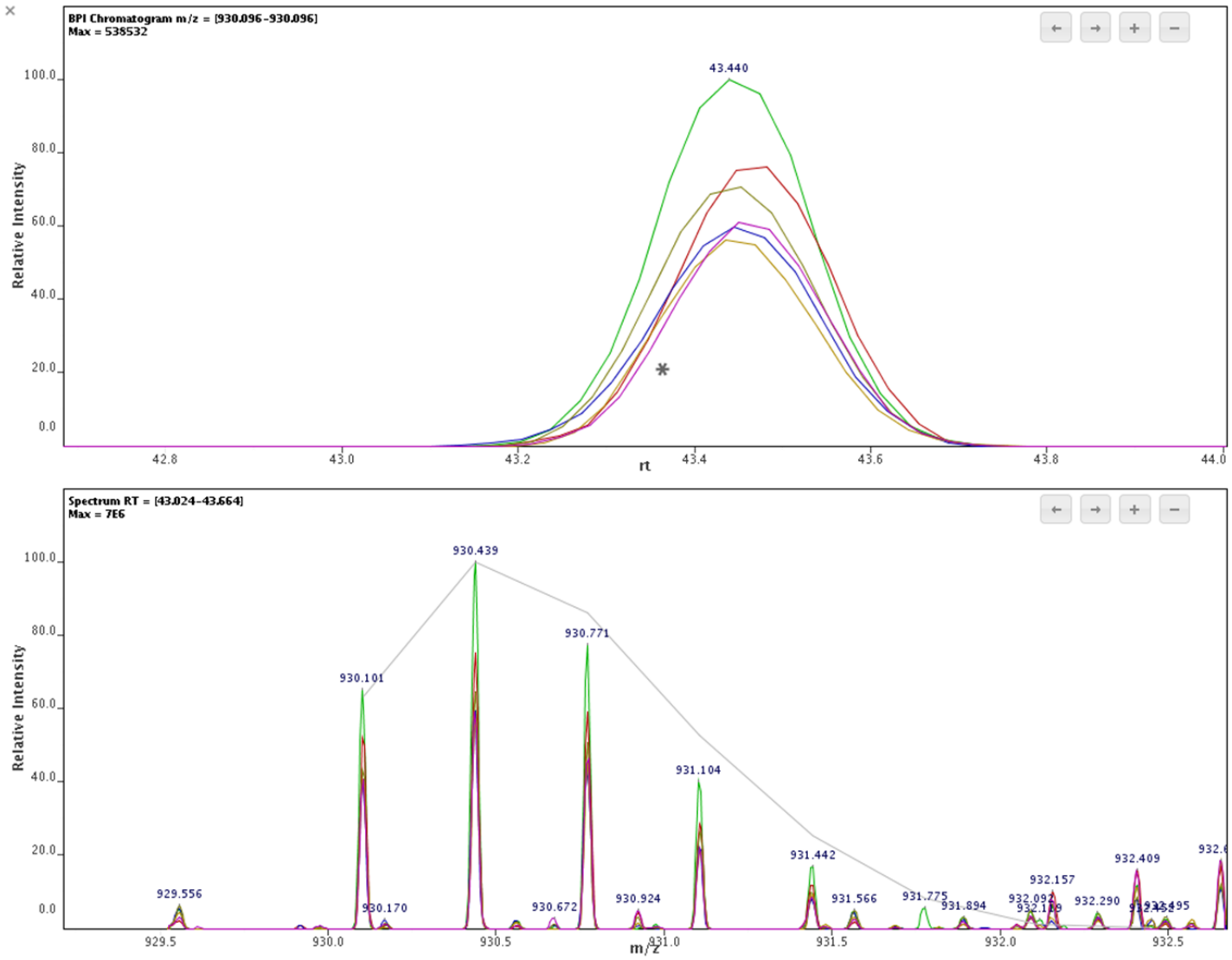

Figure 29: Isotope distribution. High-resolution dMS chromatogram (top) and mass spectrum (bottom) showing the isotope distribution for the tryptic peptide ATEMVEVGPEDDEVGAERGEATDLLR derived from Polymerase I and transcript release factor (Ptrf) with monoisotopic m/z = 930.103 Da and retention time 43.5 minutes. Colored lines show the average signal for 4 WT (blue), 4 KO (red), 4 WT+Myc

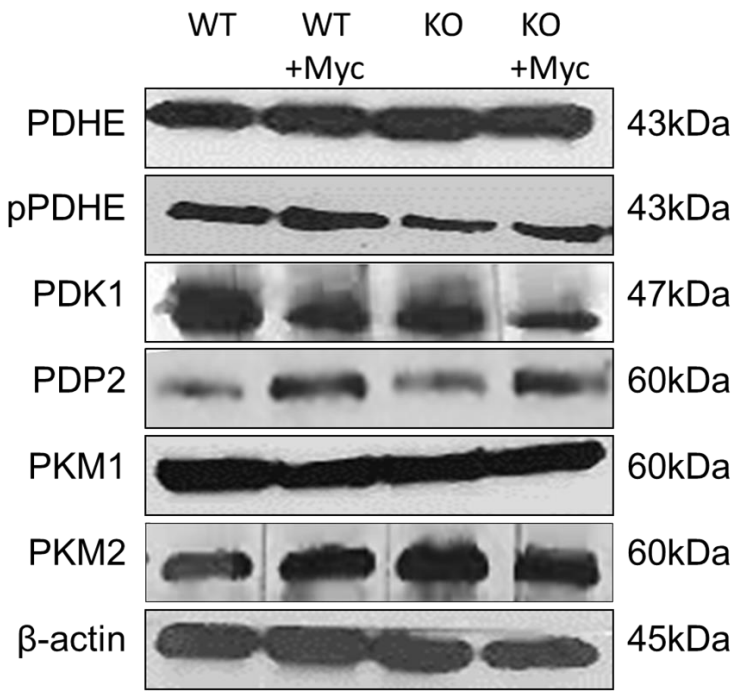

Figure 30: Immuno-blotting for selected pyruvate metabolizing enzymes. Pyruvate dehydrogenase (PHDE) and Ser293 (activated) phosphorylated PDHE. Pyruvate dehydrogenase kinase (PDK1), Pyruvate dehydrogenase phosphatase (PDP2), Pyruvate kinase M1 and M2 (PKM1/2), and β-actin loading control.

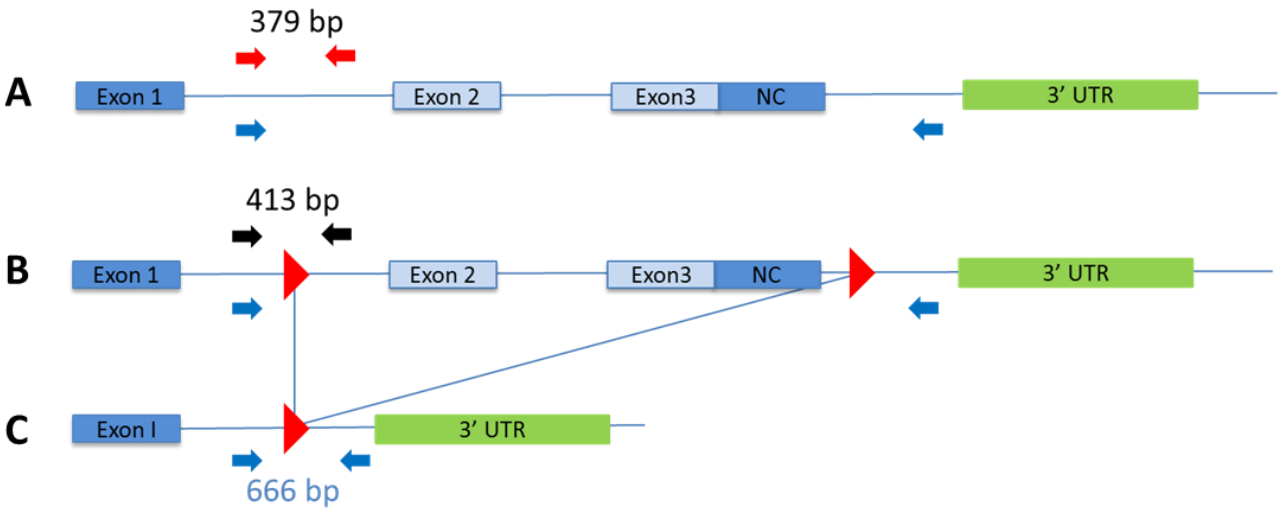

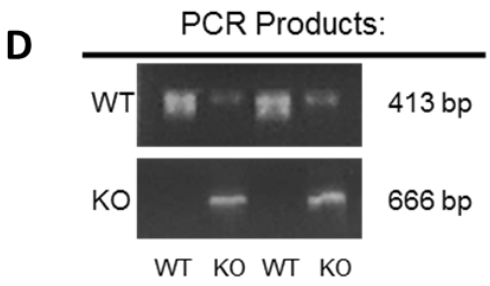

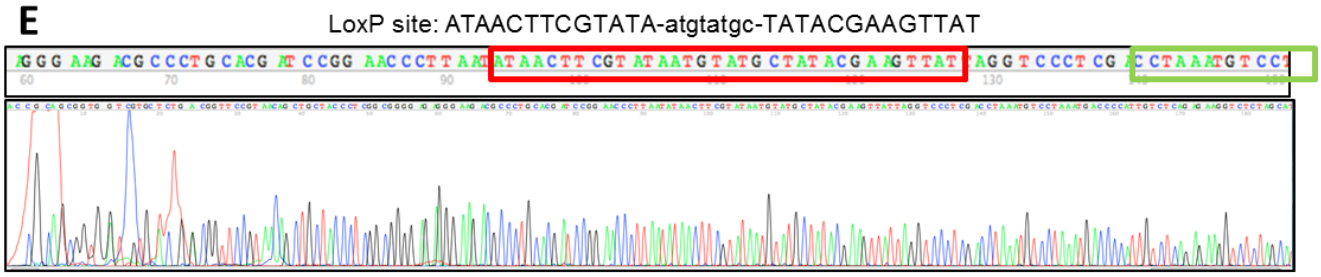

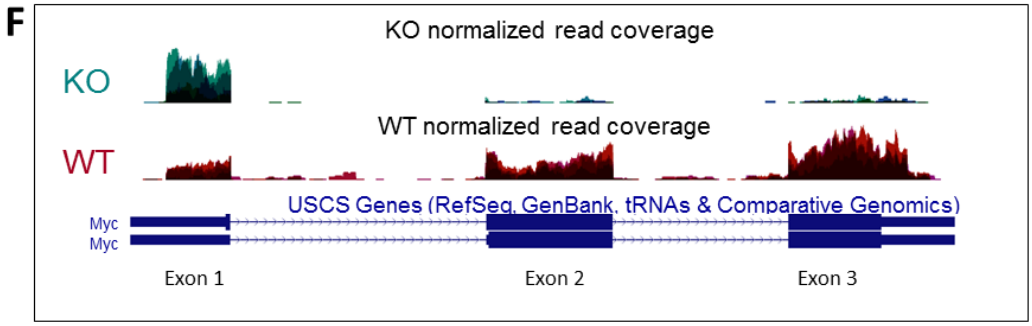

Gene ID	Gene	Description	WT abundance	KO abundance	Fold Change	p-value
17869	Myc	myelocytomatosis oncogene	200.23	34.07	-2.3	2.9×10^{-9}

Figure 31: Deletion of myc coding exons 2 and 3 from KO hepatocytes. (*A*) The myc locus in "unfloxed" WT (mycwt/wt) animals. Red arrows indicate the same set of primers as black arrows in B but with a smaller product. (*B*) The myc locus in WT (mycfl/fl) animals. LoxP sites are indicated by red triangles. PCR primers used to amplify the WT allele are indicated with black arrows with the size of the expected PCR product (in bps) indicated. (*C*) The myc locus following Cre-recombinase-mediated recombination. PCR primers used to amplify KO (myc-/-) alleles are indicated by blue arrows with the size of the PCR product indicated. (*D*) Myc alleles were amplified from WT and KO hepatocyte DNAs of 3 month old mice and resolved by agarose gel electrophoresis. Typical genotyping results are shown for two representative animals of each group. (*E*) DNA sequence of the relevant region of the KO PCR product, confirming the deletion and showing that the LoxP region (boxed in red) is flanked by intron 1 and intron 3 sequences. Note that the PCR primers depicted in A can also be used to distinguish this allele from a normal myc allele without LoxP sites. (*F*) KO hepatocytes show greatly reduced expression of myc coding exons 2 and 3. RNAseq reads across each of the 3 myc exons were compiled for both WT and KO hepatocytes. Each set of reads represents the sum of sequences generated from hepatocyte RNAs of four animals from each group.

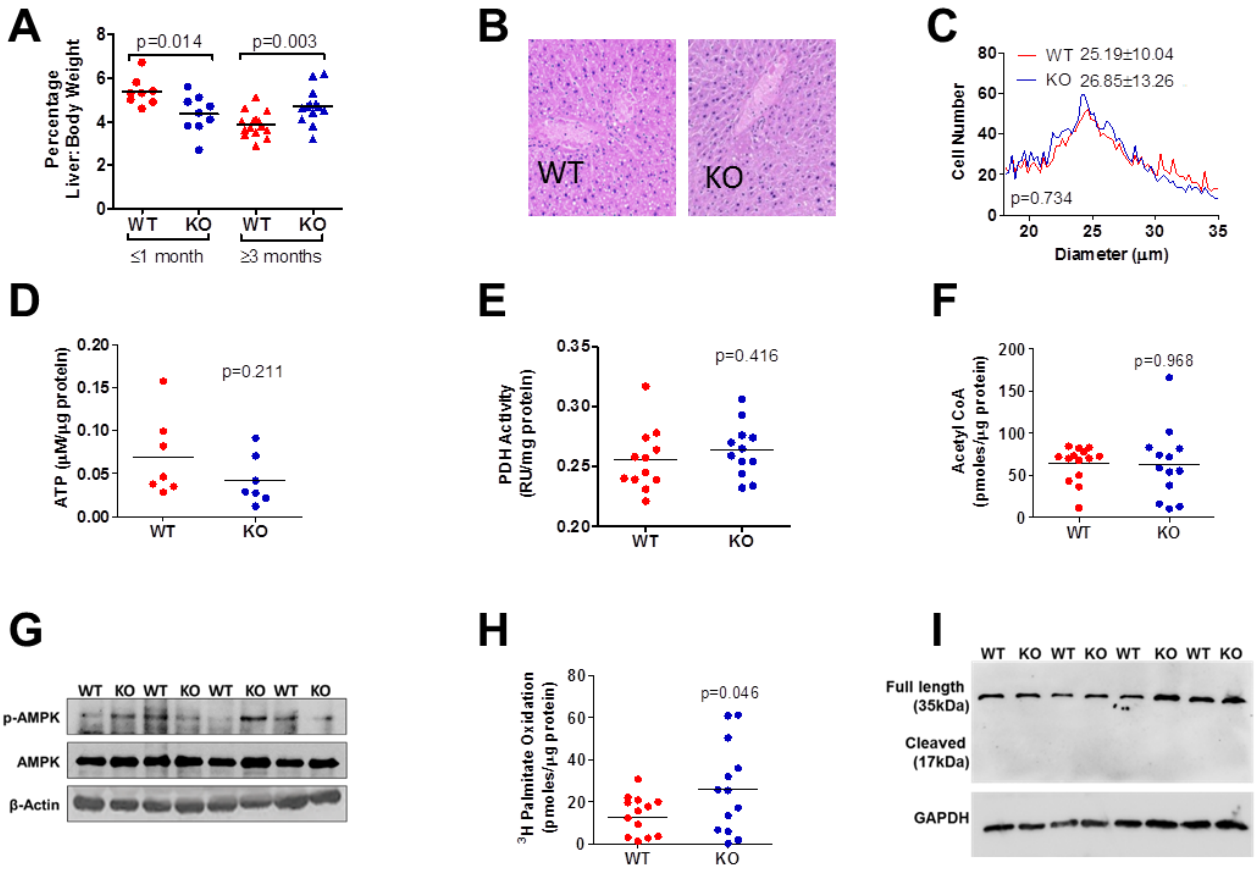

Figure 32: Characterization of WT and KO livers and hepatocytes. (*A*) Liver:body mass ratios. Weights were determined on groups of young and old mice (<1 month and >3 months old, respectively). (*B*) Typical histologic appearance of H&E-stained sections of WT and KO livers from young mice. No obvious differences were noted in examination of >10 livers from each group. (*C*) Hepatocyte sizing from ~2 month old WT and KO mice. At least 1500 hepatocytes from individual WT and KO mice were examined. Similar results were obtained from two additional sets of animals (not shown). (*D-F*) ATP content, PDH activity and acetyl CoA levels, respectively, were quantified on liver lysates. (*G*) AMPK Immunoblotting. Total liver lysates from individual WT or KO mice were immuno-blotted for total AMPK, pAMPK(Thr172) and β-actin as a loading control. (*H*) 3H-palmitate β-oxidation. Liver slices were incubated with 3H-palmitate and the amount of tritium incorporated into water-soluble products was quantified. (*I*) Caspase 3 immunblots. Total liver lysates from WT and KO mice were blotted against full length and cleaved Caspase 3 with GAPDH as a loading control.

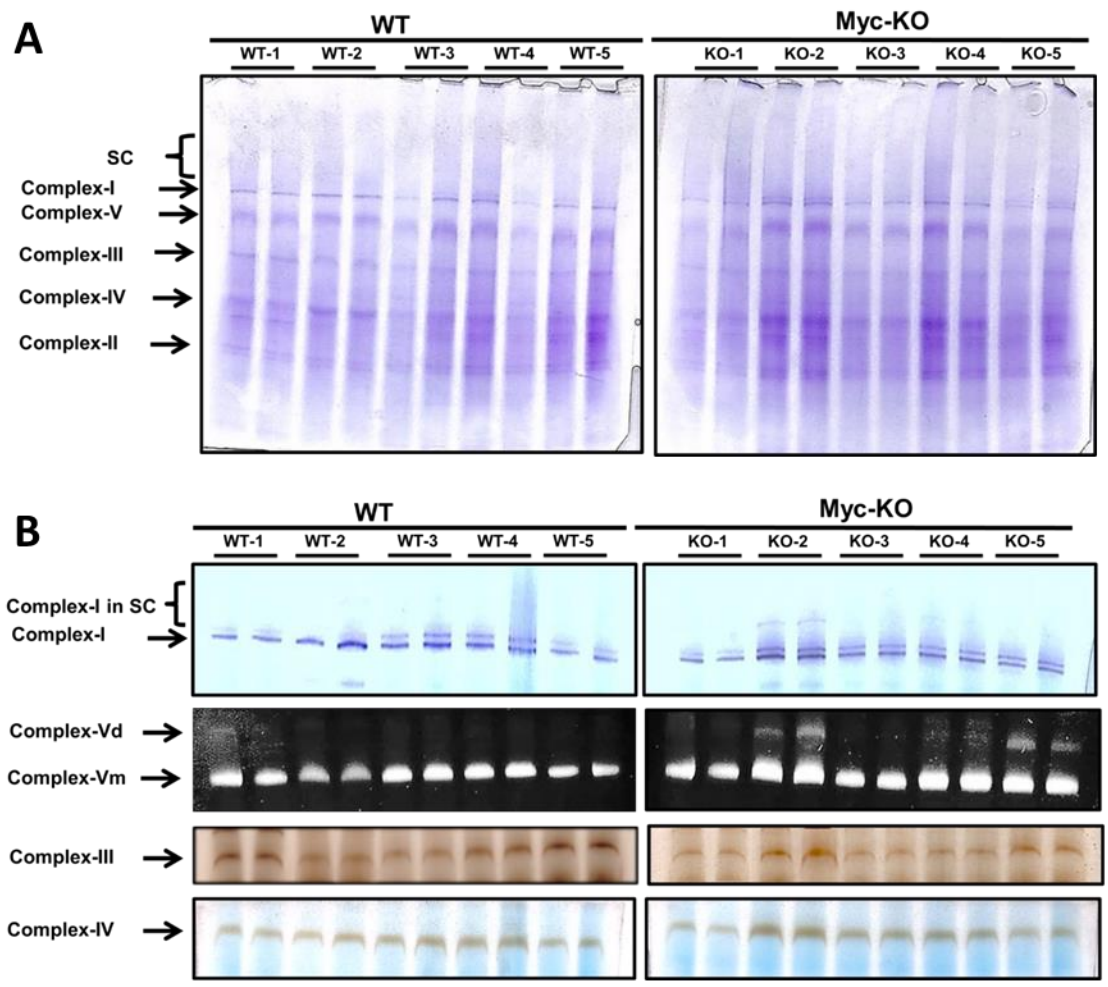
A
WT
Myc-KO
WT-1
WT-2
WT-3
WT-4
WT-5
KO-1
KO-2
KO-3
KO-4
KO-5
SC
Complex-I
Complex-V
Complex-III
Complex-IV
Complex-II
B
WT
Myc-KO
WT-1
WT-2
WT-3
WT-4
WT-5
KO-1
KO-2
KO-3
KO-4
KO-5
Complex-I in SC
Complex-I
Complex-Vd
Complex-Vm
Complex-III
Complex-IV

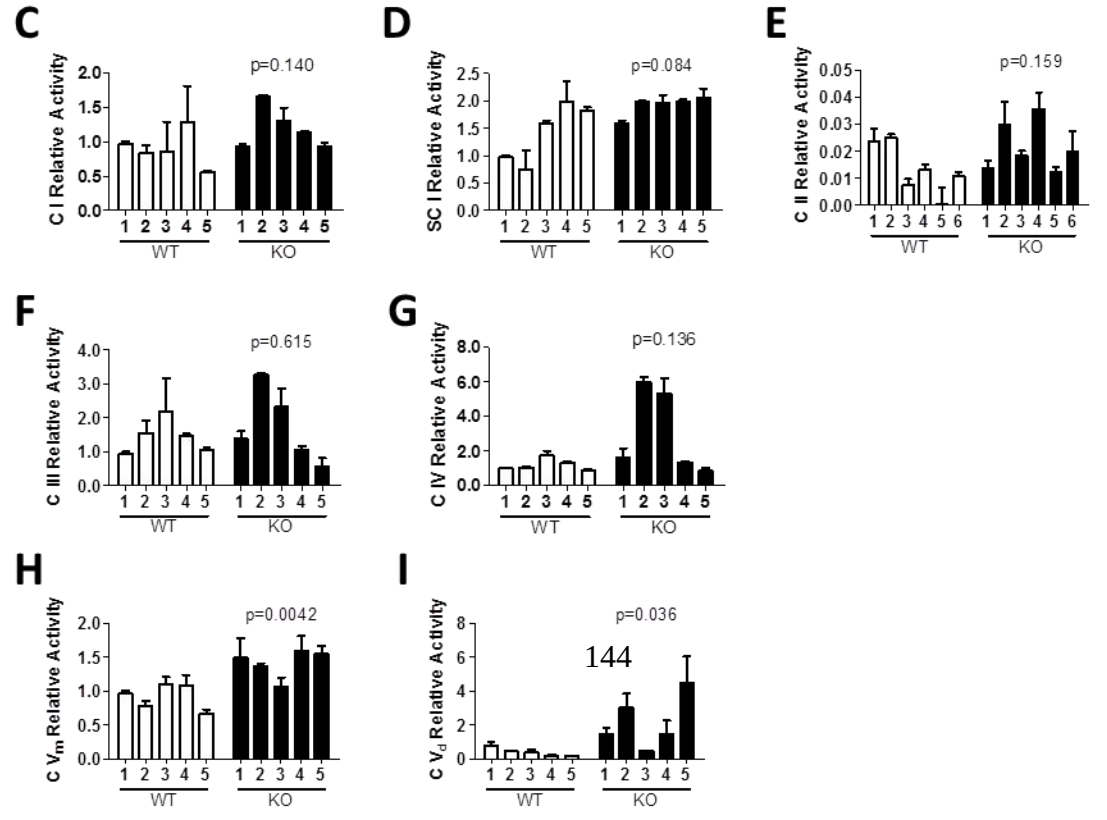
C
C I Relative Activity
p=0.140
D
SC I Relative Activity
p=0.084
E
C II Relative Activity
p=0.159
F
C III Relative Activity
p=0.615
G
C IV Relative Activity
p=0.136
H
C Vm Relative Activity
p=0.0042
I
C Vd Relative Activity
p=0.036
WT
KO

Figure 33: Comparison of ETCs in WT and KO livers. (*A*) Representative BNGE of duplicate mitochondrial samples, each prepared independently from 5 WT and 5 KO mouse livers. Mitochondria were purified as previously described [3, 4]. Arrows indicate each of the complexes as well as higher order supercomplexes (SCs) comprised primarily of different stoichiometries of complexes I, III and V [5-8]. (*B*) Examples of typical *in situ* enzymatic assays for each of the indicated SCs. Relevant regions of gels such as those shown in A were excised and assayed *in situ*. Complex II could not be measured *in situ* and was instead measured separately on isolated mitochondrial lysates as described previously [11, 12]. *In situ* enzyme activities for each of the indicated complexes are depicted here graphically after adjusting for differences in the protein content of each complex based on densitometric scanning of BNGE profiles [4]. (*C*) Complex I activity. (*D*) Complex I activity in SCs. (*E*) Complex II activity. (*F*) Complex III activity. (*G*) Complex IV activity. (*H*) Complex V_m activity. (*I*) Complex V_d activity. Each bar depicts the results of triplicate assays performed on mitochondria isolated from independent liver samples of the same animal. Standard errors and p-values were calculated based on the mean of all results.

A

Gene Symbol	p-value	q-value (for FDR)	WT 1	WT 2	WT 3	WT 4	KO 1	KO 2	KO 3	KO 4
N-Myc	1.000	1.000								
L-Myc	0.565	1.000								
B-myc	0.987	1.000								
Max	0.669	1.000								
Mnt	0.250	1.000								
Mga	0.561	1.000								
Mxd1	0.420	1.000								
Mxi1	0.974	1.000								
Mxd3	0.817	1.000								
Mxd4	0.675	1.000								
Mad1l1	0.203	1.000								
Mad2l1	0.360	1.000								
SHMT1	0.799	1.000								
Myct1	0.978	1.000								
HMGA1	0.432	1.000								
Mlx	0.331	1.000								
MondoA	0.126	1.000								
MondoB (ChREBP)	**0.008**	0.326								

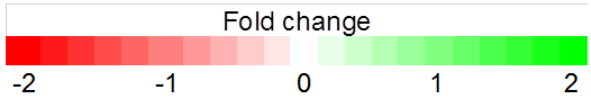

B

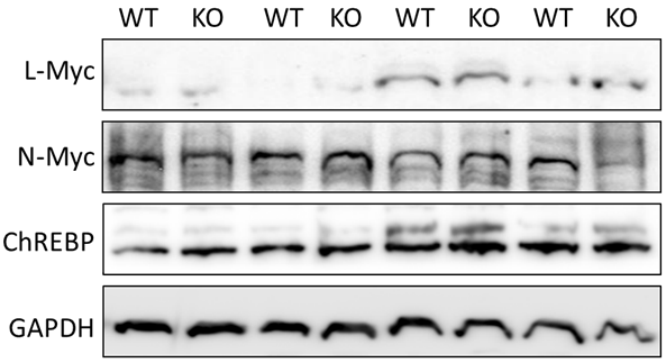

Figure 34: Lack of differential expression of most transcripts encoding Myc homologs, negative regulators of Myc function and proteins that can restore some or all Myc phenotypes in myc-/- fibroblasts. (*A*) The results shown here were extracted from RNAseq data discussed in Fig. 17. Note the modest but significant down-regulation of Mlxip1/MondoB/ChREBP expression in KO livers. (*B*) Immuno-blots for N-Myc, L-Myc, and ChREBP proteins with GAPDH as a loading control.

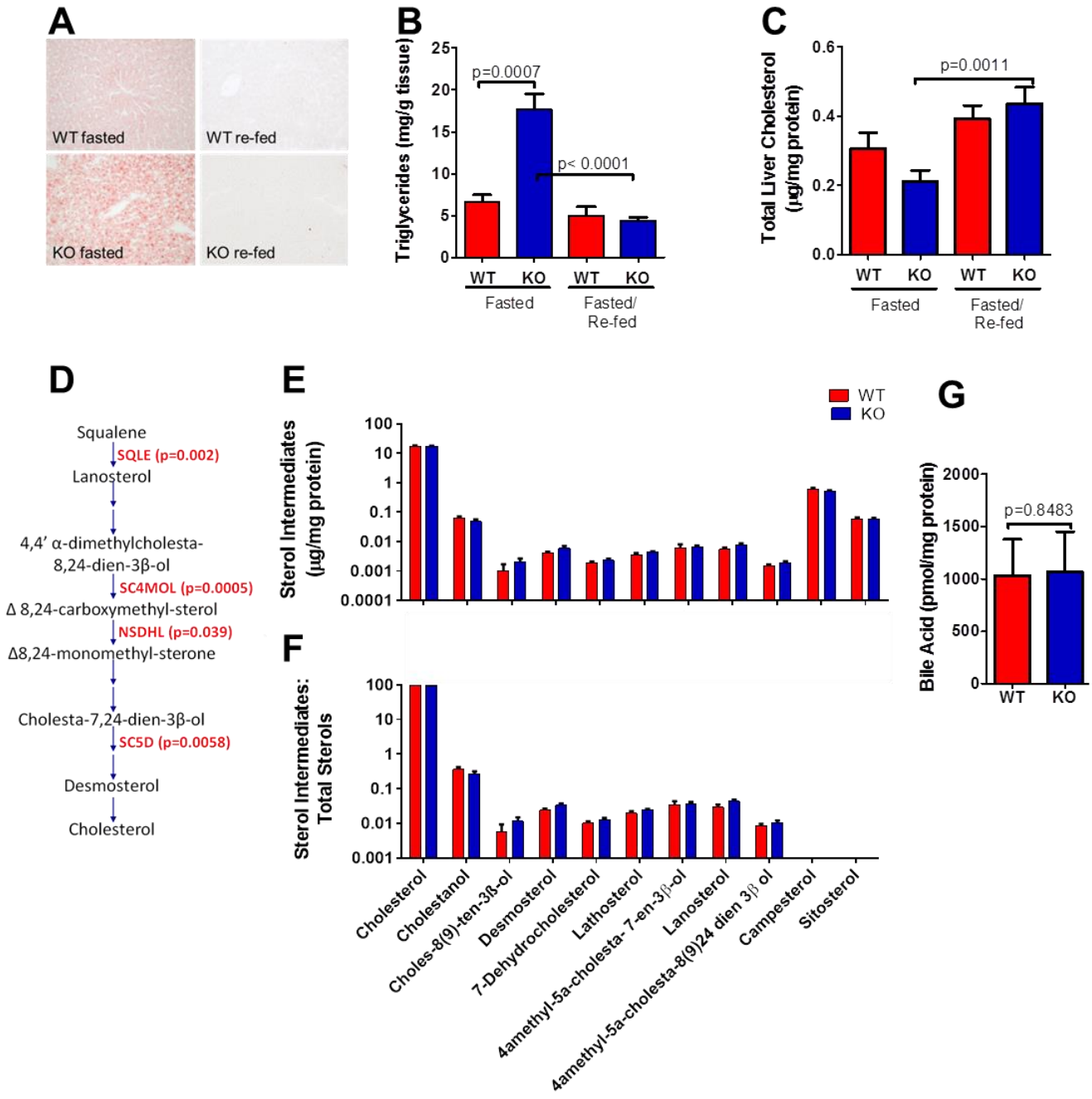

Figure 35: Triglyceride, sterol and bile acid levels in WT and KO livers. (*A*) Representative ORO-stained liver sections after fasting or fasting + re-feeding. (*B*) Quantification of total liver triglycerides in at least 6 representative animals from each of the indicated groups. (*C*) Quantification of total cholesterol levels in at least 6 animals from each of the indicated groups. (*D*) Minimal biosynthetic pathway from squalene to cholesterol showing a select sub-set of relevant sterol intermediates and enzymes (red, p-values indicated in parenthesis) whose transcripts were up-regulated in KO hepatocytes as indicated by RNAseq. (*E*) Liver sterol levels adjusted to protein content [9, 10]. (*F*) The data from (*E*) expressed as a fraction of total sterol content. (*G*) Total bile acids measured in livers of starved mice.

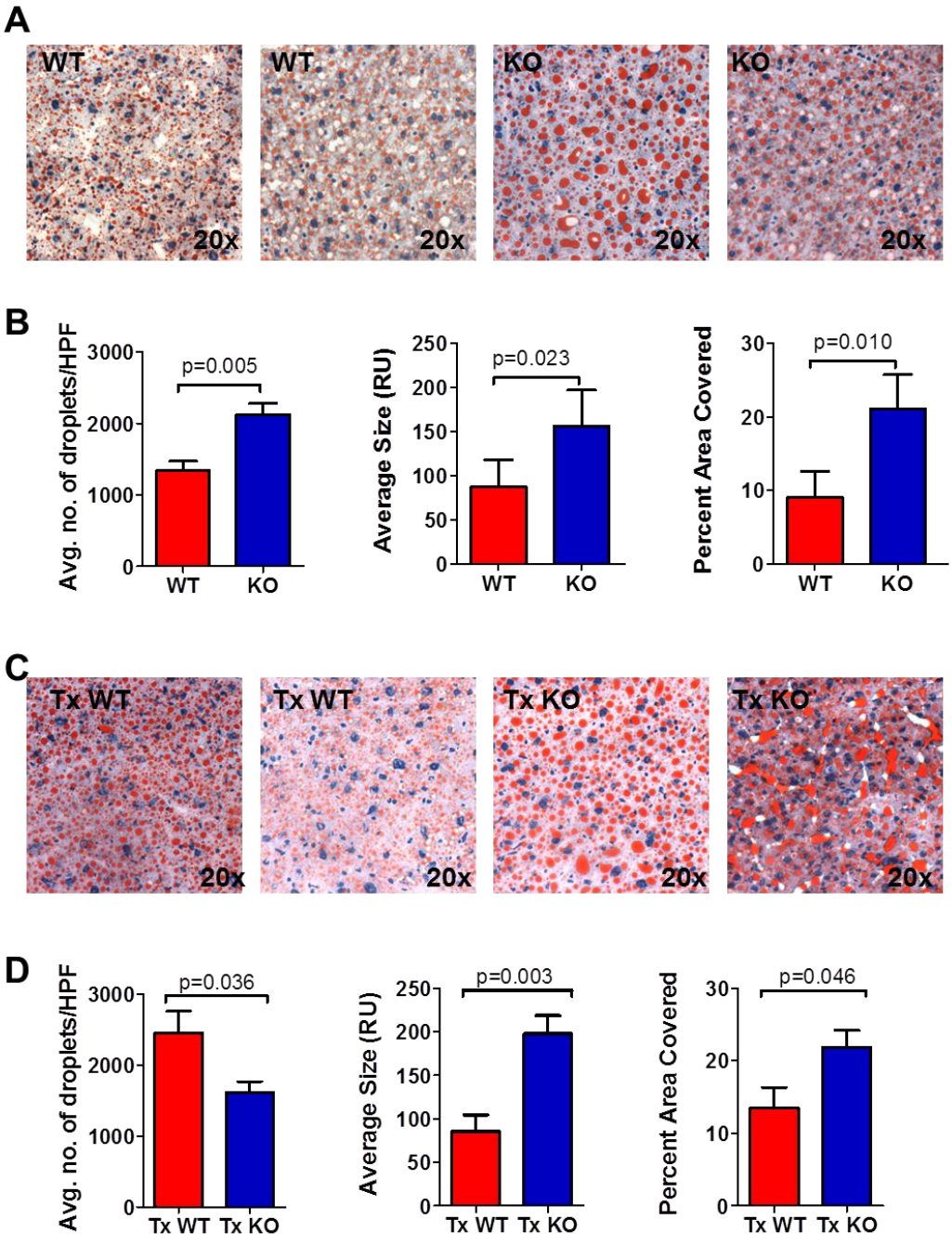

Figure 36: Lipid droplets in KO hepatocytes are more numerous and larger. (*A*) Shown are representative images similar to those depicted in Suppl. Fig. 35*A* on which analyses were performed. (*B*) Lipid droplet number, size and total average percent area occupied within hepatocytes was determined using ImageJ software (Analyze Particles function). Analyses were performed on a total of 5 mice from each group with a total of 5 independent images being taken from each histologic section. HPF=high power field. RU=relative units. (*C*) Representative images of lipid droplets in hepatocytes of recipient livers following transplantation with WT or KO hepatocytes. (*D*) Quantification was performed as described in (*B*).

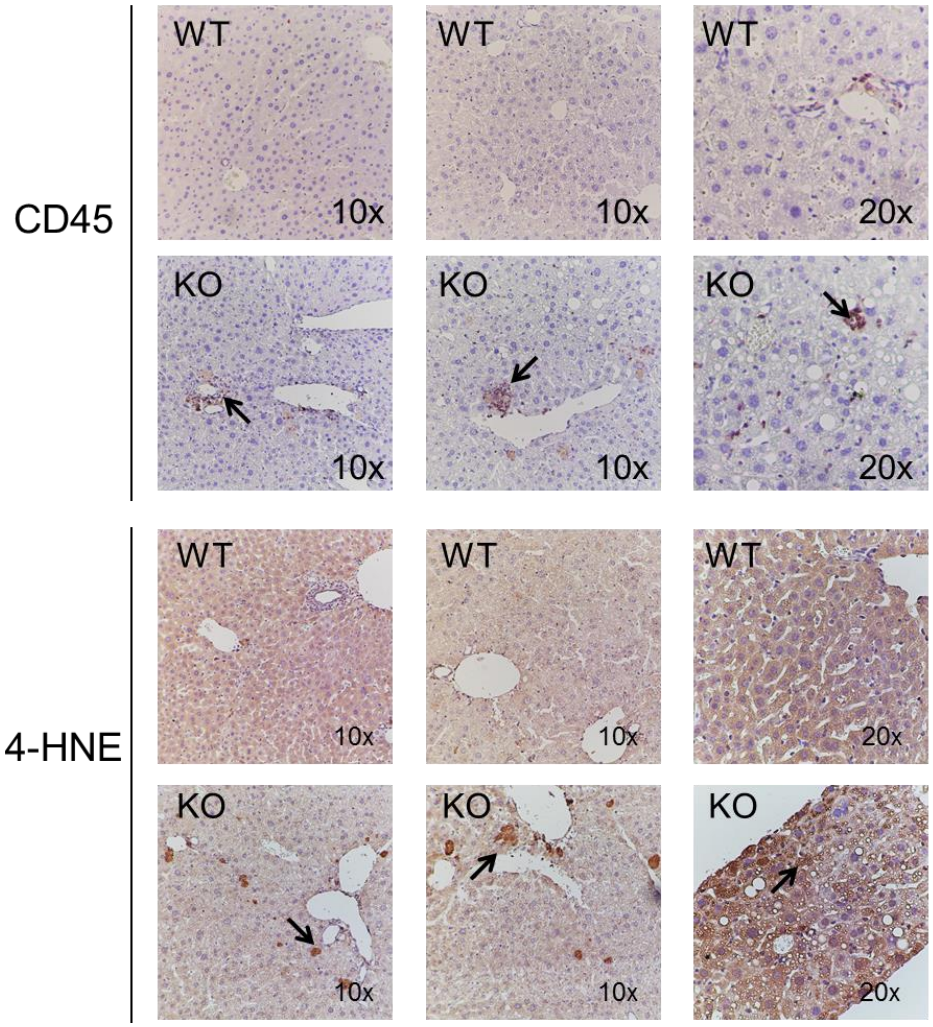

Figure 37: Post-transplant immunohistochemical staining of recipient livers for CD45 and 4-hydroxynonenal (4-HNE). Each image is typical of the remaining section and is taken from individual mice. Arrows indicate representative areas of positivity.

APPENDIX B

SUPPLEMENTAL TABLES

Table 8: Transcripts identified by Ingenuity Pathway Analysis from the top 10 deregulated pathways in transplanted livers

Gene Symbol	Fold Diff in KO cells	Log2 Diff	p-value	Adjusted p-value (for FDR)	WT		KO			
					1	2	1	2	3	4
EIF4EBP3	0.15	-2.70	0.0001	0.0011						
LEPR	0.19	-2.42	0.0001	0.0011						
DDIT4	0.40	-1.31	0.0001	0.0011						
EGFR	0.41	-1.30	0.0001	0.0011						
RPS27A	0.52	-0.94	0.0001	0.0011						
C5	0.53	-0.93	0.0004	0.0051						
RPS12	0.53	-0.92	0.0001	0.0011						
RPS21	0.53	-0.91	0.0001	0.0011						
SERPINE1	0.55	-0.87	0.0042	0.0340						
IL1R1	0.56	-0.84	0.0001	0.0019						
SDC4	0.57	-0.81	0.0004	0.0051						
RPS24	0.58	-0.80	0.0003	0.0046						
FAU	0.58	-0.78	0.0002	0.0034						
FGFR1	0.59	-0.77	0.0023	0.0216						
RPSA	0.59	-0.77	0.0004	0.0057						
RPS18	0.59	-0.75	0.0004	0.0051						
RPS9	0.60	-0.74	0.0005	0.0062						
RPS14	0.60	-0.73	0.0002	0.0034						

RPS5	0.62	-0.69	**0.0004**	**0.0051**
ATP5L	0.62	-0.69	**0.0002**	**0.0034**
RPS19	0.62	-0.68	**0.0006**	**0.0073**
RHOD	0.63	-0.67	**0.0004**	**0.0051**
RPS8	0.63	-0.67	**0.0007**	**0.0082**
RPS10	0.64	-0.64	**0.0005**	**0.0062**
RPS13	0.64	-0.64	**0.0005**	**0.0062**
Cxcl9	0.65	-0.63	**0.0042**	**0.0337**
RPS6	0.65	-0.62	**0.0023**	**0.0216**
NDUFA2	0.66	-0.61	**0.0004**	**0.0057**
RPS15A	0.66	-0.61	**0.0005**	**0.0062**
RPS20	0.66	-0.60	**0.0008**	**0.0097**
RPS28	0.66	-0.60	**0.0006**	**0.0078**
RPS16	0.68	-0.56	**0.0009**	**0.0102**
COX4I1	0.68	-0.56	**0.0045**	**0.0353**
Atp5e	0.68	-0.56	**0.0014**	**0.0143**
RPS7	0.68	-0.55	**0.0019**	**0.0183**
UQCR10	0.68	-0.55	**0.0011**	**0.0123**
RPS23	0.69	-0.54	**0.0033**	**0.0283**
GPLD1	0.70	-0.51	**0.0054**	**0.0403**
Ccl9	0.70	-0.51	**0.0022**	**0.0205**
UQCRQ	0.70	-0.51	**0.0026**	**0.0234**
RPS25	0.71	-0.50	**0.0033**	**0.0283**
NDUFA1	0.71	-0.50	**0.0017**	**0.0172**
ATP5G2	0.71	-0.50	**0.0029**	**0.0256**
AGO4	0.71	-0.50	**0.0355**	0.1513
SDHD	0.71	-0.49	**0.0052**	**0.0393**
NDUFA4	0.71	-0.49	**0.0073**	0.0500
NDUFA11	0.72	-0.48	**0.0028**	**0.0249**
Cox6c	0.72	-0.47	**0.0061**	**0.0441**
NDUFB7	0.72	-0.47	**0.0029**	**0.0256**
CCL27	0.73	-0.46	**0.0403**	0.1640
COX5A	0.73	-0.45	**0.0066**	**0.0465**
LBP	0.73	-0.44	**0.0080**	0.0529
RPS17	0.74	-0.44	**0.0076**	0.0512
UQCR11	0.74	-0.44	**0.0051**	**0.0390**
RPS3	0.74	-0.43	**0.0103**	0.0635
NDUFA3	0.76	-0.40	**0.0056**	**0.0415**
NDUFA5	0.76	-0.40	**0.0075**	0.0507
NDUFS6	0.76	-0.40	**0.0056**	**0.0415**
RPS26	0.76	-0.40	**0.0074**	0.0503

RPS2	0.76	-0.39	**0.0274**	0.1274	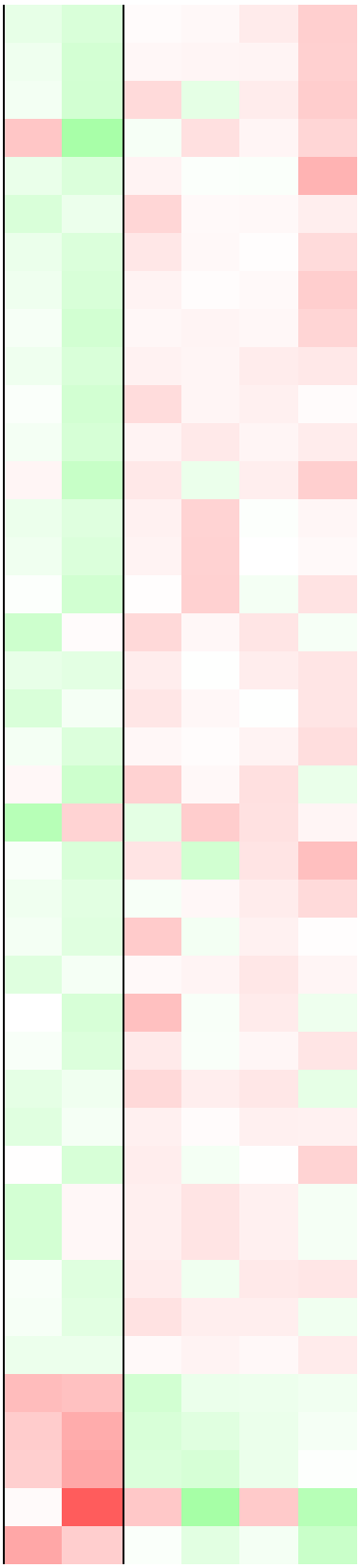
RPS4Y1	0.77	-0.38	**0.0205**	0.1043	
RPS27L	0.77	-0.37	**0.0107**	0.0653	
IL1RAP	0.78	-0.36	**0.0147**	0.0816	
ATP5G3	0.78	-0.36	**0.0276**	0.1279	
COX17	0.78	-0.36	**0.0146**	0.0814	
NDUFS4	0.78	-0.35	**0.0112**	0.0672	
NDUFB5	0.78	-0.35	**0.0141**	0.0794	
RPS29	0.78	-0.35	**0.0166**	0.0894	
NDUFS2	0.79	-0.34	**0.0220**	0.1098	
NDUFB3	0.80	-0.33	**0.0141**	0.0795	
ATP5H	0.80	-0.33	**0.0223**	0.1108	
COX7A2	0.80	-0.32	**0.0159**	0.0867	
EIF3I	0.80	-0.32	**0.0170**	0.0912	
EIF3K	0.80	-0.32	**0.0193**	0.0998	
NDUFB10	0.80	-0.32	**0.0184**	0.0966	
COX10	0.80	-0.31	**0.0432**	0.1719	
COX7A2L	0.80	-0.31	**0.0207**	0.1051	
F11R	0.81	-0.30	**0.0224**	0.1109	
RPS11	0.82	-0.29	**0.0265**	0.1247	
COL5A3	0.82	-0.29	**0.0438**	0.1734	
RICTOR	0.82	-0.29	**0.0496**	0.1888	
NDUFB6	0.82	-0.28	**0.0216**	0.1083	
EIF3F	0.82	-0.28	**0.0264**	0.1245	
NDUFB8	0.83	-0.27	**0.0330**	0.1441	
TEC	0.83	-0.27	**0.0453**	0.1775	
NDUFB4	0.83	-0.26	**0.0296**	0.1340	
NDUFA7	0.83	-0.26	**0.0322**	0.1417	
NDUFA12	0.84	-0.26	**0.0347**	0.1488	
SOS1	0.84	-0.26	**0.0366**	0.1542	
ATP5J2	0.84	-0.25	**0.0448**	0.1761	
EIF4EBP1	0.84	-0.25	**0.0416**	0.1674	
EIF4EBP1	0.84	-0.25	**0.0416**	0.1674	
NDUFA6	0.84	-0.25	**0.0373**	0.1560	
HRAS	0.84	-0.24	**0.0474**	0.1829	
NDUFA8	0.85	-0.24	**0.0387**	0.1600	
CTNND1	1.63	0.70	**0.0436**	0.1729	
EIF4EBP2	1.64	0.72	**0.0395**	0.1620	
STAT1	1.65	0.72	**0.0423**	0.1694	
TGFBR2	1.66	0.73	**0.0494**	0.1884	
BCAR1	1.66	0.73	**0.0481**	0.1850	

DLC1	1.70	0.76	**0.0264**	0.1245
PLD3	1.71	0.78	**0.0299**	0.1349
PIK3R1	1.76	0.82	**0.0185**	0.0970
VASP	1.85	0.88	**0.0156**	0.0856
IFNGR1	1.86	0.90	**0.0124**	0.0727
MYH9	1.89	0.92	**0.0045**	**0.0355**
FNBP1	1.92	0.94	**0.0462**	0.1799
IGF2	1.99	0.99	**0.0352**	0.1505
ACTN1	2.04	1.03	**0.0040**	**0.0325**
ARHGAP5	2.05	1.04	**0.0006**	**0.0078**
RPS6KA2	2.08	1.06	**0.0438**	0.1734
GNAI2	2.13	1.09	**0.0004**	**0.0057**
GNAI2	2.13	1.09	**0.0004**	**0.0057**
RPS6KA3	2.16	1.11	**0.0483**	0.1855
ARHGAP4	2.19	1.13	**0.0305**	0.1368
COL15A1	2.26	1.18	**0.0474**	0.1830
MRAS	2.26	1.18	**0.0281**	0.1296
ITGA1	2.27	1.18	**0.0159**	0.0865
ITGA1	2.27	1.18	**0.0159**	0.0865
GLG1	2.45	1.29	**0.0007**	**0.0082**
AGO2	2.45	1.30	**0.0025**	**0.0227**
COL27A1	2.62	1.39	**0.0079**	0.0527
CCL19	2.79	1.48	**0.0316**	0.1401
COL4A5	2.93	1.55	**0.0044**	**0.0348**
ITGA6	2.94	1.56	**0.0003**	**0.0040**
ITGA6	2.94	1.56	**0.0003**	**0.0040**
CLDN4	3.00	1.59	**0.0133**	0.0766
CCL5	3.37	1.75	**0.0089**	0.0570
PDGFC	3.38	1.76	**0.0002**	**0.0027**
CXCL2	3.43	1.78	0.1634	0.4068
GNAI1	3.62	1.85	**0.0006**	**0.0073**
GNAI1	3.62	1.85	**0.0006**	**0.0073**
IL33	3.62	1.86	**0.0013**	**0.0135**
Ccl2	3.67	1.88	**0.0195**	0.1004
ITGB3	3.67	1.88	**0.0001**	**0.0019**
ITGB3	3.67	1.88	**0.0001**	**0.0019**
RHOF	3.69	1.89	**0.0089**	0.0572
CX3CL1	3.72	1.90	**0.0330**	0.1441
COL6A2	3.89	1.96	**0.0025**	**0.0227**
CTGF	3.97	1.99	**0.0001**	**0.0011**
CSF3R	4.20	2.07	**0.0024**	**0.0224**

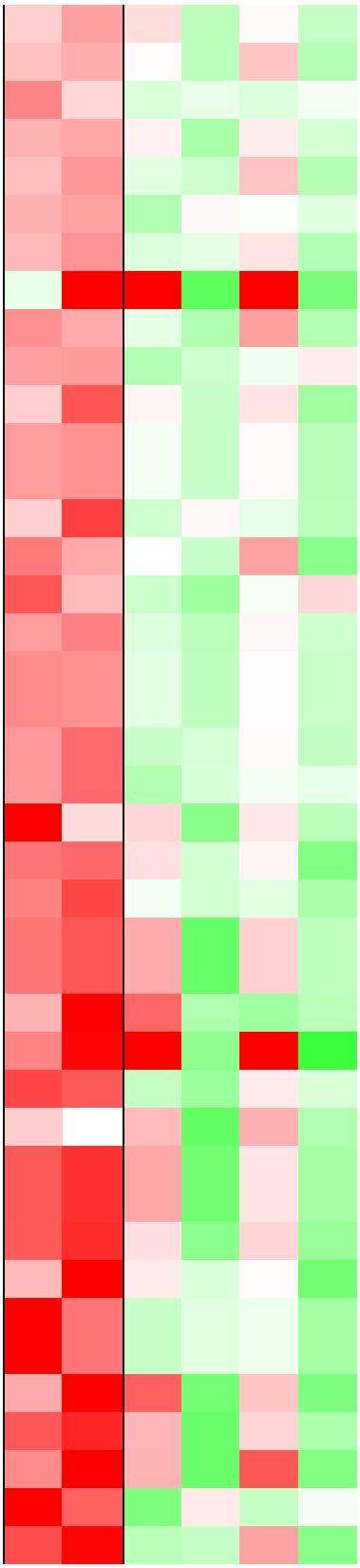

SIPA1	4.21	2.07	**0.0001**	**0.0019**	
EZR	4.26	2.09	**0.0001**	**0.0019**	
EZR	4.26	2.09	**0.0001**	**0.0019**	
MMP7	4.42	2.14	**0.0037**	**0.0306**	
MMP7	4.42	2.14	**0.0037**	**0.0306**	
VAV3	5.24	2.39	**0.0075**	0.0509	
PDGFB	5.60	2.49	**0.0064**	**0.0457**	
CXCL14	5.64	2.50	**0.0017**	**0.0168**	
THY1	5.67	2.50	**0.0348**	0.1491	
CSF1	5.78	2.53	**0.0001**	**0.0011**	
NCF4	5.84	2.55	**0.0014**	**0.0143**	
COL6A1	6.13	2.62	**0.0002**	**0.0027**	
PIK3R5	6.13	2.62	**0.0046**	**0.0359**	
RHOJ	6.17	2.63	**0.0003**	**0.0040**	
HMOX1	6.43	2.68	**0.0001**	**0.0011**	
MAPK12	6.45	2.69	**0.0002**	**0.0034**	
MAPK12	6.45	2.69	**0.0002**	**0.0034**	
CLDN5	7.00	2.81	**0.0001**	**0.0011**	
CXCL16	7.04	2.82	**0.0001**	**0.0011**	
CCL22	7.04	2.82	**0.0191**	0.0990	
PIK3R6	7.10	2.83	**0.0095**	0.0596	
PRR5L	7.29	2.87	**0.0001**	**0.0019**	
ARHGAP9	7.31	2.87	**0.0014**	**0.0143**	
PIK3CD	7.60	2.93	**0.0001**	**0.0011**	
SELPLG	7.67	2.94	**0.0003**	**0.0040**	
CXCL13	7.84	2.97	**0.0001**	**0.0011**	
WIPF1	7.84	2.97	**0.0001**	**0.0011**	
PLD4	7.85	2.97	**0.0001**	**0.0011**	
RAPGEF3	7.97	2.99	**0.0001**	**0.0011**	
RAC2	8.13	3.02	**0.0001**	**0.0011**	
IL1B	8.20	3.04	**0.0003**	**0.0046**	
NCF2	8.22	3.04	**0.0001**	**0.0011**	
TNF	8.24	3.04	**0.0061**	**0.0443**	
BTK	8.28	3.05	**0.0023**	**0.0212**	
C5AR1	8.34	3.06	**0.0011**	**0.0118**	
MAPK11	8.39	3.07	**0.0021**	**0.0197**	
MAPK11	8.39	3.07	**0.0021**	**0.0197**	
PRKCQ	8.40	3.07	**0.0017**	**0.0172**	
PLCG2	8.43	3.07	**0.0010**	**0.0115**	
CCL4	8.57	3.10	**0.0127**	0.0739	
CLDN7	8.75	3.13	**0.0074**	0.0503	

LHX2	8.77	3.13	**0.0003**	**0.0046**	
PRKCH	8.93	3.16	**0.0001**	**0.0011**	
FPR2	8.93	3.16	**0.0019**	**0.0183**	
IL10RA	8.98	3.17	**0.0001**	**0.0019**	
MSN	9.11	3.19	**0.0001**	**0.0011**	
MSN	9.11	3.19	**0.0001**	**0.0011**	
AKT3	9.19	3.20	**0.0001**	**0.0011**	
PDGFRA	9.26	3.21	**0.0001**	**0.0011**	
Ccl6	9.35	3.22	**0.0001**	**0.0011**	
PRKCB	9.99	3.32	**0.0003**	**0.0040**	
NCF1	10.25	3.36	**0.0003**	**0.0040**	
CD40	10.47	3.39	**0.0026**	**0.0234**	
IGFBP3	10.63	3.41	**0.0001**	**0.0011**	
TIMP3	10.65	3.41	**0.0001**	**0.0011**	
COL4A1	10.71	3.42	**0.0001**	**0.0011**	
CYBA	10.94	3.45	**0.0001**	**0.0011**	
VAV1	10.96	3.45	**0.0001**	**0.0019**	
Ccl7	11.09	3.47	**0.0390**	0.1608	
ITGB2	11.49	3.52	**0.0001**	**0.0011**	
ITGB2	11.49	3.52	**0.0001**	**0.0011**	
ITGAL	11.50	3.52	**0.0001**	**0.0011**	
ITGAL	11.50	3.52	**0.0001**	**0.0011**	
IL1A	11.68	3.55	**0.0001**	**0.0011**	
COL1A2	11.91	3.57	**0.0001**	**0.0011**	
JAM2	12.22	3.61	**0.0001**	**0.0011**	
ICAM2	12.22	3.61	**0.0006**	**0.0073**	
TGFB1	12.32	3.62	**0.0001**	**0.0011**	
CCR7	12.55	3.65	**0.0101**	0.0625	
MMP2	13.19	3.72	**0.0111**	0.0669	
MMP2	13.19	3.72	**0.0111**	0.0669	
CD44	13.20	3.72	**0.0001**	**0.0011**	
FLT4	13.64	3.77	**0.0001**	**0.0011**	
WAS	13.66	3.77	**0.0088**	0.0565	
CYBB	13.92	3.80	**0.0001**	**0.0011**	
PECAM1	14.01	3.81	**0.0001**	**0.0011**	
TNFRSF11B	14.61	3.87	**0.0002**	**0.0034**	
CCL3L3	14.66	3.87	**0.0116**	0.0693	
COL4A2	15.09	3.92	**0.0001**	**0.0011**	
COL5A1	15.40	3.94	**0.0001**	**0.0019**	
NGFR	15.54	3.96	**0.0272**	0.1270	
PDGFRB	15.97	4.00	**0.0001**	**0.0011**	

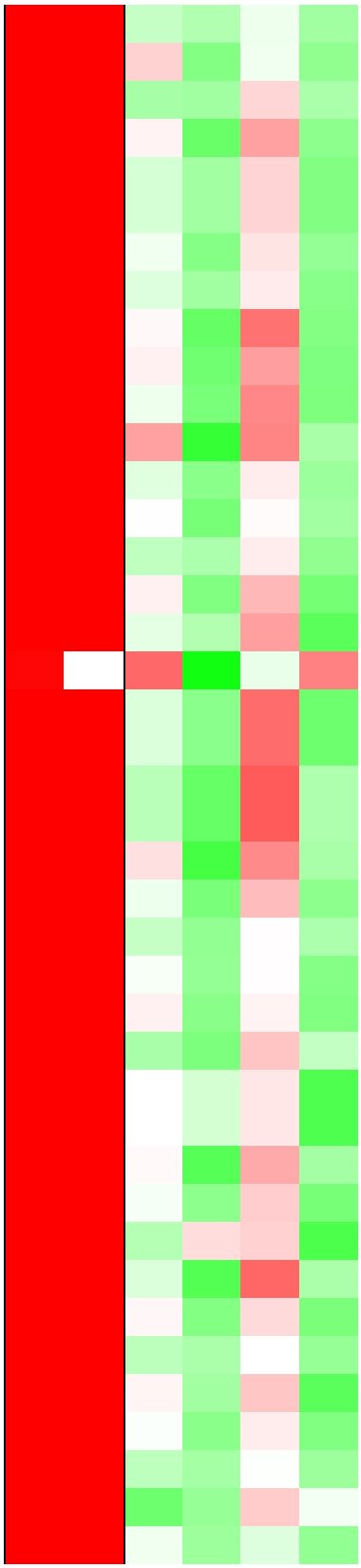

TLR4	16.61	4.05	**0.0035**	**0.0296**	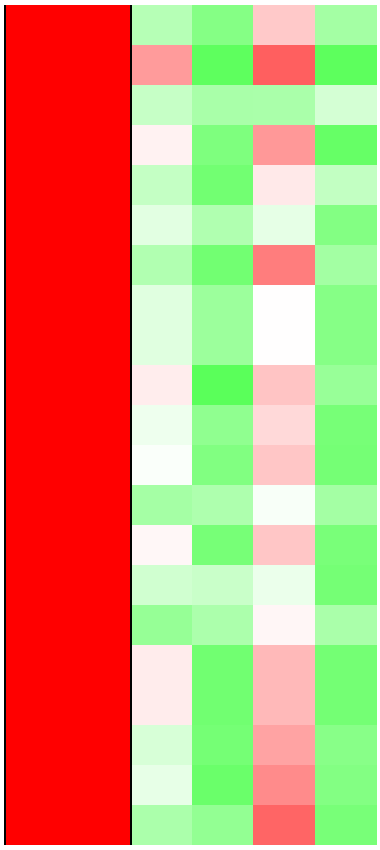
CCL24	16.74	4.06	**0.0004**	**0.0051**	
EDNRB	17.02	4.09	**0.0001**	**0.0011**	
COL3A1	17.10	4.10	**0.0001**	**0.0011**	
EDNRA	17.11	4.10	**0.0003**	**0.0046**	
JAM3	17.93	4.16	**0.0143**	0.0802	
VCAM1	18.02	4.17	**0.0001**	**0.0011**	
TIMP2	18.70	4.22	**0.0001**	**0.0011**	
TIMP2	18.70	4.22	**0.0001**	**0.0011**	
COL16A1	19.50	4.29	**0.0047**	**0.0365**	
COL13A1	19.81	4.31	**0.0001**	**0.0011**	
CDH5	22.66	4.50	**0.0001**	**0.0011**	
FLT1	23.71	4.57	**0.0002**	**0.0027**	
KDR	24.70	4.63	**0.0001**	**0.0011**	
LAMA1	25.22	4.66	**0.0024**	**0.0220**	
HGF	26.04	4.70	**0.0014**	**0.0143**	
MMP12	26.82	4.75	**0.0001**	**0.0011**	
MMP12	26.82	4.75	**0.0001**	**0.0011**	
SDC3	27.60	4.79	**0.0001**	**0.0011**	
CCR5	27.76	4.80	**0.0004**	**0.0051**	
FPR1	29.41	4.88	**0.0031**	**0.0270**	

BIBLIOGRAPHY

1. Gordan, J.D., C.B. Thompson, and M.C. Simon, *HIF and c-Myc: sibling rivals for control of cancer cell metabolism and proliferation.* Cancer Cell, 2007. **12**(2): p. 108-13.

2. Gordan, J.D., et al., *HIF-2alpha promotes hypoxic cell proliferation by enhancing c-myc transcriptional activity.* Cancer Cell, 2007. **11**(4): p. 335-47.

3. Wang, Y., et al., *Evidence for physical association of mitochondrial fatty acid oxidation and oxidative phosphorylation complexes.* J Biol Chem, 2010. **285**(39): p. 29834-41.

4. Graves, J.A., et al., *Mitochondrial structure, function and dynamics are temporally controlled by c-Myc.* PLoS One, 2012. **7**(5): p. e37699.

5. Acin-Perez, R. and J.A. Enriquez, *The function of the respiratory supercomplexes: the plasticity model.* Biochim Biophys Acta, 2014. **1837**(4): p. 444-50.

6. Barrientos, A. and C. Ugalde, *I function, therefore I am: overcoming skepticism about mitochondrial supercomplexes.* Cell Metab, 2013. **18**(2): p. 147-9.

7. Genova, M.L. and G. Lenaz, *Functional role of mitochondrial respiratory supercomplexes.* Biochim Biophys Acta, 2014. **1837**(4): p. 427-43.

8. Vartak, R., C.A. Porras, and Y. Bai, *Respiratory supercomplexes: structure, function and assembly.* Protein Cell, 2013. **4**(8): p. 582-90.

9. Kelley, R.I., et al., *Abnormal sterol metabolism in patients with Conradi-Hunermann-Happle syndrome and sporadic lethal chondrodysplasia punctata.* Am J Med Genet, 1999. **83**(3): p. 213-9.

10. Kelley, R.I., *Diagnosis of Smith-Lemli-Opitz syndrome by gas chromatography/mass spectrometry of 7-dehydrocholesterol in plasma, amniotic fluid and cultured skin fibroblasts.* Clin Chim Acta, 1995. **236**(1): p. 45-58.

11. Edmunds, L.R., et al., *c-Myc programs fatty acid metabolism and dictates acetyl-CoA abundance and fate.* J Biol Chem, 2014. **289**(36): p. 25382-92.

12. Munujos, P., et al., *Assay of succinate dehydrogenase activity by a colorimetric-continuous method using iodonitrotetrazolium chloride as electron acceptor.* Anal Biochem, 1993. **212**(2): p. 506-9.

13. Leon, J., et al., *Inhibition of cell differentiation: a critical mechanism for MYC-mediated carcinogenesis?* Cell Cycle, 2009. **8**(8): p. 1148-57.

14. Meyer, N. and L.Z. Penn, *Reflecting on 25 years with MYC.* Nat Rev Cancer, 2008. **8**(12): p. 976-90.

15. Dang, C.V., *Therapeutic targeting of Myc-reprogrammed cancer cell metabolism.* Cold Spring Harb Symp Quant Biol, 2011. **76**: p. 369-74.

16. Morrish, F. and D. Hockenbery, *MYC and mitochondrial biogenesis.* Cold Spring Harb Perspect Med, 2014. **4**(5).

17. Li, F., et al., *Myc stimulates nuclearly encoded mitochondrial genes and mitochondrial biogenesis.* Mol Cell Biol, 2005. **25**(14): p. 6225-34.

18. Dang, C.V., et al., *The c-Myc target gene network.* Semin Cancer Biol, 2006. **16**(4): p. 253-64.

19. Ward, P.S. and C.B. Thompson, *Metabolic reprogramming: a cancer hallmark even warburg did not anticipate.* Cancer Cell, 2012. **21**(3): p. 297-308.

20. Warburg, O., *On respiratory impairment in cancer cells.* Science, 1956. **124**(3215): p. 269-70.

21. Vander Heiden, M.G., L.C. Cantley, and C.B. Thompson, *Understanding the Warburg effect: the metabolic requirements of cell proliferation.* Science, 2009. **324**(5930): p. 1029-33.

22. Dang, C.V., *MYC, metabolism, cell growth, and tumorigenesis.* Cold Spring Harb Perspect Med, 2013. **3**(8).

23. Dang, C.V., A. Le, and P. Gao, *MYC-induced cancer cell energy metabolism and therapeutic opportunities.* Clin Cancer Res, 2009. **15**(21): p. 6479-83.

24. Wise, D.R., et al., *Myc regulates a transcriptional program that stimulates mitochondrial glutaminolysis and leads to glutamine addiction.* Proc Natl Acad Sci U S A, 2008. **105**(48): p. 18782-7.

25. Yuneva, M., et al., *Deficiency in glutamine but not glucose induces MYC-dependent apoptosis in human cells.* J Cell Biol, 2007. **178**(1): p. 93-105.

26. Vander Heiden, M.G., et al., *Metabolic pathway alterations that support cell proliferation.* Cold Spring Harb Symp Quant Biol, 2011. **76**: p. 325-34.

27. Jones, R.G., et al., *AMP-activated protein kinase induces a p53-dependent metabolic checkpoint.* Mol Cell, 2005. **18**(3): p. 283-93.

28. Freed-Pastor, W.A., et al., *Mutant p53 disrupts mammary tissue architecture via the mevalonate pathway.* Cell, 2012. **148**(1-2): p. 244-58.

29. Yang, W. and Z. Lu, *Regulation and function of pyruvate kinase M2 in cancer.* Cancer Lett, 2013. **339**(2): p. 153-8.

30. Yang, M., et al., *The emerging role of fumarate as an oncometabolite.* Front Oncol, 2012. **2**: p. 85.

31. Yang, M., T. Soga, and P.J. Pollard, *Oncometabolites: linking altered metabolism with cancer.* J Clin Invest, 2013. **123**(9): p. 3652-8.

32. Dang, L., et al., *Cancer-associated IDH1 mutations produce 2-hydroxyglutarate.* Nature, 2010. **465**(7300): p. 966.

33. Ward, P.S., et al., *The common feature of leukemia-associated IDH1 and IDH2 mutations is a neomorphic enzyme activity converting alpha-ketoglutarate to 2-hydroxyglutarate.* Cancer Cell, 2010. **17**(3): p. 225-34.

34. Nowicki, S. and E. Gottlieb, *Oncometabolites: tailoring our genes.* FEBS J, 2015. **282**(15): p. 2796-805.

35. Zaidi, N., J.V. Swinnen, and K. Smans, *ATP-citrate lyase: a key player in cancer metabolism.* Cancer Res, 2012. **72**(15): p. 3709-14.

36. Eilers, M. and R.N. Eisenman, *Myc's broad reach.* Genes Dev, 2008. **22**(20): p. 2755-66.

37. Wang, R., et al., *The transcription factor Myc controls metabolic reprogramming upon T lymphocyte activation.* Immunity, 2011. **35**(6): p. 871-82.

38. Semenza, G.L., et al., *'The metabolism of tumours': 70 years later.* Novartis Found Symp, 2001. **240**: p. 251-60; discussion 260-4.

39. David, C.J., et al., *HnRNP proteins controlled by c-Myc deregulate pyruvate kinase mRNA splicing in cancer.* Nature, 2010. **463**(7279): p. 364-8.

40. Carroll, P.A., et al., *Deregulated Myc requires MondoA/Mlx for metabolic reprogramming and tumorigenesis.* Cancer Cell, 2015. **27**(2): p. 271-85.

41. Diolaiti, D., et al., *Functional interactions among members of the MAX and MLX transcriptional network during oncogenesis.* Biochim Biophys Acta, 2015. **1849**(5): p. 484-500.

42. Berg JM, T.J., Stryer L., *Each Organ Has a Unique Metabolic Profile*, in *Biochemistry*. 2002, W H Freeman: New York. p. 30.2.

43. Handler, J.A. and R.G. Thurman, *Catalase-dependent ethanol oxidation in perfused rat liver. Requirement for fatty-acid-stimulated H2O2 production by peroxisomes.* Eur J Biochem, 1988. **176**(2): p. 477-84.

44. Ganning, A.E., et al., *Fatty acid oxidation in hepatic peroxisomes and mitochondria after treatment of rats with di(2-ethylhexyl)phthalate.* Pharmacol Toxicol, 1989. **65**(4): p. 265-8.

45. Cherkaoui-Malki, M., et al., *Hepatic steatosis and peroxisomal fatty acid beta-oxidation.* Curr Drug Metab, 2012. **13**(10): p. 1412-21.

46. Gusdon, A.M., K.X. Song, and S. Qu, *Nonalcoholic Fatty liver disease: pathogenesis and therapeutics from a mitochondria-centric perspective.* Oxid Med Cell Longev, 2014. **2014**: p. 637027.

47. Papamandjaris, A.A., D.E. MacDougall, and P.J. Jones, *Medium chain fatty acid metabolism and energy expenditure: obesity treatment implications.* Life Sci, 1998. **62**(14): p. 1203-15.

48. Kashfi, K. and G.A. Cook, *Topology of hepatic mitochondrial carnitine palmitoyltransferase I.* Adv Exp Med Biol, 1999. **466**: p. 27-42.

49. Murthy, M.S. and S.V. Pande, *Malonyl-CoA binding site and the overt carnitine palmitoyltransferase activity reside on the opposite sides of the outer mitochondrial membrane.* Proc Natl Acad Sci U S A, 1987. **84**(2): p. 378-82.

50. Santos, C.R. and A. Schulze, *Lipid metabolism in cancer.* FEBS J, 2012. **279**(15): p. 2610-23.

51. Liu, Y., *Fatty acid oxidation is a dominant bioenergetic pathway in prostate cancer.* Prostate Cancer Prostatic Dis, 2006. **9**(3): p. 230-4.

52. Khasawneh, J., et al., *Inflammation and mitochondrial fatty acid beta-oxidation link obesity to early tumor promotion.* Proc Natl Acad Sci U S A, 2009. **106**(9): p. 3354-9.

53. Samudio, I., et al., *Pharmacologic inhibition of fatty acid oxidation sensitizes human leukemia cells to apoptosis induction.* J Clin Invest, 2010. **120**(1): p. 142-56.

54. Pike, L.S., et al., *Inhibition of fatty acid oxidation by etomoxir impairs NADPH production and increases reactive oxygen species resulting in ATP depletion and cell death in human glioblastoma cells.* Biochim Biophys Acta, 2011. **1807**(6): p. 726-34.

55. Price, D.T., et al., *Comparison of [18 F]fluorocholine and [18 F]fluorodeoxyglucose for positron emission tomography of androgen dependent and androgen independent prostate cancer.* J Urol, 2002. **168**(1): p. 273-80.

56. Effert, P.J., et al., *Metabolic imaging of untreated prostate cancer by positron emission tomography with 18fluorine-labeled deoxyglucose.* J Urol, 1996. **155**(3): p. 994-8.

57. Liu, T., et al., *Fluorine-18 deoxyglucose positron emission tomography, magnetic resonance imaging and bone scintigraphy for the diagnosis of bone metastases in patients with lung cancer: which one is the best?--a meta-analysis.* Clin Oncol (R Coll Radiol), 2011. **23**(5): p. 350-8.

58. Zha, S., et al., *Peroxisomal branched chain fatty acid beta-oxidation pathway is upregulated in prostate cancer.* Prostate, 2005. **63**(4): p. 316-23.

59. Louie, S.M., et al., *Cancer cells incorporate and remodel exogenous palmitate into structural and oncogenic signaling lipids.* Biochim Biophys Acta, 2013. **1831**(10): p. 1566-72.

60. Hardie, D.G., et al., *Regulation of lipid metabolism by the AMP-activated protein kinase.* Biochem Soc Trans, 1997. **25**(4): p. 1229-31.

61. Baron, A., et al., *Fatty acid synthase: a metabolic oncogene in prostate cancer?* J Cell Biochem, 2004. **91**(1): p. 47-53.

62. Kuhajda, F.P., *Fatty acid synthase and cancer: new application of an old pathway.* Cancer Res, 2006. **66**(12): p. 5977-80.

63. Lupu, R. and J.A. Menendez, *Pharmacological inhibitors of Fatty Acid Synthase (FASN)--catalyzed endogenous fatty acid biogenesis: a new family of anti-cancer agents?* Curr Pharm Biotechnol, 2006. **7**(6): p. 483-93.

64. Yoon, S., et al., *Up-regulation of acetyl-CoA carboxylase alpha and fatty acid synthase by human epidermal growth factor receptor 2 at the translational level in breast cancer cells.* J Biol Chem, 2007. **282**(36): p. 26122-31.

65. Li, J.N., et al., *Sterol regulatory element-binding protein-1 participates in the regulation of fatty acid synthase expression in colorectal neoplasia.* Exp Cell Res, 2000. **261**(1): p. 159-65.

66. Swinnen, J.V., et al., *Stimulation of tumor-associated fatty acid synthase expression by growth factor activation of the sterol regulatory element-binding protein pathway.* Oncogene, 2000. **19**(45): p. 5173-81.

67. Bauer, D.E., et al., *ATP citrate lyase is an important component of cell growth and transformation.* Oncogene, 2005. **24**(41): p. 6314-22.

68. Hatzivassiliou, G., et al., *ATP citrate lyase inhibition can suppress tumor cell growth.* Cancer Cell, 2005. **8**(4): p. 311-21.

69. Zirath, H., et al., *MYC inhibition induces metabolic changes leading to accumulation of lipid droplets in tumor cells.* Proc Natl Acad Sci U S A, 2013. **110**(25): p. 10258-63.

70. Morrish, F., et al., *Myc-dependent mitochondrial generation of acetyl-CoA contributes to fatty acid biosynthesis and histone acetylation during cell cycle entry.* J Biol Chem, 2010. **285**(47): p. 36267-74.

71. Fan, Y., K.G. Dickman, and W.X. Zong, *Akt and c-Myc differentially activate cellular metabolic programs and prime cells to bioenergetic inhibition.* J Biol Chem, 2010. **285**(10): p. 7324-33.

72. Wang, H., et al., *Structurally diverse c-Myc inhibitors share a common mechanism of action involving ATP depletion.* Oncotarget, 2015. **6**(18): p. 15857-70.

73. Hardie, D.G., *AMP-activated protein kinase: an energy sensor that regulates all aspects of cell function.* Genes Dev, 2011. **25**(18): p. 1895-908.

74. Hardie, D.G., F.A. Ross, and S.A. Hawley, *AMPK: a nutrient and energy sensor that maintains energy homeostasis.* Nat Rev Mol Cell Biol, 2012. **13**(4): p. 251-62.

75. Bergeron, R., et al., *Chronic activation of AMP kinase results in NRF-1 activation and mitochondrial biogenesis.* Am J Physiol Endocrinol Metab, 2001. **281**(6): p. E1340-6.

76. Hardie, D.G., *AMPK: positive and negative regulation, and its role in whole-body energy homeostasis.* Curr Opin Cell Biol, 2014. **33C**: p. 1-7.

77. Inoki, K., T. Zhu, and K.L. Guan, *TSC2 mediates cellular energy response to control cell growth and survival.* Cell, 2003. **115**(5): p. 577-90.

78. Hofmann, J.W., et al., *Reduced Expression of MYC Increases Longevity and Enhances Healthspan.* Cell, 2015. **160**(3): p. 477-88.

79. Faubert, B., et al., *AMPK is a negative regulator of the Warburg effect and suppresses tumor growth in vivo.* Cell Metab, 2013. **17**(1): p. 113-24.

80. Liu, L., et al., *Deregulated MYC expression induces dependence upon AMPK-related kinase 5.* Nature, 2012. **483**(7391): p. 608-12.

81. Dang, C.V., *c-Myc target genes involved in cell growth, apoptosis, and metabolism.* Mol Cell Biol, 1999. **19**(1): p. 1-11.

82. Levens, D., *Disentangling the MYC web.* Proc Natl Acad Sci U S A, 2002. **99**(9): p. 5757-9.

83. Wilson, A., et al., *c-Myc controls the balance between hematopoietic stem cell self-renewal and differentiation.* Genes Dev, 2004. **18**(22): p. 2747-63.

84. Trumpp, A., et al., *c-Myc regulates mammalian body size by controlling cell number but not cell size.* Nature, 2001. **414**(6865): p. 768-73.

85. Bettess, M.D., et al., *c-Myc is required for the formation of intestinal crypts but dispensable for homeostasis of the adult intestinal epithelium.* Mol Cell Biol, 2005. **25**(17): p. 7868-78.

86. Soucek, L., et al., *Modelling Myc inhibition as a cancer therapy.* Nature, 2008. **455**(7213): p. 679-83.

87. Sanders, J.A., et al., *Postnatal liver growth and regeneration are independent of c-myc in a mouse model of conditional hepatic c-myc deletion.* BMC Physiol, 2012. **12**: p. 1.

88. Li, F., et al., *Conditional deletion of c-myc does not impair liver regeneration.* Cancer Res, 2006. **66**(11): p. 5608-12.

89. Baena, E., et al., *c-Myc regulates cell size and ploidy but is not essential for postnatal proliferation in liver.* Proc Natl Acad Sci U S A, 2005. **102**(20): p. 7286-91.

90. Tariq, Z., C.J. Green, and L. Hodson, *Are oxidative stress mechanisms the common denominator in the progression from hepatic steatosis towards non-alcoholic steatohepatitis (NASH)?* Liver Int, 2014. **34**(7): p. e180-90.

91. Dang, C.V., *MYC, microRNAs and glutamine addiction in cancers.* Cell Cycle, 2009. **8**(20): p. 3243-5.

92. Dang, C.V., *Rethinking the Warburg effect with Myc micromanaging glutamine metabolism.* Cancer Res, 2010. **70**(3): p. 859-62.

93. Rodriguez-Enriquez, S., et al., *Oxidative phosphorylation as a target to arrest malignant neoplasias.* Curr Med Chem, 2011. **18**(21): p. 3156-67.

94. Jose, C., N. Bellance, and R. Rossignol, *Choosing between glycolysis and oxidative phosphorylation: a tumor's dilemma?* Biochim Biophys Acta, 2011. **1807**(6): p. 552-61.

95. Mateyak, M.K., et al., *Phenotypes of c-Myc-deficient rat fibroblasts isolated by targeted homologous recombination.* Cell Growth Differ, 1997. **8**(10): p. 1039-48.

96. Sato, R. and T. Takano, *Regulation of intracellular cholesterol metabolism.* Cell Struct Funct, 1995. **20**(6): p. 421-7.

97. Delmastro-Greenwood, M.M., et al., *Mn porphyrin regulation of aerobic glycolysis: implications on the activation of diabetogenic immune cells.* Antioxid Redox Signal, 2013. **19**(16): p. 1902-15.

98. Rardin, M.J., et al., *SIRT5 Regulates the Mitochondrial Lysine Succinylome and Metabolic Networks.* Cell Metab, 2013. **18**(6): p. 920-33.

99. Goetzman, E.S., *Modeling disorders of fatty acid metabolism in the mouse.* Prog Mol Biol Transl Sci, 2011. **100**: p. 389-417.

100. Gregersen, N., et al., *Mutation analysis in mitochondrial fatty acid oxidation defects: Exemplified by acyl-CoA dehydrogenase deficiencies, with special focus on genotype-phenotype relationship.* Hum Mutat, 2001. **18**(3): p. 169-89.

101. Vockley, J., et al., *Mammalian branched-chain acyl-CoA dehydrogenases: molecular cloning and characterization of recombinant enzymes.* Methods Enzymol, 2000. **324**: p. 241-58.

102. Yin, X., et al., *Low molecular weight inhibitors of Myc-Max interaction and function.* Oncogene, 2003. **22**(40): p. 6151-9.

103. Patel, M.S. and L.G. Korotchkina, *Regulation of the pyruvate dehydrogenase complex.* Biochem Soc Trans, 2006. **34**(Pt 2): p. 217-22.

104. Wallace, J.C., S. Jitrapakdee, and A. Chapman-Smith, *Pyruvate carboxylase.* Int J Biochem Cell Biol, 1998. **30**(1): p. 1-5.

105. Gupta, V. and R.N. Bamezai, *Human pyruvate kinase M2: a multifunctional protein.* Protein Sci, 2010. **19**(11): p. 2031-44.

106. Tamada, M., M. Suematsu, and H. Saya, *Pyruvate kinase M2: multiple faces for conferring benefits on cancer cells.* Clin Cancer Res, 2012. **18**(20): p. 5554-61.

107. Chaneton, B. and E. Gottlieb, *Rocking cell metabolism: revised functions of the key glycolytic regulator PKM2 in cancer.* Trends Biochem Sci, 2012. **37**(8): p. 309-16.

108. Barber, M.C., N.T. Price, and M.T. Travers, *Structure and regulation of acetyl-CoA carboxylase genes of metazoa.* Biochim Biophys Acta, 2005. **1733**(1): p. 1-28.

109. Athenstaedt, K. and G. Daum, *The life cycle of neutral lipids: synthesis, storage and degradation.* Cell Mol Life Sci, 2006. **63**(12): p. 1355-69.

110. Fujimoto, T. and R.G. Parton, *Not just fat: the structure and function of the lipid droplet.* Cold Spring Harb Perspect Biol, 2011. **3**(3).

111. Fullerton, M.D., et al., *Single phosphorylation sites in Acc1 and Acc2 regulate lipid homeostasis and the insulin-sensitizing effects of metformin.* Nat Med, 2013. **19**(12): p. 1649-54.

112. Aguer, C., et al., *Increased FAT/CD36 cycling and lipid accumulation in myotubes derived from obese type 2 diabetic patients.* PLoS One, 2011. **6**(12): p. e28981.

113. Holloway, G.P., et al., *Contribution of FAT/CD36 to the regulation of skeletal muscle fatty acid oxidation: an overview.* Acta Physiol (Oxf), 2008. **194**(4): p. 293-309.

114. Cuthbert, K.D. and J.R. Dyck, *Malonyl-CoA decarboxylase is a major regulator of myocardial fatty acid oxidation.* Curr Hypertens Rep, 2005. **7**(6): p. 407-11.

115. Sugden, M.C. and M.J. Holness, *Mechanisms underlying regulation of the expression and activities of the mammalian pyruvate dehydrogenase kinases.* Arch Physiol Biochem, 2006. **112**(3): p. 139-49.

116. Kolobova, E., et al., *Regulation of pyruvate dehydrogenase activity through phosphorylation at multiple sites.* Biochem J, 2001. **358**(Pt 1): p. 69-77.

117. Kaplon, J., et al., *A key role for mitochondrial gatekeeper pyruvate dehydrogenase in oncogene-induced senescence.* Nature, 2013. **498**(7452): p. 109-12.

118. Pettit, F.H., J.W. Pelley, and L.J. Reed, *Regulation of pyruvate dehydrogenase kinase and phosphatase by acetyl-CoA/CoA and NADH/NAD ratios.* Biochem Biophys Res Commun, 1975. **65**(2): p. 575-82.

119. Shimazu, T., et al., *Acetate metabolism and aging: An emerging connection.* Mech Ageing Dev, 2010. **131**(7-8): p. 511-6.

120. Fujino, T., et al., *Acetyl-CoA synthetase 2, a mitochondrial matrix enzyme involved in the oxidation of acetate.* J Biol Chem, 2001. **276**(14): p. 11420-6.

121. Ziegler, D.M., *Role of reversible oxidation-reduction of enzyme thiols-disulfides in metabolic regulation.* Annu Rev Biochem, 1985. **54**: p. 305-29.

122. Wang, H., et al., *c-Myc depletion inhibits proliferation of human tumor cells at various stages of the cell cycle.* Oncogene, 2008. **27**(13): p. 1905-15.

123. Fernandez, P.C., et al., *Genomic targets of the human c-Myc protein.* Genes Dev, 2003. **17**(9): p. 1115-29.

124. O'Connell, B.C., et al., *A large scale genetic analysis of c-Myc-regulated gene expression patterns.* J Biol Chem, 2003. **278**(14): p. 12563-73.

125. Faergeman, N.J. and J. Knudsen, *Role of long-chain fatty acyl-CoA esters in the regulation of metabolism and in cell signalling.* Biochem J, 1997. **323 (Pt 1)**: p. 1-12.

126. Jo, Y. and R.A. Debose-Boyd, *Control of cholesterol synthesis through regulated ER-associated degradation of HMG CoA reductase.* Crit Rev Biochem Mol Biol, 2010. **45**(3): p. 185-98.

127. Mazurek, S., et al., *Pyruvate kinase type M2: a crossroad in the tumor metabolome.* Br J Nutr, 2002. **87 Suppl 1**: p. S23-9.

128. Gocze, P.M. and D.A. Freeman, *Factors underlying the variability of lipid droplet fluorescence in MA-10 Leydig tumor cells.* Cytometry, 1994. **17**(2): p. 151-8.

129. Nesbit, C.E., J.M. Tersak, and E.V. Prochownik, *MYC oncogenes and human neoplastic disease.* Oncogene, 1999. **18**(19): p. 3004-16.

130. Petrich, A.M., C. Nabhan, and S.M. Smith, *MYC-associated and double-hit lymphomas: A review of pathobiology, prognosis, and therapeutic approaches.* Cancer, 2014.

131. Roussel, M.F. and G.W. Robinson, *Role of MYC in Medulloblastoma.* Cold Spring Harb Perspect Med, 2013. **3**(11).

132. Gomez-Roman, N., et al., *Direct activation of RNA polymerase III transcription by c-Myc.* Nature, 2003. **421**(6920): p. 290-4.

133. Grandori, C., et al., *c-Myc binds to human ribosomal DNA and stimulates transcription of rRNA genes by RNA polymerase I.* Nat Cell Biol, 2005. **7**(3): p. 311-8.

134. Nie, Z., et al., *c-Myc is a universal amplifier of expressed genes in lymphocytes and embryonic stem cells.* Cell, 2012. **151**(1): p. 68-79.

135. Lin, C.Y., et al., *Transcriptional amplification in tumor cells with elevated c-Myc.* Cell, 2012. **151**(1): p. 56-67.

136. Sabo, A. and B. Amati, *Genome recognition by MYC.* Cold Spring Harb Perspect Med, 2014. **4**(2).

137. Walz, S., et al., *Activation and repression by oncogenic MYC shape tumour-specific gene expression profiles.* Nature, 2014. **511**(7510): p. 483-7.

138. Hann, S.R., *MYC cofactors: molecular switches controlling diverse biological outcomes.* Cold Spring Harb Perspect Med, 2014. **4**(9): p. a014399.

139. Sabo, A., et al., *Selective transcriptional regulation by Myc in cellular growth control and lymphomagenesis.* Nature, 2014. **511**(7510): p. 488-92.

140. Wahlstrom, T. and M. Arsenian Henriksson, *Impact of MYC in regulation of tumor cell metabolism.* Biochim Biophys Acta, 2014.

141. Bayley, J.P. and P. Devilee, *The Warburg effect in 2012.* Curr Opin Oncol, 2012. **24**(1): p. 62-7.

142. Olson, A.K., et al., *C-Myc induced compensated cardiac hypertrophy increases free fatty acid utilization for the citric acid cycle.* J Mol Cell Cardiol, 2013. **55**: p. 156-64.

143. Pacilli, A., et al., *Carnitine-acyltransferase system inhibition, cancer cell death, and prevention of myc-induced lymphomagenesis.* J Natl Cancer Inst, 2013. **105**(7): p. 489-98.

144. DeBerardinis, R.J. and T. Cheng, *Q's next: the diverse functions of glutamine in metabolism, cell biology and cancer.* Oncogene, 2010. **29**(3): p. 313-24.

145. Kim, I. and Y.Y. He, *Targeting the AMP-Activated Protein Kinase for Cancer Prevention and Therapy.* Front Oncol, 2013. **3**: p. 175.

146. Shirwany, N.A. and M.H. Zou, *AMPK: a cellular metabolic and redox sensor. A minireview.* Front Biosci (Landmark Ed), 2014. **19**: p. 447-74.

147. Sanz, P., *AMP-activated protein kinase: structure and regulation.* Curr Protein Pept Sci, 2008. **9**(5): p. 478-92.

148. Russo, G.L., M. Russo, and P. Ungaro, *AMP-activated protein kinase: a target for old drugs against diabetes and cancer.* Biochem Pharmacol, 2013. **86**(3): p. 339-50.

149. O'Neill, H.M., G.P. Holloway, and G.R. Steinberg, *AMPK regulation of fatty acid metabolism and mitochondrial biogenesis: implications for obesity.* Mol Cell Endocrinol, 2013. **366**(2): p. 135-51.

150. Reznick, R.M. and G.I. Shulman, *The role of AMP-activated protein kinase in mitochondrial biogenesis.* J Physiol, 2006. **574**(Pt 1): p. 33-9.

151. Eilers, M., et al., *Chimaeras of myc oncoprotein and steroid receptors cause hormone-dependent transformation of cells.* Nature, 1989. **340**(6228): p. 66-8.

152. Vafa, O., et al., *c-Myc can induce DNA damage, increase reactive oxygen species, and mitigate p53 function: a mechanism for oncogene-induced genetic instability.* Mol Cell, 2002. **9**(5): p. 1031-44.

153. Colombo, S.L. and S. Moncada, *AMPKalpha1 regulates the antioxidant status of vascular endothelial cells.* Biochem J, 2009. **421**(2): p. 163-9.

154. Quintero, M., et al., *Mitochondria as signaling organelles in the vascular endothelium.* Proc Natl Acad Sci U S A, 2006. **103**(14): p. 5379-84.

155. Sid, B., J. Verrax, and P.B. Calderon, *Role of AMPK activation in oxidative cell damage: Implications for alcohol-induced liver disease.* Biochem Pharmacol, 2013. **86**(2): p. 200-9.

156. Toyoda, T., et al., *Possible involvement of the alpha1 isoform of 5'AMP-activated protein kinase in oxidative stress-stimulated glucose transport in skeletal muscle.* Am J Physiol Endocrinol Metab, 2004. **287**(1): p. E166-73.

157. Lenaz, G., et al., *Mitochondrial respiratory chain super-complex I-III in physiology and pathology.* Biochim Biophys Acta, 2010. **1797**(6-7): p. 633-40.

158. Genova, M.L., et al., *Is supercomplex organization of the respiratory chain required for optimal electron transfer activity?* Biochim Biophys Acta, 2008. **1777**(7-8): p. 740-6.

159. Chen, G., et al., *Discordant protein and mRNA expression in lung adenocarcinomas.* Mol Cell Proteomics, 2002. **1**(4): p. 304-13.

160. de Sousa Abreu, R., et al., *Global signatures of protein and mRNA expression levels.* Mol Biosyst, 2009. **5**(12): p. 1512-26.

161. Ghazalpour, A., et al., *Comparative analysis of proteome and transcriptome variation in mouse.* PLoS Genet, 2011. **7**(6): p. e1001393.

162. Kristensen, A.R., J. Gsponer, and L.J. Foster, *Protein synthesis rate is the predominant regulator of protein expression during differentiation.* Mol Syst Biol, 2013. **9**: p. 689.

163. Matalon, O., A. Horovitz, and E.D. Levy, *Different subunits belonging to the same protein complex often exhibit discordant expression levels and evolutionary properties.* Curr Opin Struct Biol, 2014. **26**: p. 113-20.

164. Pascal, L.E., et al., *Correlation of mRNA and protein levels: cell type-specific gene expression of cluster designation antigens in the prostate.* BMC Genomics, 2008. **9**: p. 246.

165. Zhang, B., et al., *Proteogenomic characterization of human colon and rectal cancer.* Nature, 2014. **513**(7518): p. 382-7.

166. Alaynick, W.A., *Nuclear receptors, mitochondria and lipid metabolism.* Mitochondrion, 2008. **8**(4): p. 329-37.

167. Roberti, M., et al., *The MTERF family proteins: mitochondrial transcription regulators and beyond.* Biochim Biophys Acta, 2009. **1787**(5): p. 303-11.

168. Scarpulla, R.C., R.B. Vega, and D.P. Kelly, *Transcriptional integration of mitochondrial biogenesis.* Trends Endocrinol Metab, 2012. **23**(9): p. 459-66.

169. Yakubovskaya, E., et al., *Organization of the human mitochondrial transcription initiation complex.* Nucleic Acids Res, 2014. **42**(6): p. 4100-12.

170. Meng, F., et al., *Quantitative analysis of complex peptide mixtures using FTMS and differential mass spectrometry.* J Am Soc Mass Spectrom, 2007. **18**(2): p. 226-33.

171. Paweletz, C.P., et al., *Application of an end-to-end biomarker discovery platform to identify target engagement markers in cerebrospinal fluid by high resolution differential mass spectrometry.* J Proteome Res, 2010. **9**(3): p. 1392-401.

172. Gellerich, F.N., et al., *The regulation of OXPHOS by extramitochondrial calcium.* Biochim Biophys Acta, 2010. **1797**(6-7): p. 1018-27.

173. Huttemann, M., et al., *Regulation of oxidative phosphorylation, the mitochondrial membrane potential, and their role in human disease.* J Bioenerg Biomembr, 2008. **40**(5): p. 445-56.

174. Pierron, D., et al., *Cytochrome c oxidase: evolution of control via nuclear subunit addition.* Biochim Biophys Acta, 2012. **1817**(4): p. 590-7.

175. Scheller, K. and C.E. Sekeris, *The effects of steroid hormones on the transcription of genes encoding enzymes of oxidative phosphorylation.* Exp Physiol, 2003. **88**(1): p. 129-40.

176. Hanson, G.T., et al., *Investigating mitochondrial redox potential with redox-sensitive green fluorescent protein indicators.* J Biol Chem, 2004. **279**(13): p. 13044-53.

177. Schwarzlander, M., et al., *Confocal imaging of glutathione redox potential in living plant cells.* J Microsc, 2008. **231**(2): p. 299-316.

178. Dooley, C.T., et al., *Imaging dynamic redox changes in mammalian cells with green fluorescent protein indicators.* J Biol Chem, 2004. **279**(21): p. 22284-93.

179. Trachootham, D., et al., *Redox regulation of cell survival.* Antioxid Redox Signal, 2008. **10**(8): p. 1343-74.

180. Jiang, K., et al., *Expression and characterization of a redox-sensing green fluorescent protein (reduction-oxidation-sensitive green fluorescent protein) in Arabidopsis.* Plant Physiol, 2006. **141**(2): p. 397-403.

181. Janssen-Heininger, Y.M., et al., *Emerging mechanisms of glutathione-dependent chemistry in biology and disease.* J Cell Biochem, 2013. **114**(9): p. 1962-8.

182. Iqbal, M.A., et al., *Pyruvate kinase M2 and cancer: an updated assessment.* FEBS Lett, 2014. **588**(16): p. 2685-92.

183. Morgan, H.P., et al., *M2 pyruvate kinase provides a mechanism for nutrient sensing and regulation of cell proliferation.* Proc Natl Acad Sci U S A, 2013. **110**(15): p. 5881-6.

184. Patel, M.S. and L.G. Korotchkina, *Regulation of mammalian pyruvate dehydrogenase complex by phosphorylation: complexity of multiple phosphorylation sites and kinases.* Exp Mol Med, 2001. **33**(4): p. 191-7.

185. Wong, N., J. De Melo, and D. Tang, *PKM2, a Central Point of Regulation in Cancer Metabolism.* Int J Cell Biol, 2013. **2013**: p. 242513.

186. Li, Z., P. Yang, and Z. Li, *The multifaceted regulation and functions of PKM2 in tumor progression.* Biochim Biophys Acta, 2014. **1846**(2): p. 285-296.

187. Jeon, S.M., N.S. Chandel, and N. Hay, *AMPK regulates NADPH homeostasis to promote tumour cell survival during energy stress.* Nature, 2012. **485**(7400): p. 661-5.

188. Bardeesy, N., et al., *Loss of the Lkb1 tumour suppressor provokes intestinal polyposis but resistance to transformation.* Nature, 2002. **419**(6903): p. 162-7.

189. Laderoute, K.R., et al., *5'-AMP-activated protein kinase (AMPK) is induced by low-oxygen and glucose deprivation conditions found in solid-tumor microenvironments.* Mol Cell Biol, 2006. **26**(14): p. 5336-47.

190. Kuehl, W.M. and P.L. Bergsagel, *MYC addiction: a potential therapeutic target in MM.* Blood, 2012. **120**(12): p. 2351-2.

191. Sodir, N.M. and G.I. Evan, *Finding cancer's weakest link.* Oncotarget, 2011. **2**(12): p. 1307-13.

192. Salt, I., et al., *AMP-activated protein kinase: greater AMP dependence, and preferential nuclear localization, of complexes containing the alpha2 isoform.* Biochem J, 1998. **334 (Pt 1)**: p. 177-87.

193. Ju, T.C., et al., *Nuclear translocation of AMPK-alpha1 potentiates striatal neurodegeneration in Huntington's disease.* J Cell Biol, 2011. **194**(2): p. 209-27.

194. Kazgan, N., et al., *Identification of a nuclear export signal in the catalytic subunit of AMP-activated protein kinase.* Mol Biol Cell, 2010. **21**(19): p. 3433-42.

195. Zhang, P., et al., *c-Myc is required for the CHREBP-dependent activation of glucose-responsive genes.* Mol Endocrinol, 2010. **24**(6): p. 1274-86.

196. Attie, A.D. and C.M. Kendziorski, *PGC-1alpha at the crossroads of type 2 diabetes.* Nat Genet, 2003. **34**(3): p. 244-5.

197. Kukidome, D., et al., *Activation of AMP-activated protein kinase reduces hyperglycemia-induced mitochondrial reactive oxygen species production and promotes mitochondrial biogenesis in human umbilical vein endothelial cells.* Diabetes, 2006. **55**(1): p. 120-7.

198. Kawaguchi, T., et al., *Mechanism for fatty acid "sparing" effect on glucose-induced transcription: regulation of carbohydrate-responsive element-binding protein by AMP-activated protein kinase.* J Biol Chem, 2002. **277**(6): p. 3829-35.

199. Mihaylova, M.M. and R.J. Shaw, *The AMPK signalling pathway coordinates cell growth, autophagy and metabolism.* Nat Cell Biol, 2011. **13**(9): p. 1016-23.

200. Bres, V., S.M. Yoh, and K.A. Jones, *The multi-tasking P-TEFb complex.* Curr Opin Cell Biol, 2008. **20**(3): p. 334-40.

201. Rahl, P.B. and R.A. Young, *MYC and transcription elongation.* Cold Spring Harb Perspect Med, 2014. **4**(1): p. a020990.

202. Cao, Z., J.G. Lindsay, and N.W. Isaacs, *Mitochondrial peroxiredoxins.* Subcell Biochem, 2007. **44**: p. 295-315.

203. Go, Y.M. and D.P. Jones, *Redox compartmentalization in eukaryotic cells.* Biochim Biophys Acta, 2008. **1780**(11): p. 1273-90.

204. Miranda-Vizuete, A., A.E. Damdimopoulos, and G. Spyrou, *The mitochondrial thioredoxin system.* Antioxid Redox Signal, 2000. **2**(4): p. 801-10.

205. Raha, S. and B.H. Robinson, *Mitochondria, oxygen free radicals, and apoptosis.* Am J Med Genet, 2001. **106**(1): p. 62-70.

206. Raha, S. and B.H. Robinson, *Mitochondria, oxygen free radicals, disease and ageing.* Trends Biochem Sci, 2000. **25**(10): p. 502-8.

207. Pitkanen, S. and B.H. Robinson, *Mitochondrial complex I deficiency leads to increased production of superoxide radicals and induction of superoxide dismutase.* J Clin Invest, 1996. **98**(2): p. 345-51.

208. Robinson, B.H., *Human complex I deficiency: clinical spectrum and involvement of oxygen free radicals in the pathogenicity of the defect.* Biochim Biophys Acta, 1998. **1364**(2): p. 271-86.

209. Irani, K., *Oxidant signaling in vascular cell growth, death, and survival : a review of the roles of reactive oxygen species in smooth muscle and endothelial cell mitogenic and apoptotic signaling.* Circ Res, 2000. **87**(3): p. 179-83.

210. Sarsour, E.H., et al., *Redox control of the cell cycle in health and disease.* Antioxid Redox Signal, 2009. **11**(12): p. 2985-3011.

211. Viollet, B., et al., *Physiological role of AMP-activated protein kinase (AMPK): insights from knockout mouse models.* Biochem Soc Trans, 2003. **31**(Pt 1): p. 216-9.

212. Jorgensen, S.B., et al., *Knockout of the alpha2 but not alpha1 5'-AMP-activated protein kinase isoform abolishes 5-aminoimidazole-4-carboxamide-1-beta-4-ribofuranosidebut not contraction-induced glucose uptake in skeletal muscle.* J Biol Chem, 2004. **279**(2): p. 1070-9.

213. Van Coster, R., et al., *Blue native polyacrylamide gel electrophoresis: a powerful tool in diagnosis of oxidative phosphorylation defects.* Pediatr Res, 2001. **50**(5): p. 658-65.

214. Wittig, I., M. Karas, and H. Schagger, *High resolution clear native electrophoresis for in-gel functional assays and fluorescence studies of membrane protein complexes.* Mol Cell Proteomics, 2007. **6**(7): p. 1215-25.

215. Zeng, X., et al., *Lung cancer serum biomarker discovery using label-free liquid chromatography-tandem mass spectrometry.* J Thorac Oncol, 2011. **6**(4): p. 725-34.

216. Miedel, M.T., et al., *Isolation of serpin-interacting proteins in C. elegans using protein affinity purification.* Methods, 2014. **68**(3): p. 536-41.

217. Eng, J.K., T.A. Jahan, and M.R. Hoopmann, *Comet: an open-source MS/MS sequence database search tool.* Proteomics, 2013. **13**(1): p. 22-4.

218. Paredes, R.M., et al., *Metabolomic profiling of schizophrenia patients at risk for metabolic syndrome.* Int J Neuropsychopharmacol, 2014. **17**(8): p. 1139-48.

219. Zhou, J.Z., et al., *Differential impact of adenosine nucleotides released by osteocytes on breast cancer growth and bone metastasis.* Oncogene, 2015. **34**(14): p. 1831-42.

220. Sheiness, D., et al., *Avian retroviruses that cause carcinoma and leukemia: identification of nucleotide sequences associated with pathogenicity.* J Virol, 1980. **33**(3): p. 962-8.

221. Arvanitis, C. and D.W. Felsher, *Conditional transgenic models define how MYC initiates and maintains tumorigenesis.* Semin Cancer Biol, 2006. **16**(4): p. 313-7.

222. Fernandez, D., V.J. Sanchez-Arevalo, and I.M. de Alboran, *The role of the proto-oncogene c-myc in B lymphocyte differentiation.* Crit Rev Immunol, 2012. **32**(4): p. 321-34.

223. Davis, A.C., et al., *A null c-myc mutation causes lethality before 10.5 days of gestation in homozygotes and reduced fertility in heterozygous female mice.* Genes Dev, 1993. **7**(4): p. 671-82.

224. Michalopoulos, G.K., *Liver regeneration after partial hepatectomy: critical analysis of mechanistic dilemmas.* Am J Pathol, 2010. **176**(1): p. 2-13.

225. Qu, A., et al., *Role of Myc in hepatocellular proliferation and hepatocarcinogenesis.* J Hepatol, 2014. **60**(2): p. 331-8.

226. Kvittingen, E.A., *Tyrosinaemia--treatment and outcome.* J Inherit Metab Dis, 1995. **18**(4): p. 375-9.

227. Grompe, M., et al., *Pharmacological correction of neonatal lethal hepatic dysfunction in a murine model of hereditary tyrosinaemia type I.* Nat Genet, 1995. **10**(4): p. 453-60.

228. Overturf, K., et al., *Hepatocytes corrected by gene therapy are selected in vivo in a murine model of hereditary tyrosinaemia type I.* Nat Genet, 1996. **12**(3): p. 266-73.

229. Duncan, A.W., et al., *Aneuploidy as a mechanism for stress-induced liver adaptation.* J Clin Invest, 2012. **122**(9): p. 3307-15.

230. Jonkers, J. and A. Berns, *Oncogene addiction: sometimes a temporary slavery.* Cancer Cell, 2004. **6**(6): p. 535-8.

231. Hoffman, B. and D.A. Liebermann, *Apoptotic signaling by c-MYC.* Oncogene, 2008. **27**(50): p. 6462-72.

232. Edmunds, L.R., et al., *c-Myc and AMPK Control Cellular Energy Levels by Cooperatively Regulating Mitochondrial Structure and Function.* PLoS One, 2015. **10**(7): p. e0134049.

233. Nelson, D.R., et al., *Comparison of cytochrome P450 (CYP) genes from the mouse and human genomes, including nomenclature recommendations for genes, pseudogenes and alternative-splice variants.* Pharmacogenetics, 2004. **14**(1): p. 1-18.

234. Kim, S., et al., *Induction of ribosomal genes and hepatocyte hypertrophy by adenovirus-mediated expression of c-Myc in vivo.* Proc Natl Acad Sci U S A, 2000. **97**(21): p. 11198-202.

235. Calkin, A.C. and P. Tontonoz, *Transcriptional integration of metabolism by the nuclear sterol-activated receptors LXR and FXR.* Nat Rev Mol Cell Biol, 2012. **13**(4): p. 213-24.

236. Rothermund, K., et al., *C-Myc-independent restoration of multiple phenotypes by two C-Myc target genes with overlapping functions.* Cancer Res, 2005. **65**(6): p. 2097-107.

237. Nikiforov, M.A., et al., *A functional screen for Myc-responsive genes reveals serine hydroxymethyltransferase, a major source of the one-carbon unit for cell metabolism.* Mol Cell Biol, 2002. **22**(16): p. 5793-800.

238. Mashek, D.G., et al., *Hepatic lipid droplet biology: Getting to the root of fatty liver.* Hepatology, 2015.

239. Russell, D.W., *The enzymes, regulation, and genetics of bile acid synthesis.* Annu Rev Biochem, 2003. **72**: p. 137-74.

240. Azuma, H., et al., *Robust expansion of human hepatocytes in Fah-/-/Rag2-/-/Il2rg-/- mice.* Nat Biotechnol, 2007. **25**(8): p. 903-10.

241. Vartak, R.S., M.K. Semwal, and Y. Bai, *An update on complex I assembly: the assembly of players.* J Bioenerg Biomembr, 2014. **46**(4): p. 323-8.

242. Cobbold, S.P., *The mTOR pathway and integrating immune regulation.* Immunology, 2013. **140**(4): p. 391-8.

243. Boudina, S. and E.D. Abel, *Mitochondrial uncoupling: a key contributor to reduced cardiac efficiency in diabetes.* Physiology (Bethesda), 2006. **21**: p. 250-8.

244. Speijer, D., *How the mitochondrion was shaped by radical differences in substrates: what carnitine shuttles and uncoupling tell us about mitochondrial evolution in response to ROS.* Bioessays, 2014. **36**(7): p. 634-43.

245. Das, A.M., *Regulation of mitochondrial ATP synthase activity in human myocardium.* Clin Sci (Lond), 1998. **94**(5): p. 499-504.

246. Nebert, D.W., K. Wikvall, and W.L. Miller, *Human cytochromes P450 in health and disease.* Philos Trans R Soc Lond B Biol Sci, 2013. **368**(1612): p. 20120431.

247. Hafner, M., T. Rezen, and D. Rozman, *Regulation of hepatic cytochromes p450 by lipids and cholesterol.* Curr Drug Metab, 2011. **12**(2): p. 173-85.

248. Tetri, L.H., et al., *Severe NAFLD with hepatic necroinflammatory changes in mice fed trans fats and a high-fructose corn syrup equivalent.* Am J Physiol Gastrointest Liver Physiol, 2008. **295**(5): p. G987-95.

249. Brunt, E.M., *Pathology of nonalcoholic fatty liver disease.* Nat Rev Gastroenterol Hepatol, 2010. **7**(4): p. 195-203.

250. Baena, E., et al., *c-Myc is essential for hematopoietic stem cell differentiation and regulates Lin(-)Sca-1(+)c-Kit(-) cell generation through p21.* Exp Hematol, 2007. **35**(9): p. 1333-43.

251. Wilson, E.M., et al., *Extensive double humanization of both liver and hematopoiesis in FRGN mice.* Stem Cell Res, 2014. **13**(3 Pt A): p. 404-12.

252. MacLean, B., et al., *Skyline: an open source document editor for creating and analyzing targeted proteomics experiments.* Bioinformatics, 2010. **26**(7): p. 966-8.

253. Benjamini, Y. and Y. Hochberg, *Controlling the false discovery rate: a practical and powerful approach to multiple testing.* Journal of the Royal Statistical Society. Series B (Methodological), 1995: p. 289-300.

254. Trapnell, C., et al., *Differential analysis of gene regulation at transcript resolution with RNA-seq.* Nat Biotechnol, 2013. **31**(1): p. 46-53.

255. Trapnell, C., et al., *Transcript assembly and quantification by RNA-Seq reveals unannotated transcripts and isoform switching during cell differentiation.* Nat Biotechnol, 2010. **28**(5): p. 511-5.

256. Basantani, M.K., et al., *Pnpla3/Adiponutrin deficiency in mice does not contribute to fatty liver disease or metabolic syndrome.* J Lipid Res, 2011. **52**(2): p. 318-29.

257. Choi, T.Y., et al., *Hepatocyte-specific ablation in zebrafish to study biliary-driven liver regeneration.* J Vis Exp, 2015(99): p. e52785.

258. Rankin, E.B., et al., *Hypoxia-inducible factor 2 regulates hepatic lipid metabolism.* Mol Cell Biol, 2009. **29**(16): p. 4527-38.

259. Wiesener, M.S., et al., *Widespread hypoxia-inducible expression of HIF-2alpha in distinct cell populations of different organs.* FASEB J, 2003. **17**(2): p. 271-3.

260. Postic, C., et al., *ChREBP, a transcriptional regulator of glucose and lipid metabolism.* Annu Rev Nutr, 2007. **27**: p. 179-92.

261. Zaidi, N., et al., *ATP citrate lyase knockdown induces growth arrest and apoptosis through different cell- and environment-dependent mechanisms.* Mol Cancer Ther, 2012. **11**(9): p. 1925-35.

262. Mason, P., et al., *SCD1 inhibition causes cancer cell death by depleting mono-unsaturated fatty acids.* PLoS One, 2012. **7**(3): p. e33823.

263. Baenke, F., et al., *Hooked on fat: the role of lipid synthesis in cancer metabolism and tumour development.* Dis Model Mech, 2013. **6**(6): p. 1353-63.

264. Zhou, G., et al., *Role of AMP-activated protein kinase in mechanism of metformin action.* J Clin Invest, 2001. **108**(8): p. 1167-74.

265. Hawley, S.A., et al., *The antidiabetic drug metformin activates the AMP-activated protein kinase cascade via an adenine nucleotide-independent mechanism.* Diabetes, 2002. **51**(8): p. 2420-5.

266. Polyak, K., et al., *A model for p53-induced apoptosis.* Nature, 1997. **389**(6648): p. 300-5.

267. Packham, G. and J.L. Cleveland, *Ornithine decarboxylase is a mediator of c-Myc-induced apoptosis.* Mol Cell Biol, 1994. **14**(9): p. 5741-7.

268. Sanders, S. and S.S. Thorgeirsson, *Promotion of hepatocarcinogenesis by phenobarbital in c-myc/TGF-alpha transgenic mice.* Mol Carcinog, 2000. **28**(3): p. 168-73.